UNIVERSITÀ DEGLI STUDI DI PADOVA

DIPARTIMENTO DI INGEGNERIA INDUSTRIALE

(ex DM 270/2004)

BIOMECHANICAL ANALYSIS OF THE SIDESTEP CUTTING MANEUVER IN FOOTBALL PLAYERS WITH OPENSIM

Relatori: Prof. Nicola Petrone

Prof. Josep Maria Font Llagunes

Dott. Ventura Ferrer Roca

Laureando: Dennis Da Corte

Matricola: 1036513

ANNO ACCADEMICO 2013/2014

Abstract

The use of mechanical vibrations has become a very common technique in the training of athletes. Some studies highlight that this kind of training is able to increase the force of the muscles, but is seems to decrease the capacity of controlling the movements by the subject. This aspect could increase the risk of ACL injuries.

The aim of this project is to develop a computational model to analyze how a warming up with mechanical vibrations can affect the biomechanical behavior of the lower limbs, with a particular attention to the aspects related to the noncontact ACL injuries. For this purpose, a lower limb model is implemented using the OpenSim software (Stanford University) to obtain the evolution of joint angles, joint torques and muscle forces during a sidestep cutting maneuver (before and after warming up). Those results are obtained by means of multibody dynamics and optimization techniques.

The work also includes an economic study and an analysis of the social and environmental impact.

Contents

Chapter 1

Introduction

The ACL injury is a very common problem in sports like football, alpine skiing, basketball, handball, rugby, etc., that just in the United States affects more than 100000 people each year. This kind of injury requires a very long convalescence, in some cases longer than 6 months.

In this prospective the sports trainers are trying to work in order to find strategies of training designed to reduce the risk of occurrence of ACL injuries. However, on the other hand, they design the trainings in order to increase the performances of the athletes. Could these two aims be at odds with each other?

Some studies on the full body mechanical vibrations warming up highlight that this kind of training seems to increase the muscular performance of the athletes but, on the other hand, to decrease the capacity of control and of perception of the knee, bringing to an increase of possibilities to develop an ACL injury.

The aim of the project is to develop a three-dimensional lower limb multibody model to investigate the biomechanical effects related to the loss of control of the knee after a mechanical vibrations warming up. The model, that has a total of 36 degrees of freedom, consists of 6 segments and is actuated by 43 muscles. This project is done in the framework of a collaborative work among the Biomechanics Division of CREB-UPC at ETSEIB, the CAR of Sant Cugat and the University of Lleida.

Chapter 2

Anatomy of the lower limb

2.1 Knee joint behavior

2.1.1 Introduction

The knee can be considered as a double condylar articulation together with a trochlea. The lower limb can be divided mainly in two parts: the thigh and the shank. The first one is situated between the hip joint and the knee joint and it's coincident with the femur, the second one is situated between the knee joint and the ankle joint and it's coincident with the tibia and the fibula.

The biomechanical analysis of this joint highlights a principal degree of freedom (DOF) of flexion. The internal rotation and the adduction have a very low range of motion and they are often neglected in the mechanical models; anyway the amplitude of these two degrees of freedom is considered as a good factor to see if there is any problem on the ligaments that constrain the joint motion.

All the degrees of freedom of the knee joint are shown in Figure 2.1. The range of motion of the knee reported in literature is the following:

- Flexion: from 0° to 120°;
- Adduction: more or less from -10° to +10°;
- Internal rotation: more or less from -15° to 13° [11].

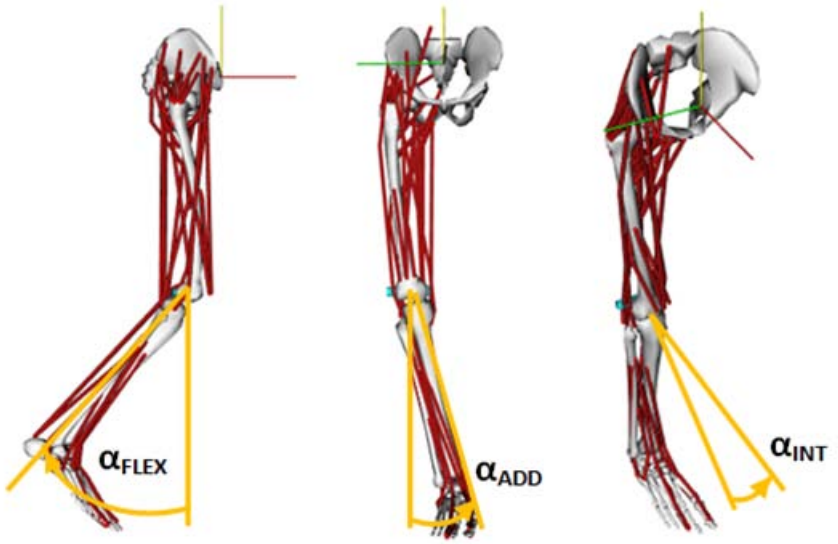

Figure 2.1: Degrees of freedom of the knee. On the left flexion, on the center adduction, on the right internal rotation.

2.1.2 Bones

Femur:

The femur, represented in Figure 2.2, is the longest, heaviest and by most measures the strongest bone in the human body. Its length is 26% of the person's height, a ratio that is useful in anthropology because it offers a basis for a reasonable estimate of a subject's height from an incomplete skeleton.

The femur comprises a diaphysis (or shaft) and two epiphysis or extremities that articulate with adjacent bones in the hip and knee. In the proximal extremity of this bone there is a big protrusion called neck of the femur with a semi-spherical part called head of the femur that articulates with the acetabulum of the pelvis. There are also two smaller protrusions called greater and lesser trochanter, which are lever arms for some important muscles.

In a frontal plane, a normal neck of the femur has an inclination of more or less 125-130° with respect to the axis of the shaft; an inclination lower than 120° is considered as coxa vara, an inclination higher than 135° is considered as coxa valga, two pathologies that influence the posture of the whole body. A graphical explanation of this can be seen in Figure 2.3.

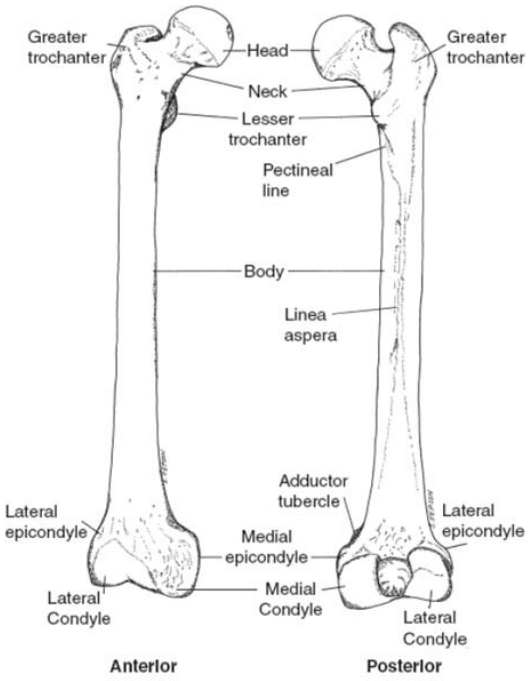

Figure 2.2: Anterior and posterior views of the femur, source [1].

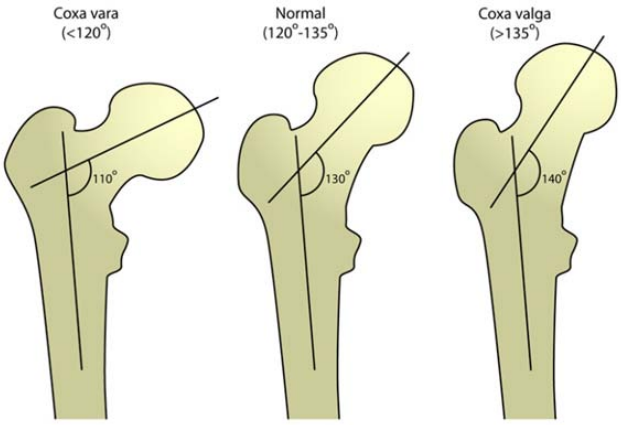

Figure 2.3: Typical angles of inclination of the head of the femur respect to its axial direction. On the left an example of coxa vara pathology, on the center a normal head of the femur, on the right an example of coxa valga pathology.

In a transversal view of the femur we can see an inclination between the neck and the axis that passes between the two condyles that can be quantified around 12-14°. An anteversion of the femur can be identified for angles greater than those, in the opposite case we would talk about retroversion. A graphical explanation of this can be seen in Figure 2.4.

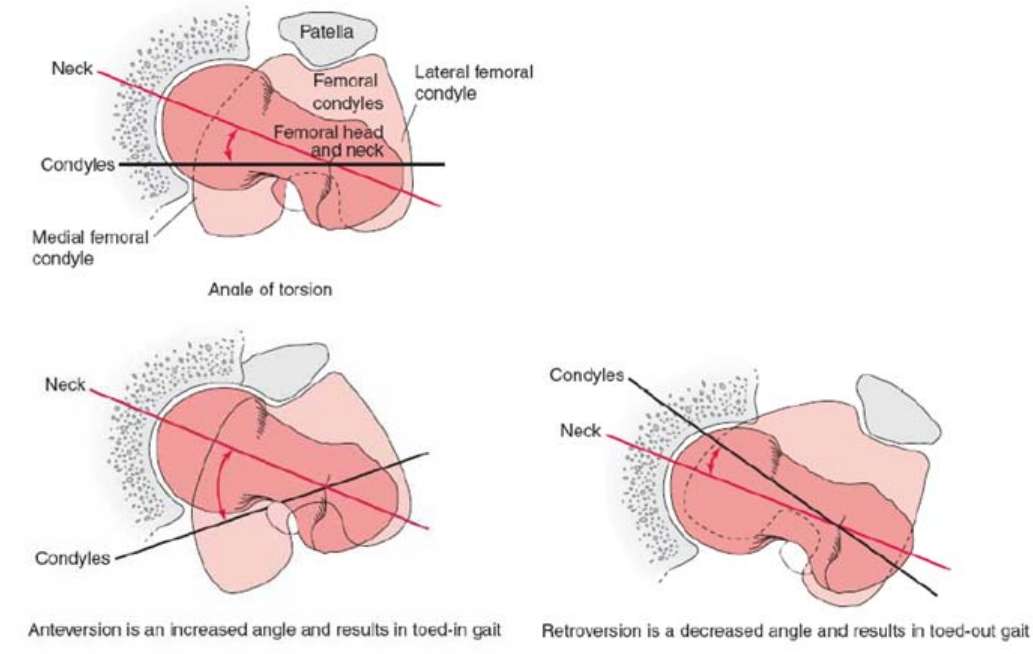

Figure 2.4: Typical angles of inclination of the axis passing between the two femoral condyles with respect to the direction of the neck of the femur. On the top the normal inclination, below on the left an example of anteversion pathology, below on the right an example of retroversion pathology.

The distal part of the femur has two condyles with a shape that matches the two glenoid cavities of the upper part of the tibia; between these there are two C-shaped pieces of fibro-cartilaginous tissue called medial and lateral menisci: their function is to act as shock absorbers between the femur and tibia.

The frontal part of the femur has a groove where the patella can slide during the flexion-extension of the knee; the contact surfaces are covered of articular cartilage, in order to reduce the friction between the bones and preserve them from usury. The articular surfaces of the knee can be seen in Figure 2.5.

Tibia and fibula:

The tibia is the largest and strongest bone of the shank; it's composed of a diaphysis (or shaft) and two epiphyses. The proximal part it's composed by the tibial plateau, a part larger than the rest of the bone that presents two condyles, one lateral and one medial; their upper surface presents a little glenoid concavity covered with articular cartilage, in order to permit the contact with the femoral condyles.

Between these two condyles there is a protrusion called intercondylar eminence that matches with the notch in the middle of the two condyles of the femur. The distal extremity of the tibia

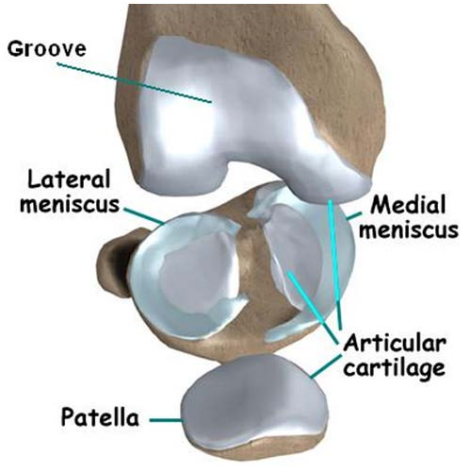

Figure 2.5: Surfaces of the knee and the two menisci, adapted from [15] .

presents a concave articular surface that develops in the medial part in the medial malleolus.

The fibula is the other bone part of the shank. It's very thin and it's situated in the lateral part of the tibia. It's composed of a diaphysis and two epiphyses. The proximal one has a planar articular facet, the contact part with the tibia; the distal part becomes the lateral malleolus. An anterior and posterior view of the tibia and the fibula bones can be seen in Figure 2.6.

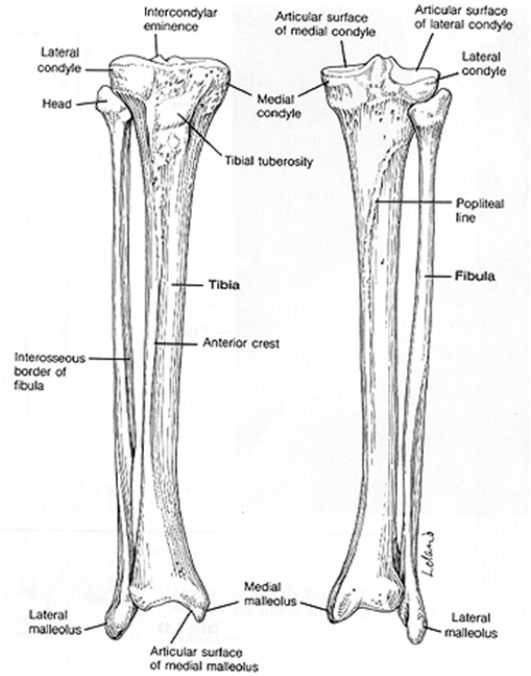

Figure 2.6: Anterior and posterior views of the tibia and the fibula.

Patella:

The patella, as we can see in Figure 2.7, is a flat, circular-triangular bone which articulates with the femur and covers and protects the anterior articular surface of the knee joint. It is the largest sesamoid bone in the human body. Its thickness can be considered as included in the thickness of the tendon of insertion of the quadriceps muscle. The patella has a very important role in the extension of the knee and its main importance is in the increasing of the lever arm of the quadriceps muscle.

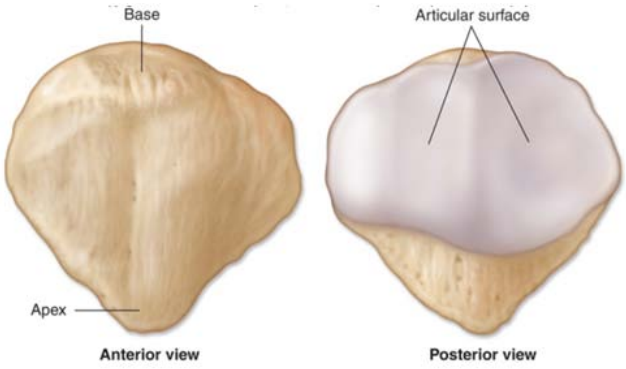

Figure 2.7: Anterior and posterior views of the patella, source [16].

2.2 Anatomy and phisiology of the skeletal muscle

2.2.1 Introduction

The muscle tissue is a fundamental part of the human structure. According with the different structures, functionalities and mechanism of control, we can divide it in three main categories: the skeletal muscle tissue, the cardiac muscle tissue and the smooth muscle tissue.

- Skeletal muscle tissue: as its name suggests, most skeletal muscles are attached to bones by bundles of collagen fibers known as tendons. This tissue is striated and is controlled by the somatic nervous system, so it can be activated voluntarily;

- Cardiac muscle tissue: this tissue is striated and composes the heart; its control is involuntary;

- Smooth muscle tissue: this tissue is not striated and composes most of the structure of the digestive system; its control is involuntary.

In this study we are interested just in the skeletal muscle tissue, so we will focus on this explaining which is its structure and how does it work. In the human body, there are 660 skeletal muscles, representing the 40-45% of the total mass of the body. Each muscle has two points where it is attached to the bones, namely, the origin and the insertion points. The origin is the proximal one and the insertion is the distal one.

2.2.2 Actions of the skeletal muscles

When we talk about action of the muscles we have to distinguish between three different kinds of action, as we can see in Figure 2.8.

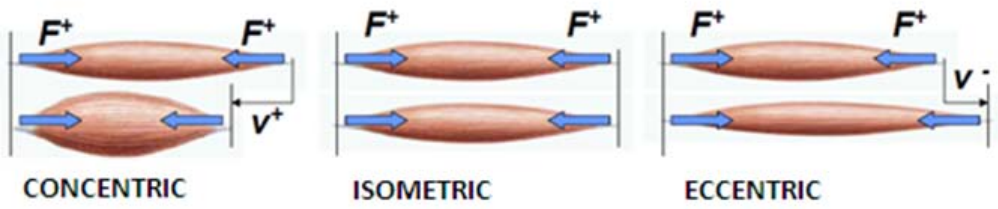

Figure 2.8: Actions of the skeletal muscle. On the left a concentric action, on the center an isometric action, on the right an eccentric action.

The fibers of the muscles are always generating a contraction force. During the concentric action there is a shortening of the length of the muscle, the force and the velocity of shortening have the same sign, so the work and the power produced by the muscle are both positive. During an isometric action there is not any movement of the two heads of the muscle, so the work and the power produced are zero. The eccentric action provides an elongation of the muscle, so the work and the power produced by the muscle are both negative, because the force and the velocity have different signs.

2.2.3 Macroscopic structure of the skeletal muscle

As shown in Figure 2.9, the skeletal muscle is wrapped by a connective tissue sheath called epimysium; this sheath separates the muscle from the adjacent tissues and holds together the fascicles which constitute the muscle.

All the fascicles are covered by a membrane called perimysium and they are composed by fibers (more or less 150 each) covered themselves by the endomysium. The diameter of the fibers can be around 100 μm and their length can reach some centimetres.

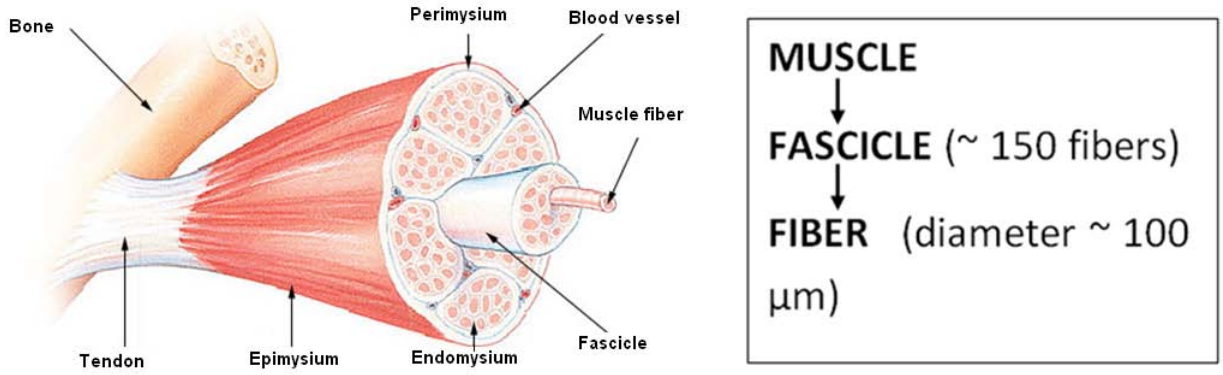

Figure 2.9: Macroscopic structure of the skeletal muscle.

2.2.4 Architecture of the skeletal muscle

We can distinguish between different kinds of architecture depending on the disposal of the fibers respect to the direction of the line connecting the origin and the insertion of the muscle; we describe the inclination of the fibers respect to the line of action of the muscle with the angle of pennation (α) as we can see in Figure 2.10.

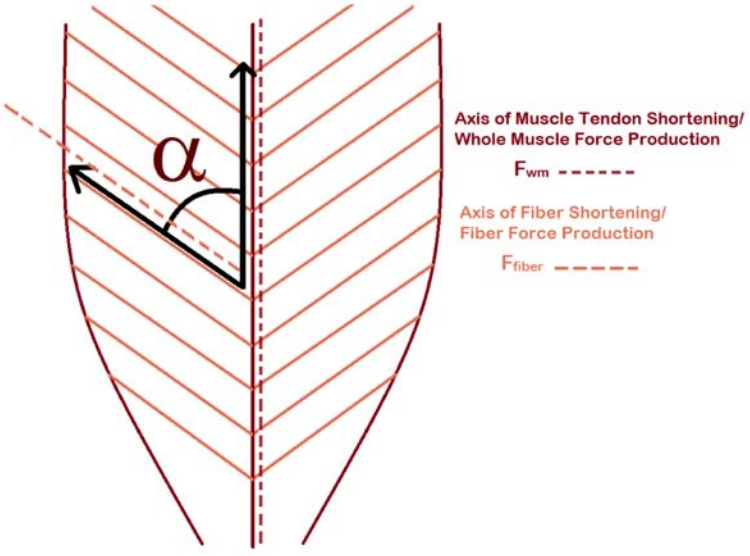

Figure 2.10: Definition of angle of pennation (α), source [3].

In this way we can distinguish between fusiform muscles and pennate muscles; the latter can be divided in different categories, according with the number of different directions in which the

fibers are oriented. The classification of the skeletal muscles respect to this criterion can be seen in Figure 2.11.

Figure 2.11: Classification of the skeletal muscles according with the macroscopic disposition of the fibers respect to the line of action of the tendon.

According with the definitions shown in Figure 2.12, it is possible to introduce an index called "index of architecture" (i_a) in order to give an idea of the kind of architecture of the muscle, considering the ratio between the length of the fibers (l_f) and the length of the muscle (l_m) in a particular optimal condition (Eq. 2.1).

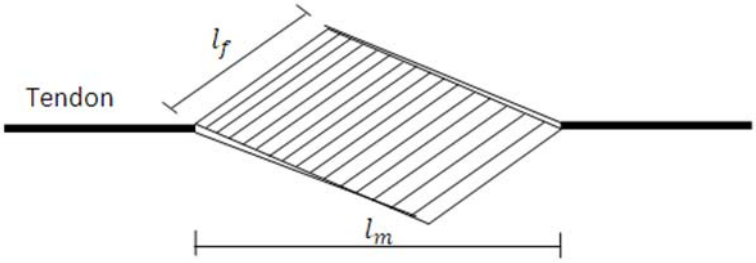

Figure 2.12: Schematization of a pennate muscle.

$$i_a = \frac{l_f}{l_m} \tag{2.1}$$

Obviously for a fusiform muscle the index of architecture is 1, because the angle of pennation is zero, so the length of the fibers coincides with the length of the muscle.

Every muscle has a parameter that describes which is the nominal strength of the muscle σ_0, the maximum isometric tension that can be generated by the fibers along their direction. The relationship between strength and force for the muscle has to pass through the definition of two geometrical parameters:

- Physiological Cross Section Area:

$$PCSA = \frac{Vol}{l_f} \tag{2.2}$$

- Cross Section Area:

$$CSA = \frac{Vol}{l_m} \tag{2.3}$$

where "Vol" si the volume of the muscle.

As we can see in Figure 2.13, the CSA is a section area perpendicular to the line that connects the two heads of the muscle; conversely the PCSA is a section area perpendicular to the direction of the fibers. In a fusiform muscle these two parameters are coincident, but in a pennate muscle they are different.

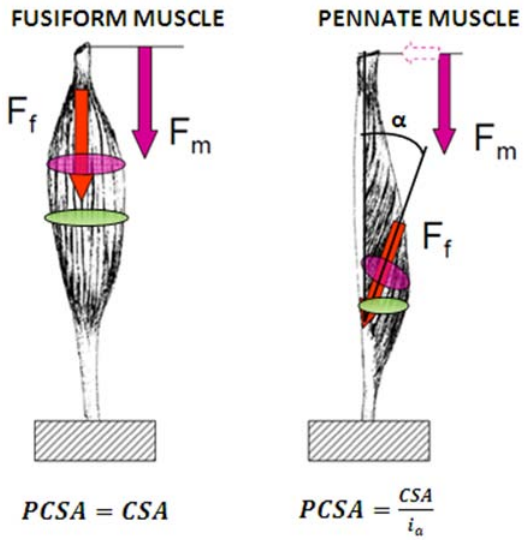

Figure 2.13: Graphical presentation of the PCSA (in pink) and of the CSA (in green) in a fusiform muscle and in a pennate muscle.

The relationship between the muscular force and the nominal strength of the muscle is, for all kinds of muscle, the following:

$$F_m = \sigma_0 \cdot PCSA \cdot \cos\alpha \tag{2.4}$$

2.2.5 Microstructure of the skeletal muscle

We can have an idea of the miscro structure of the skeletal muscle in Figure 2.14.

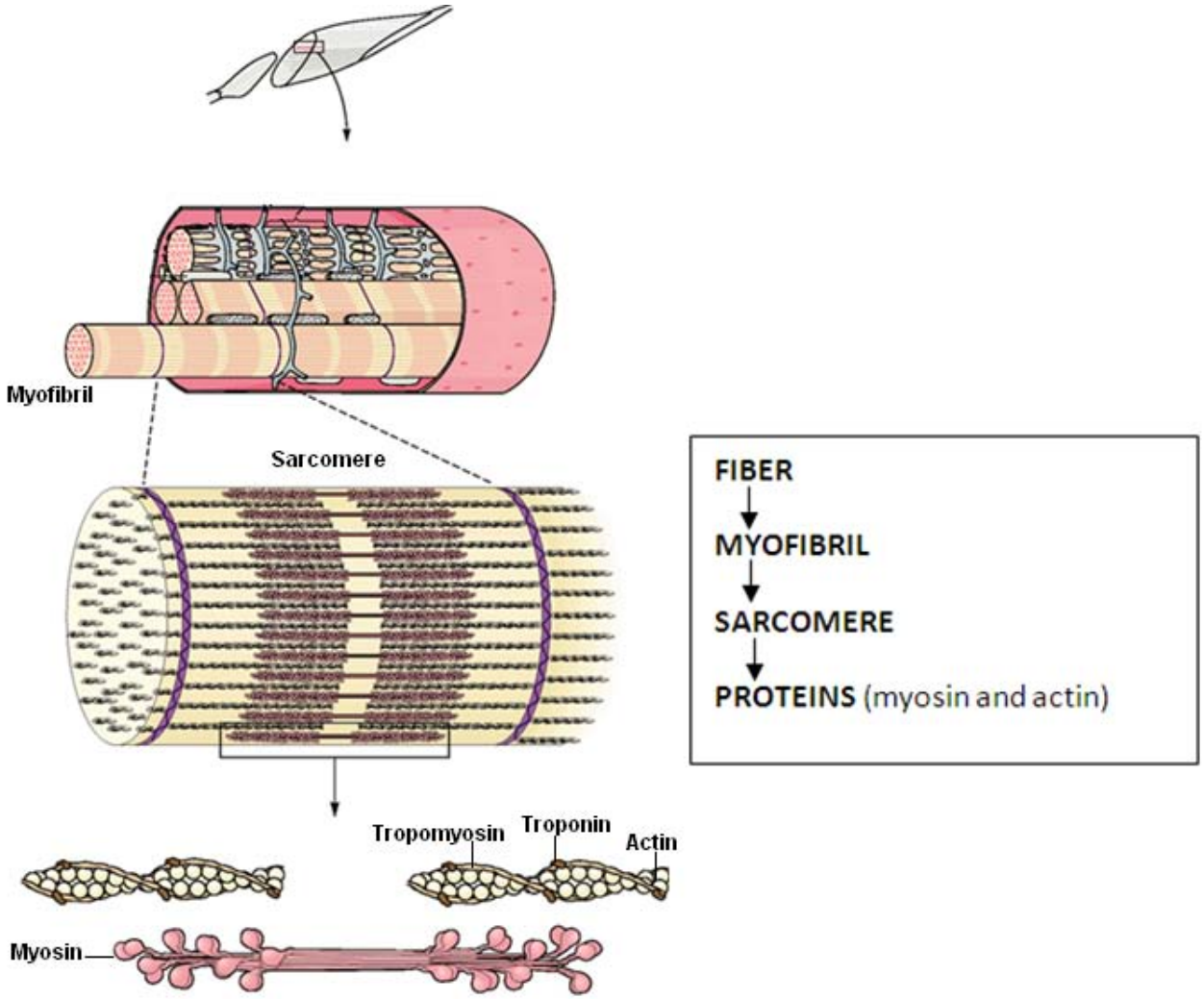

Figure 2.14: Micro structure of the skeletal muscle, source [8].

The smallest component of the macroscopic structure of the muscle is the muscle fiber with a diameter around 100 μm. The fiber is composed by a lot of filaments called myofibrils. Each myofibril is divided in different portions by transversal lines; in the portion between two contiguous Z lines we can identify the sarcomere, the elementary structure of the muscle. This is composed by filaments of different proteins: the actin and the myosin.

The myosin has a lot of protrusions that, thanks to Ca^{++} ions, can attach to the filament of actin and, thanks to the ATP that gives the energy for the process, can drag it.

2.2.6 Activation of the skeletal muscle

The skeletal muscles are activated through an electric impulse coming from the nervous system. The motor unit is the minimum quantity of muscle tissue that the nervous system can control independently. From a place of the spinal cord starts a particular motor neuron, the element that can control the contraction of the whole motor unit. The motor neuron then divides in nervous fibers, responsible to bring the signal to each muscle fiber part of the motor unit; each of these nervous fibers is attached to the muscle fiber through a motor endplate, that transforms the potential of action of the motor neuron into a potential of action in the muscle fiber that runs along the membrane of the muscle fiber in both the directions.

A scheme of the mechanism of activation of the motor units can is presented in Figure 2.15.

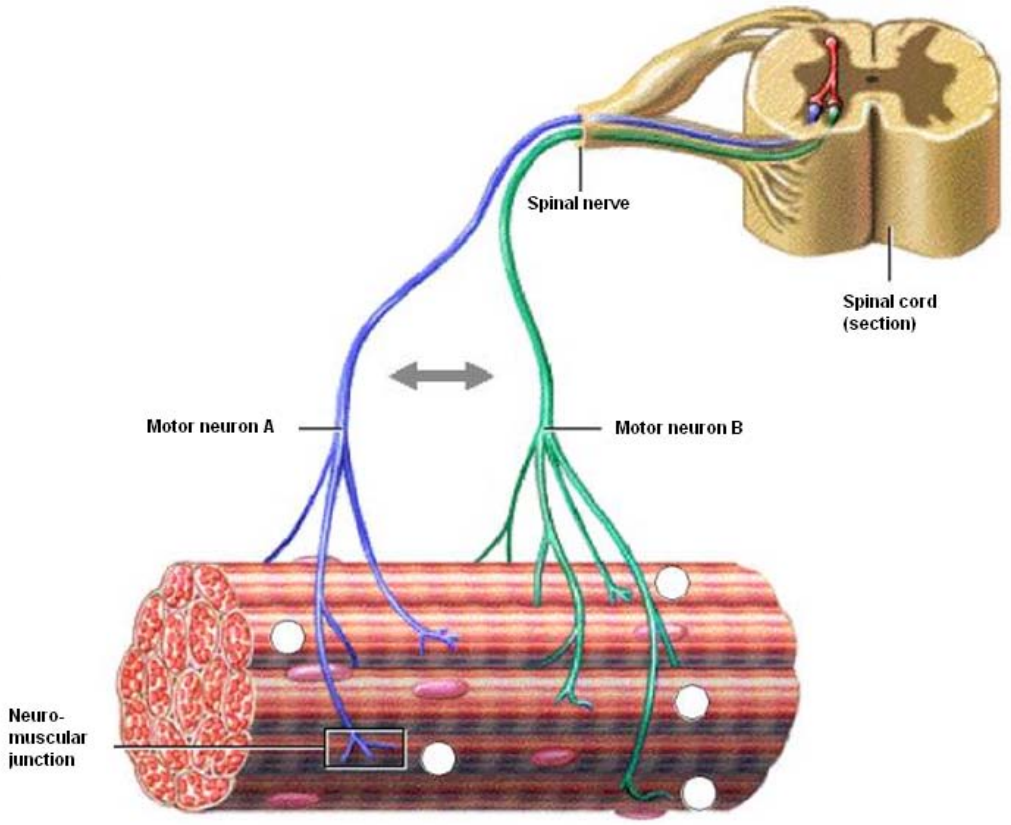

Figure 2.15: Scheme of the activation system of two different motor units of a muscle, source [17] .

The muscular fibers of each motor unit are scattered in the muscle, mixed with the fibers of other motor units. The fibers of each motor unit are scattered in a volume that is more or less the 20-30% of the whole volume of the muscle; in this way, even with a small number of motor units activated, it's possible to have a force well distributed in the volume of the muscle.

There are different types of motor units, according with the magnitude of the force that they can product and the time they can maintain it:

- S type (Slow): it produces a relatively low level of force, but it can maintain it for a long time without many changes on it;
- FF type (Fast Fatigable): it produces forces higher than the S type, but it can maintain it for a short time;
- FR type (Fast Resistant): it has avarage charachteristics between type S and type FF.

The motor units are never activated all together but they have an asynchronus activity, in order to have a force as constant as possible during the time, without the occurrence of fatigue.

The potential of action can be considered as a dipole that lasts more or less 1-5 ms, that runs along the membrane of the muscle fiber at a speed of 3-5 m/s. The electromyography (EMG) electrodes can detect it and give an idea of the excitation of the muscle.

This is the concept of working of the EMG, but we have to consider that the motor units in the muscle are many, of different type and at different depth, so the signal that is read by the EMG electrodes is an overlap of different signals. We have moreover to consider that the electrodes are located on the skin surface and not on the membrane surface; between the membrane surface and the electrodes there are other tissues that alter the signal that can be read by the EMG electrodes.

All these things are influencing the reliability of the EMG results and we have to take care of this when we are analyzing the results of an EMG system. That's why in the biomechanical analysis most researchers trust just on the shape of the EMG signals, and not on the amplitude of them.

2.3 Ligaments

The ligaments are filaments mainly made of collagen and water that connect bones to other bones to form a joint. They don't have to be confused with the tendons that are made more or less in the same way but they connect muscles and bones.

The structure of the ligaments is composed, as we can see in Figure 2.16, at the lower level, of micro-fibrils of tropo-collagen that, aggregate together, form sub-fibrils. At a higher lever there are the fibrils that, aggregate together, form fascicles.

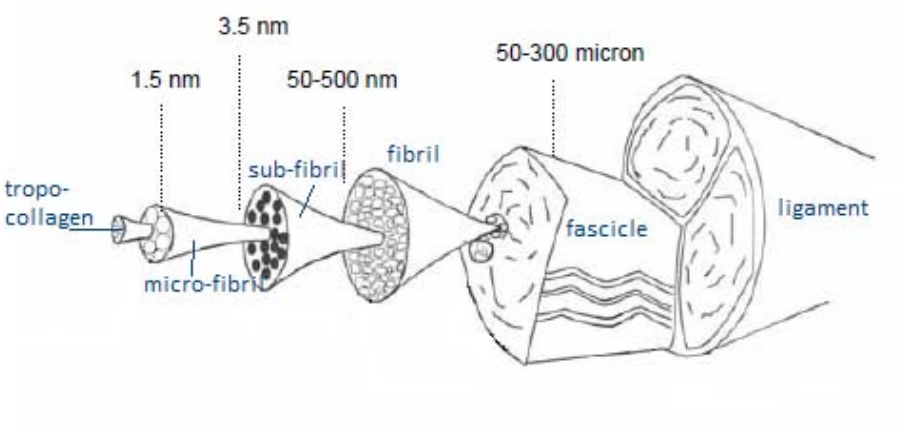

Figure 2.16: Structure of a ligament.

Ligaments are viscoelastic; they gradually elongate when under tension, and return to their original shape when the tension is removed. However, they cannot retain their original shape when the elongation passes a certain point or if it's maintained for a prolonged period of time. This is one reason why dislocated joints must be set as quickly as possible: if the ligaments lengthen too much, then the joint will be weakened, becoming prone to future dislocations. Athletes use to perform stretching exercises to lengthen their ligaments, making their joints more flexible.

In the case of the knee the articular surfaces are covered with cartilage and are connected by ligaments that maintain the contiguity between the different bones. The most important ligaments of the knee can be seen in Figure 2.17 and are:

- The Medial Collateral Ligament (MCL) that connects the medial femoral epicondyle to the upper part of the medial face of the tibia;
- The lateral Collateral Ligament (LCL) that connects the lateral femoral epicondyle to the head of the fibula;
- The two Cruciate Ligaments, called in this way because of their crossing with an "X" shape in the middle of the articulation of the knee, connect the intercondylar part of the femur to the tubercles of the tibial. Cruciate ligaments prevent the front-back movements of the tibia respect to the femur (anterior-posterior dislocation). They are urged in every position but in particular in the complete flexion and the complete extension of the knee. They can be distinguished into:
  - Anterior Cruciate Ligament (ACL), that originates from the internal face of the lat-

eral condyle of the femur and inserts in the anterior intercondylar area of the tibia; the main function of this ligament is to prevent the anterior dislocation of the tibia respect to the femur and it's the most commonly injured during sports like football, ski, rugby, volleyball, basketball, etc.

– Posterior Cruciate Ligament (PCL), that originates from the internal face of the medial condyle of the femur and inserts in the posterior intercondylar area of the tibia; the main function of this ligament is to prevent the posterior dislocation of the tibia respect to the femur and it's the most commonly injured during car accidents.

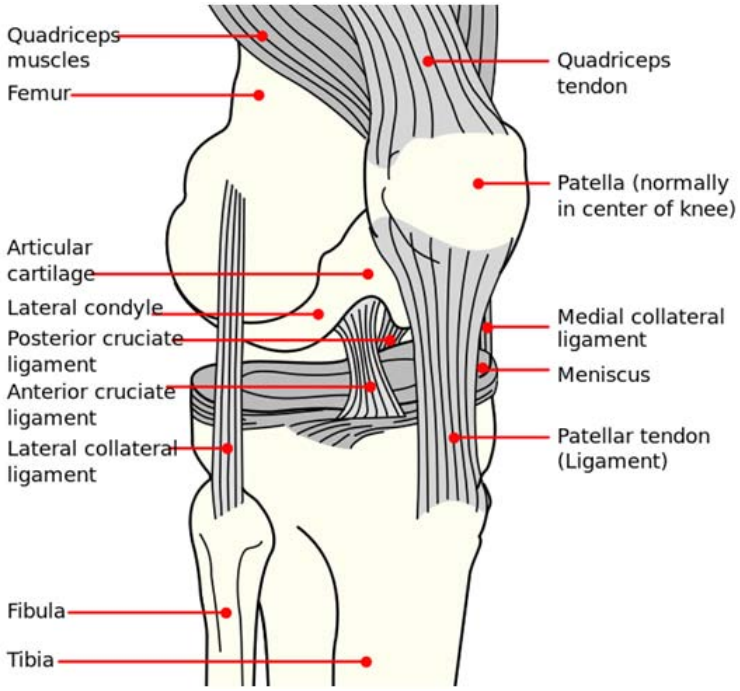

Figure 2.17: View of the knee with in evidence the main ligaments, source [2].

Since in this chapter we explained the anatomy of the lower limb, we are ready to understand the main hypotheses of occurrence of ACL non contact injuries that will be presented in the following chapter.

Chapter 3

State of the art

3.1 Mechanism of ACL non contact injuries

The knee is a very complex system and its mechanical behavior is affected by many different factors. The mechanisms of ACL non contact injury are very controversial and they are still under complete evaluation and study; there are a lot of hypothesis that try to explain how the injuries occur.

De Morat et al. [5], based on a study on cadavers, demonstrated that aggressive quadriceps loading ($\sim$4500 N) could take the ACL to failure and proposed that aggressive quadriceps loading was the responsible factor of ACL non contact injuries. A graphical representation of this hypothesis can be seen in Figure 3.1.

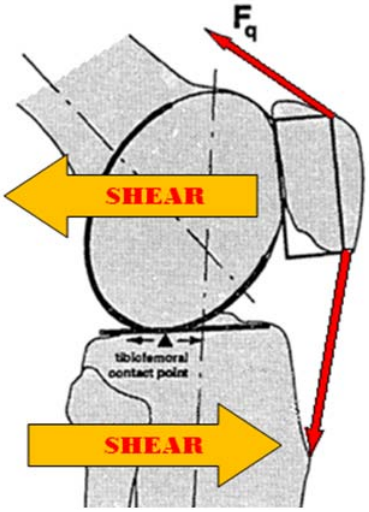

Figure 3.1: Hypothesis of ACL injury mechanism by De Morat et al.: an aggressive quadriceps loading generates a shear on the knee that urges the ligament causing its rupture.

In contrast, McLean et al. [19] using a mathematical simulation model, argued that pure sagittal plane loading could not produce such injuries.

Another study among female athletes showing that high valgus load increased injury risk, led Hewett et al. [22] to suggest valgus loading as an important component for ACL injuries. A schematic representation of the valgus loading can be seen in Figure 3.2.

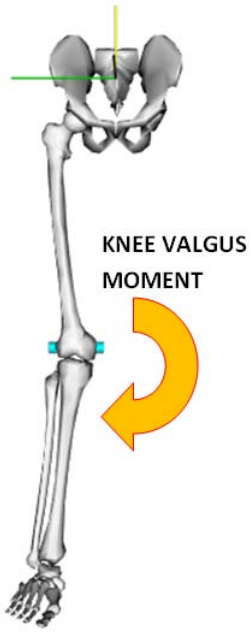

Figure 3.2: Schematic representation of a knee valgus loading, suggested by Hewett et al. as an important component for ACL injuries.

Some video analyses also showed that valgus collapse seemed to be the main mechanism among female athletes. However, studies on cadavers and mathematical simulation have shown that pure valgus loading would not produce ACL injuries without tearing the medial collateral ligament first.

However, other simulation studies suggested that valgus loading would substantially increase ACL force in situations where anterior tibial shear force is applied, for instance through quadriceps contraction. Furthermore, it has been shown that valgus loading induces a coupled motion of valgus and internal tibial rotation [10].

Speer et al. [13], analyzing the Magnetic Resonance Imaging (MRI) of some patients with acute non contact ACL injuries, reported bone bruises of the lateral femoral condyle or of the posterolateral portion of the tibial plateau in more than 80% of them (see Figure 3.3). They concluded that valgus in combination with internal rotation and/or anterior tibial translation

Figure 3.3: Points where Speer et al. noted the presence of bruises, sign of a high loading in those points.

occurred at the time of ACL injuries, consistent with the current observations.

After this first overview of controversial possible explanations of the mechanism of ACL non contact injury, we can say that maybe the best way to understand it is to investigate it during the occurrence of a real ACL injury, without limiting the study to the loads acting just in one particular plane.

Right now, the only non invasive method available to extract data from real injury's situations is a video analysis. Koga et al. [9] analyzed the video sequences of ten ACL injuries from women handball and basketball players and one ACL injury from a male football player, using the model-based image-matching method (MBIM) that allowed the researchers to calculate the complete kinematics of the knee (angles of flexion-extension, abduction-adduction and internal-external rotation) combining the views of different cameras; they could estimate also the ground reaction forces estimating the accelerations of the center of mass and solving the dynamic's equations.

From these studies they formulated the hypothesis of mechanism of ACL non contact injury shown in Figure 3.4.

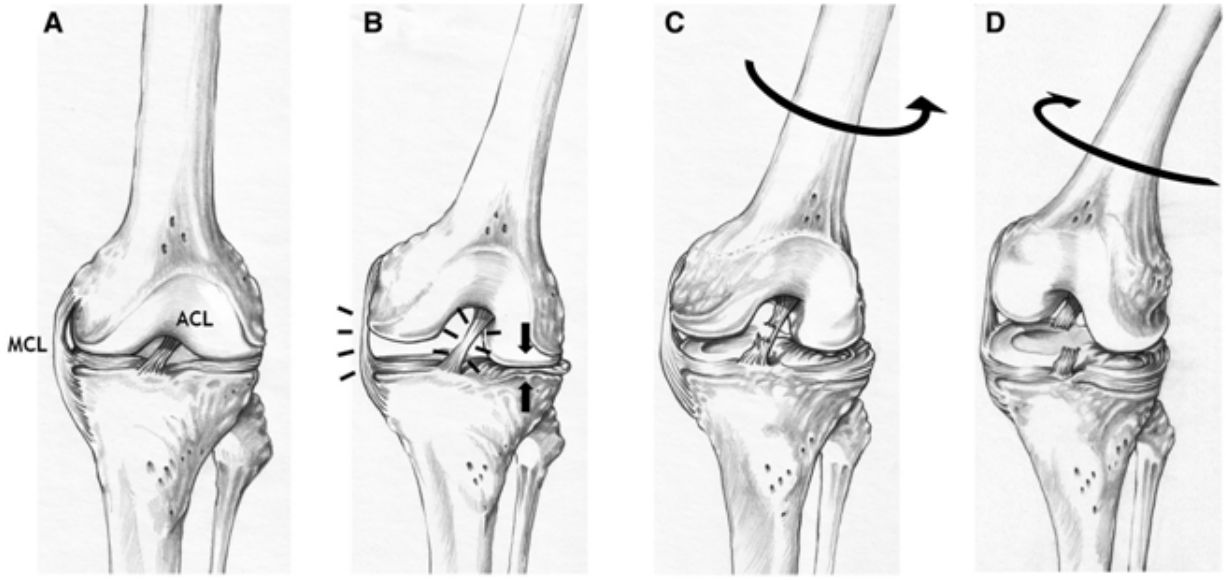

Figure 3.4: Hypothesis of non contact ACL injury mechanism by Koga et al., source [9].

A) Situation of rest of the knee.

B) When valgus loading is applied, the medial collateral ligament becomes taut and lateral compression occurs.

C) This compressive load, together with the force caused by quadriceps contraction pushing back the femur, causes a displacement of the femur with respect to the tibia and, because of the particular shape of the contact surfaces, the lateral femoral condyle shifts posteriorly and the tibia translates anteriorly and rotates internally, resulting in ACL rupture (in more than the 80% of ACL injuries, the MRI highlights bone bruises of the lateral femoral condyle or posterolateral portion of the tibial plateau).

D) After the ACL is torn, the primary restraint to anterior translation of the tibia is gone. This causes the medial femoral condyle to also be displaced posteriorly, resulting in external rotation of the tibia.

Moreover these studies highlighted that the injury occurs in the first 40 *ms* after the initial contact of the foot with the ground so the movements highlighted in these studies can be seen just with high speed cameras (acquiring at a frequency up to 50 *Hz*).

In the following chapter we will present the experimental methodology we followed for the execution of the tests.

Chapter 4

Experimental methodology

4.1 Instrumentation

4.1.1 Motion capture system

In order to acquire the movement of the athletes performing the maneuver object of the study, we needed to use a motion capture system; in our case the system used was a Peak Motus, Version 9.2.0 (Peak Performance Technologies, Inc. USA) with 4 digital cameras Basler A602fc (Basler AG Ahrensburg Germany) acquiring at 150 *Hz* with the characteristics shown in Table 4.1. An image of the cameras used can be seen in Figure 4.1.

There is the possibility to acquire at a higher frequency, reducing the resolution of the sensor; the sampling frequencies permitted by Vicon Motus are 50, 60, 75, 80, 120, 125, 150, 200, 240, 250 and 300 *Hz*. In our case we used a sampling rate of 150 *Hz* with a resolution horizontal/vertical of 536 x 400 *pixels*.

The athlete is wearing some passive reflecting markers in particular landmarks of the body described in the marker protocol chosen for the test, the digital cameras acquire the execution of the movement and the trajectories of the markers can be reconstructed during the processing with the software Vicon Motus 9 (Vicon UK), an example of the process of recognition of the markers is shown in Figure 4.2.

Figure 4.1: Basler A602fc camera.

Basler A602fc specifications:	
Resolution horizontal/vertical (*pixels*)	656 x 490
Pixel Size horizontal/vertical	9.9 μm x 9.9 μm
Frame Rate	100 *fps*
Synchronization	External trigger Via the 1394 bus Free-run
Exposure Control	programmable via the 1394 bus
Housing Temperature	0 $^\circ C$ - 50 $^\circ C$
Power Consumption (typical)	1.7 W
Weight (typical)	100 g
Sensor Technology	Progressive Scan CMOS, global shutter
Sensor Size (optical)	1/2 *inch*
Sensor Type	CMOS
Sensor Size [mm]	6.49 x 4.86

Table 4.1: Characteristics of Basler A602fc cameras.

Working with the contrast and the brightness, it is possible to distinguish the reflections of the passive markers, because they are covered with a reflective material made of aluminum powder. Starting from a manual detection of all the markers done by the user, the software is able to follow the markers during the movement (if they can be seen in every frame) and recognize their positions in the view of each camera.

Then, using a Direct Linear Transformation (DLT) the software is able to combine the views of the different cameras in order to reconstruct the three-dimensional position of each marker

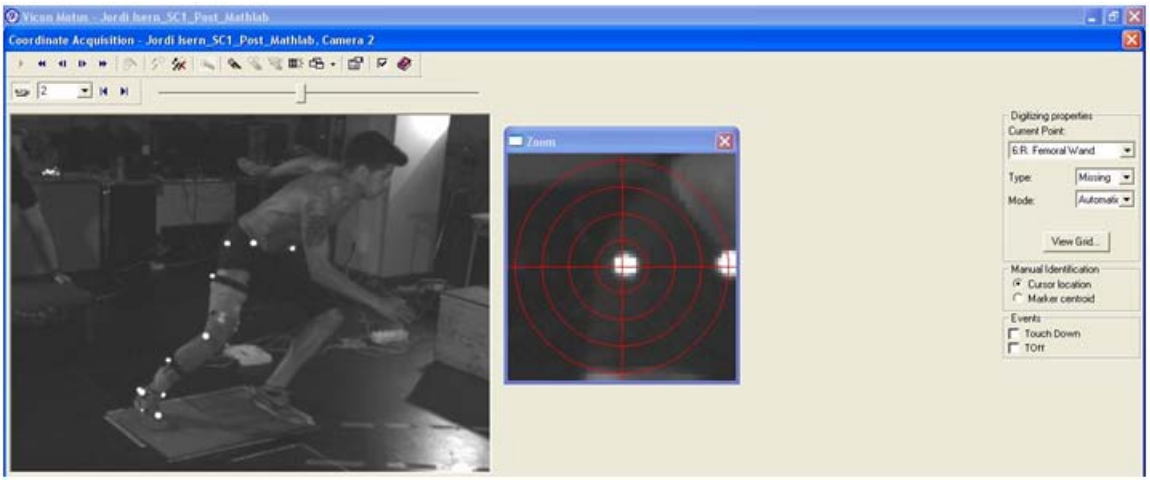

Figure 4.2: Example of the process of recognition of the markers in the Vicon Motus 9 environment.

frame by frame. We have to take care because the DLT method will not work if two cameras have their optical axes at exactly 180°. We know that, in order to be able to do all the reconstruction of the trajectories of the markers, each marker has to be seen at least by two cameras in every instant, according to the triangulation principle, and the higher is the number of cameras that can see simultaneously a marker, the higher is the accuracy in the determination of its position.

Recording all the positions of the markers during the movement, the software can reconstruct the trajectories of each marker and then, deriving once and twice with respect to time, also the velocities and the accelerations. The results coming from the Motion Capture system are not correct in absolute, but they are very dependent on the position of the cameras, the quality of the calibration of the system, the errors and artifacts.

Position of the cameras:

As we said before if we want the Direct Linear Transformation (DLT) working, we have to be sure that the angles between all the optical axes of the cameras has to be always different from 180°.

Then, as we said, in order to reconstruct correctly the trajectories of the markers, every marker has to be seen in every frame by at least two cameras; this depends a lot on the position and on the number of the cameras and, of course, on the nature of the movement. In general, the higher is the number of cameras, the higher is the accuracy in the determination of the markers position.

The position of the cameras depends a lot on the kind of movement and on the set of markers that has been used and in general we have to take into account that during the execution of the

movement we should have a complete view of all the markers. In our case we used four cameras fixed on easels at a height of more or less 1,70 m and disposed in a plane view as shown in Figure 4.3.

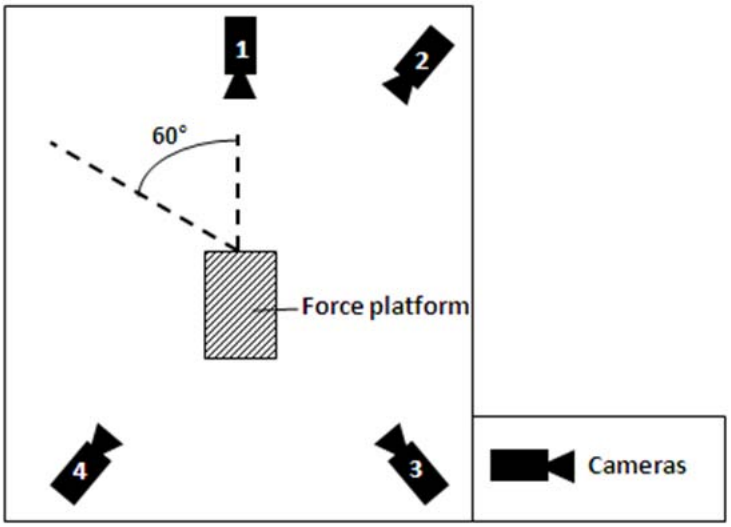

Figure 4.3: Plan view of the disposition of the four cameras and the force platform. It's possible to see also the longitudinal direction and the direction of the movement inclined at 60° with respect to the longitudinal direction.

Calibration:

The calibration is the process that allows the system to fix a reference system and to generate the relations that allow calculating the distances in a defined volume called volume of calibration.

First of all we put three reflecting markers on the floor defining the directions of the two horizontal axes (perpendicular to each other) of the laboratory reference system (X and Y in our case) as we can see in Figure 4.4.

Then we can assemble and place the control object called "32-point Frame" that is represented in Figure 4.5. This is composed by an easel with a central body where there are eight rods attached: these sticks have four markers each placed at a known distance from each other. It's possible to extend the sticks adding more parts in order to increase the volume of control.

After making an acquisition of the control object and the three markers placed on the floor, the user has to detect each marker and mark it with its name, in order to make the system recognize it.

The horizontal axes of the laboratory reference system are detected using the three markers placed on the floor and the vertical axis can be defined as the cross product of the two horizontal

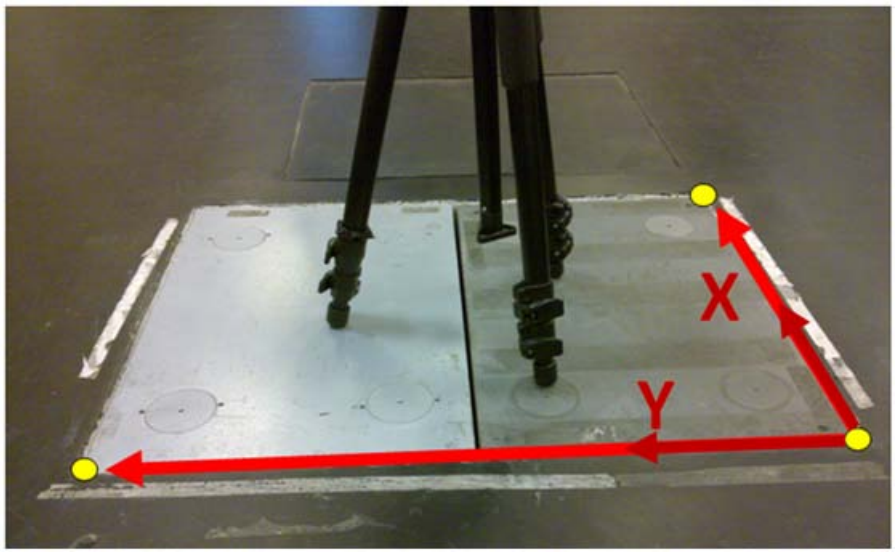

Figure 4.4: Identification of the two horizontal axes X and Y of the laboratory reference system during the process of calibration.

unitary vectors. The system knows how the control object is defined, because the coordinates of each marker are known as we can see in Table 4.2, so it is possible to calculate the coordinates of all the points inside the volume of control.

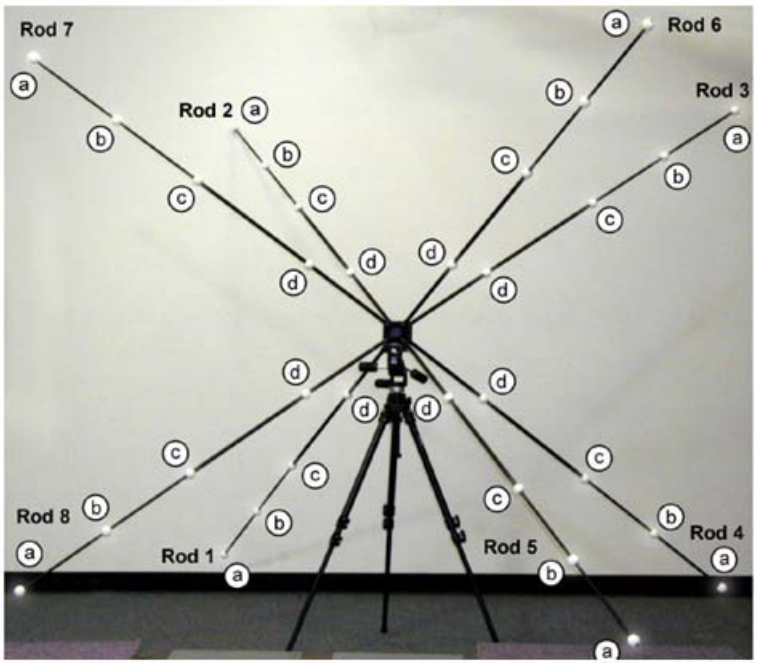

Figure 4.5: The "32-point Frame" object used for the calibration.

Calibration Frame standard orientation (meters)									
	full frame			inner 17 points			inner 9 points		
	X	Y	Z	X	Y	Z	X	Y	Z
A	0.0000	0.0000	0.0000						
B	0.4789	0.4259	0.3420	0.0000	0.0000	0.0000			
C	0.8231	0.7280	0.5879	0.3442	0.3021	0.2459	0.0000	0.0000	0.0000
D	-0.0190	1.9143	-0.0113						
E	0.4712	1.5079	0.3375	-0.0077	1.0820	-0.0045			
F	0.8211	1.2146	0.5867	0.3422	0.7887	0.2447	-0.0021	0.4866	-0.0012
G	2.2298	1.9150	-0.0111						
H	1.7396	1.5085	0.3376	1.2607	1.0826	-0.0044			
I	1.3903	1.2149	0.5869	0.9113	0.7890	0.2449	0.5671	0.4869	-0.0010
J	2.2116	0.0000	0.0000						
K	1.7323	0.4257	0.3423	1.2534	-0.0002	0.0003			
L	1.3880	0.7279	0.5880	0.9091	0.3020	0.2460	0.5648	-0.0001	0.0001
M	2.2141	-0.0005	1.5743						
N	1.7335	0.4254	1.2349	1.2546	-0.0005	0.8929			
O	1.3888	0.7279	0.9905	0.9099	0.3020	0.6485	0.5657	-0.0001	0.4026
P	2.2282	1.9169	1.5913						
Q	1.7392	1.5093	1.2418	1.2602	1.0834	0.8998			
R	1.3901	1.2153	0.9926	0.9112	0.7894	0.6505	0.5669	0.4873	0.4047
S	-0.0191	1.9119	1.5935						
T	0.4709	1.5077	1.2418	-0.0080	1.0818	0.8997			
U	0.8208	1.2146	0.9928	0.3418	0.7887	0.6508	-0.0024	0.4866	0.4049
V	-0.0023	0.0000	1.5763						
W	0.4780	0.4254	1.2359	-0.0009	-0.0005	0.8939			
X	0.8229	0.7278	0.9908	0.3439	0.3019	0.6487	-0.0003	-0.0002	0.4029
Y	1.1056	1.1239	0.7900	0.6267	0.6980	0.4480	0.2825	0.3959	0.2021

Table 4.2: Definition of the coordinates of each markers of the calibration object.

Artifacts and errors:

The markers are objects attached to particular landmarks of the body in order to be representative of a certain point of the body considered; since the models used for our analysis are rigid bodies, we consider the markers as representative of a particular point located on a bone. The only non-invasive way we have to place a marker and make it representative of the landmark, is attaching it on the skin surface with an adhesive.

We have to consider that during the movement the soft tissues between the marker and the point of the bone we want to represent is moving too: we are mainly talking about the skin, the layers of fat and the muscles. These are real movements but they are considered as errors, because they affect the real position of the point we want to represent that is part of the bone.

This kind of errors cannot be avoided if we attach the markers to the skin surface, but if we want to reduce the amplitude of these artifacts, we have to choose in a good way the anatomical landmarks, in order to have the minimum soft tissue artifacts between the skin and the bone and filter the coordinates of the markers in order to remove the unwanted frequencies from the signal.

During the acquisition there could be other kind of errors depending on different factors; there could be errors due to a wrong calibration, errors due to particular problems in the cameras or

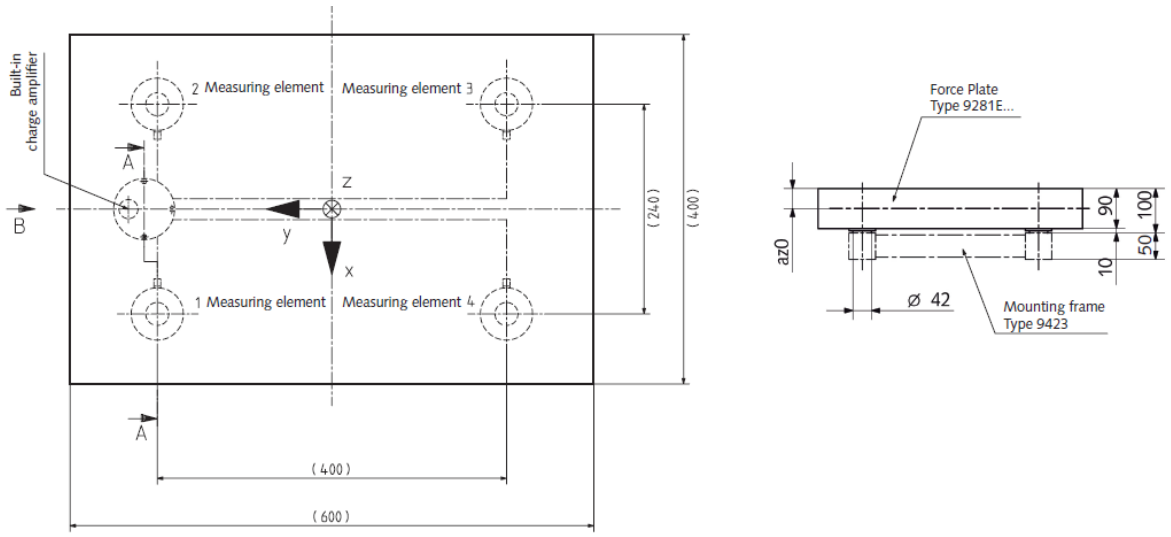

Figure 4.6: Geometrical characteristics of the force platform Kistler 9281B.

due to electronic noise in the environment. Considering if the error is systematic or random, we can identify it and proceed to the resolution or reduction of the problem.

4.1.2 Force platform

Force platforms are instruments that measure the ground reaction forces, the moments and the position of the center of pressure. This tool is essential in our study in order to have accurate results about the dynamics of the movement and not just estimations of it.

The force platform used in our study is a Kistler 9281B (Kistler instruments LTD, Winterthur, Switzerland) acquiring at 900 *Hz* and its geometrical characteristics are shown in Figure 4.6. The maximum frequency of acquisition is 1000 *Hz*, but we decided to acquire at 900 *Hz* in order to have a frequency multiple integer of the frequency of acquisition of the Motion Capture system (150 *Hz*).

Physically it is a 600x400x100 *mm* aluminum sandwich top plate equipped with four built-in piezoelectric 3-component force sensors, so in total the force platform gives 12 force components. Then the system transforms those into 8 channels (fx12, fx34, fy14, fy23, fz1, fz2, fz3, fz4) described in Table 4.3 and it calculates the forces, the moments and the coordinates of the center of pressure in the same Table.

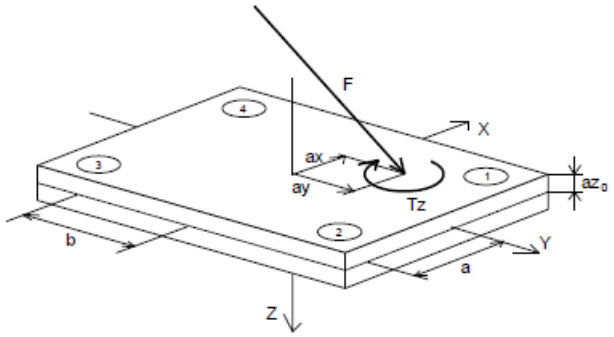

Force plate output signals

Output signal	Channel	Description
fx12	1	Force in X-direction measured by sensor 1 + sensor 2
fx34	2	Force in X-direction measured by sensor 3 + sensor 4
fy14	3	Force in Y-direction measured by sensor 1 + sensor 4
fy23	4	Force in Y-direction measured by sensor 2 + sensor 3
fz1 ... fz4	5 ... 8	Force in Z direction measured by sensor 1 ... 4

Calculated parameters

Parameter	Calculation	Description
Fx	= fx12 + fx34	Medio-lateral force 1)
Fy	= fy14 + fy23	Anterior-posterior force 1)
Fz	= fz1 + fz2 + fz3 + fz4	Vertical force
Mx	= b * (fz1 + fz2 - fz3 - fz4)	Plate moment about X-axis 3)
My	= a * (-fz1 + fz2 + fz3 - fz4)	Plate moment about Y-axis 3)
Mz	= b * (-fx12 + fx34) + a * (fy14 - fy23)	Plate moment about Z-axis 3)
Mx'	= Mx + Fy*az0	Plate moment about top plate surface 2)
My'	= My - Fx*az0	Plate moment about top plate surface 2)
ax	= -My' / Fz	X-Coordinate of force application point (COP) 2)
ay	= Mx' / Fz	Y-Coordinate of force application point (COP) 2)
Tz	= Mz - Fy * ax + Fx * ay	Free moment, Vertical torque, „Frictional" torque
COFx	= Fx/Fz	Coefficient of Friction x-component
COFy	= Fy/Fz	Coefficient of Friction y-component
COFxy	= sqrt (COFx^2 + COFy^2)	Coefficient of Friction absolute

Table 4.3: Definition of the channels of the force platform and calculation of the main variables.

4.1.3 Electromyography

Electromyography (EMG) is a technique for evaluating and recording the electrical activity produced by skeletal muscles [6]. An electromyograph detects the electrical potential (mV) generated by muscles when they are activated.

There are two kinds of electromyography systems: the surface EMG that requires to attach the electrodes on the skin, it is quite non-invasive but the accuracy of the results that can give

Figure 4.7: Mega WBA EMG system: above the receiver and below the sensors attached on the charging/synchronizing module.

is low, and the needle EMG that requires the electrodes to be put under the skin and it is more accurate but of course also more invasive.

In our study the electromyography data have not been used for any kind of evaluation, but they have been collected too for any future kind of evaluation. For this purpose we used the 8 channels surface electromyography system Mega WBA (Mega Electronics LTD, Kupio, Finland) shown in Figure 4.7. The system is composed by the sensors and the receiver.

Sensors:

Each sensor corresponds to one channel and is the set of one wireless transmitter and three cables with connectors where disposable surface electrodes can be attached on; we can see a representation of one sensor in Figure 4.8.

Each channel can work independently from the others and does not need any wire of connection, neither for the supply, neither for the transmission of the data. This system does not have a common ground for all the channels, but each channel has its own ground, this solution requires one electrode more for each channel, but it allows a better modularity and compactness of the system.

The wireless transmitter is needed to collect the signals from the electrodes and to send them to the receiver; it contains the electronic circuit that is able to send the data wirelessly and a battery, needed to make working the sensor without any supply wire; the battery can be

Figure 4.8: One of the sensor of the Mega WBA EMG system: the three electrodes and the wireless transmitter.

recharged connecting the sensors to the charging module. The characteristics of the sensors are shown in Table 4.4.

Mega WBA EMG sensors specifications:	
Sampling rate	1000 *Hz*
CMRR	Typ. 104 *dB*
Channels	Up to 16
Sensor freq band	20-500 *Hz* (EMG model)
Data transfer	Bluetooth 2.0 EDR
Power	Internal rechargeable batteries
Weight	16 *g* / module
Size	35 x 35 x 15 *mm*
Electrodes	Lead wires with snap connectors for disposable electrodes

Table 4.4: Characteristics of the sensors of the WBA Mega EMG system.

Receiver:

The receiver is an instrument that is able to collect all the wireless data coming from the sensors and to transmit them through an analog cable to the computer. The characteristics of the receiver are shown in Table 4.5.

It has to be considered that, since the data are passing from the sensors to the receiver through a wireless connection, there is a delay of the data that arrive to the computer and the real instant when they are collected. This delay has been quantified in 60 *ms* and it is corrected manually by the user in the Vicon software.

Mega WBA EMG receiver specifications:	
D/A conversion	16 *bits*
Analog output	Yes, Isolated
Power supply	100-240 *V*, Medical Approved (UL60601) power supply
Interfaces	Analog, Bluetooth

Table 4.5: Characteristics of the receiver of the WBA Mega EMG system.

4.1.4 Mechanical vibrations machine

To see which are the effects of mechanical vibrations on the execution of a sidestep cutting movement, we needed a mechanical vibration machine and we used a ViBalance (Biomedic System, Barcelona, Spain) that is shown in Figure 4.9.

This machine can produce three-dimensional mechanical vibrations in a frequency from 20 to 50 *Hz* and an amplitude from 1 to 2 *mm*. The characteristics of the ViBalance can be seen in Table 4.6.

Figure 4.9: Mechanical vibrations machine ViBalance.

ViBalance specifications:	
Motors (2)	0.18 KW, 3000 rpm
Frequency	20-50 Hz (adjustable Hz to Hz)
Pre-set Frequency	20,25,30,35,40,45,50 Hz
Amplitude	HIGH (2 mm), LOW (1 mm) peak-to-peak
Maximal acceleration	7G
Weight	49 Kg
Dimensions	990 x 740 x 315 mm
Vibratory surface	Diameter 698 mm
Maximum load	200 Kg
Maximum inclination	$23° \pm 2°$

Table 4.6: Characteristics of the mechanical vibrations machine ViBalance.

4.2 Execution of the test

The subjects that took part in these tests were footballers that had never had any injury at the knee or at the ankle in the last months. Moreover any of them had never had any lesion in the anterior cruciate ligament (ACL) before the tests. Before the execution of the test each subject had to sign an informed consent and the ethics committee of the Catalan sport's council licensed the protocol of execution of the test.

4.2.1 Preparation of the tester

The preparation of the testers is essential in order to have good data concerning the kinematics and the electromyography and has to be done in the most precise way possible.

First of all the anthropometric data of the subjects were collected, in particular the length of the limbs and the mass. In this preliminary part of the subjects' preparation, the places of positioning of the electrodes were also signed.

Application of the EMG electrodes:

The application of the EMG electrodes it is an operation that in our case took more or less 20 minutes of time. The procedure of application of the electrodes is standard and it has been collected and unified in the SENIAM project (Surface Electromyography for the Non-Invasive Assessment of Muscles); the main guidelines used for the project have been taken from the SENIAM website [18].

Before applying the electrodes, the skin has been prepared as shown in Figure 4.10: shaving and cleaning with cotton and alcohol in order to reduce the impedance due to the hair, the sebum and the sweat on the surface of the skin.

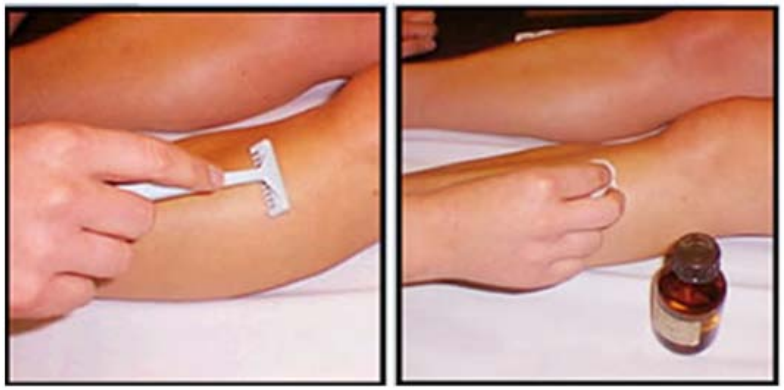

Figure 4.10: Preparation of the skin for the application of the electrodes: shaving and cleaning with cotton and alcohol.

As we saw previously, for each muscle we want to collect the data, we need one EMG sensor that has three electrodes each: two of them are collecting the potential passing along the skin that will be treated passing through a differential or a double differential amplifier, the other one is the ground electrode that gives the value of reference to the system. We can see a schematic example of the treatment of the signals coming from the three electrodes in Figure 4.11.

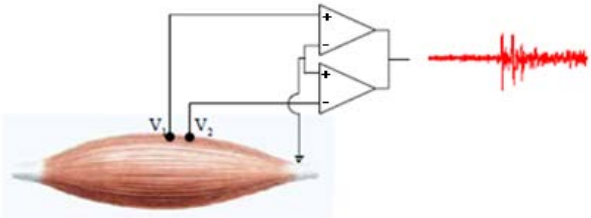

Figure 4.11: Representation of the treatment of the data coming from the EMG electrodes with a double differential amplifier.

Each electrode is attached to the shaved, cleaned and dried skin with its adhesive part then the three electrodes and the transmitter are fixed to the limb with a porous gauze that allows a better transmission of the data from the transmitter to the receiver.

The muscles we are interested in studying are the vastus lateralis, rectus anterior of quadriceps, biceps femoris, semitendinosus and soleus and the precise point of application of the

electrodes is described below and can be seen in Figure 4.12:

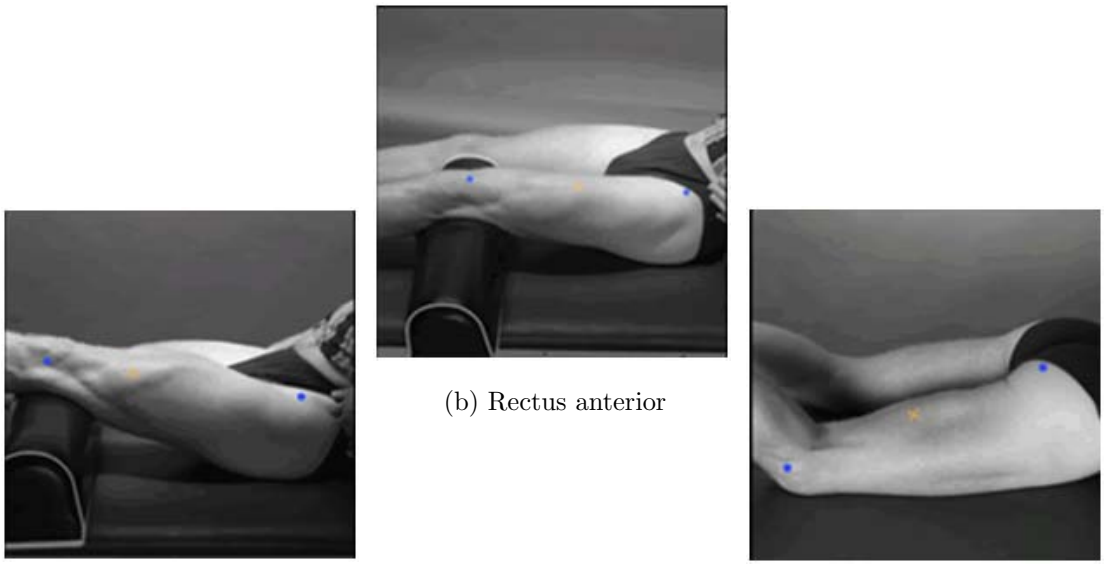

(a) Vastus lateralis

(b) Rectus anterior

(c) Biceps femoris

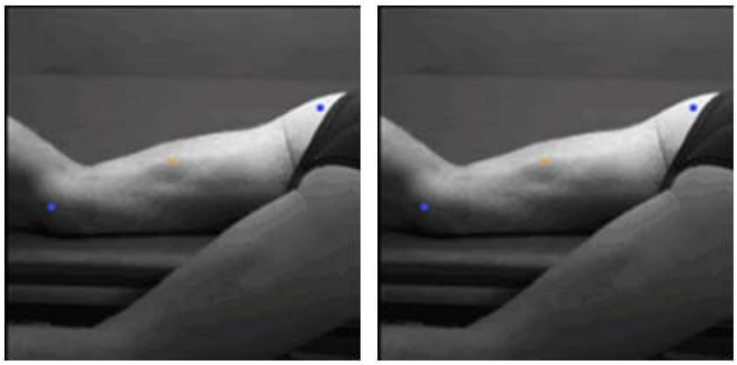

(d) Semitendinosus

(e) Soleus

Figure 4.12: Position of the electrodes of the muscles considered.

- Vastus lateralis: electrodes attached at 2/3 of the line connecting the iliac spine and the lateral corner of the patella.

- Rectus anterior of quadriceps: electrodes attached at the half of the line connecting the anterior part of the iliac spine and the superior part of the patella.

- Biceps femoris: electrodes attached at the half of the line connecting the ischial tuberosity and the lateral epicondyle of the tibia.

- Semitendinosus: electrodes attached at the half of the line connecting the ischial tuberosity and the medial epicondyle of the tibia.

- Soleus: electrodes attached at the half of the line connecting the medial condyle of the femur and the medial malleolus.

All the positions of the ground electrodes are described in the guide of the Megawin software.

Marker placement:

The application of the markers it is an operation that in our case took more or less 15 minutes of time. The markers are plastic balls covered with a reflecting material made of aluminum powder and they are used to represent a particular point of the body; in our case we used two different kind of markers as we can see in Figure 4.13: the normal markers have a diameter of 15 *mm* and are attached on the skin with a piece of double-sided tape; the wand markers have a diameter of 10 *mm* and are connected with a stick attached on the limb with a Velcro strap.

Figure 4.13: On the left normal reflecting marker, on the right a particular of a wand with the Velcro strap.

Since we wanted to make a three-dimensional analysis, each body of the model needed at least three markers attached in order to describe its complete orientation and position in the space.

The set of markers chosen for the tests is a Helen Hayes marker set for one leg with the addition of three more markers: one on the greater trochanter, one on the medial femoral epicondyle and one on the medial malleolus for a total of 12 markers. We can see the protocol of markers used for the tests in Figure 4.14.

The description of the precise position of each marker of the Helen Hayes marker protocol is shown in Table 4.7.

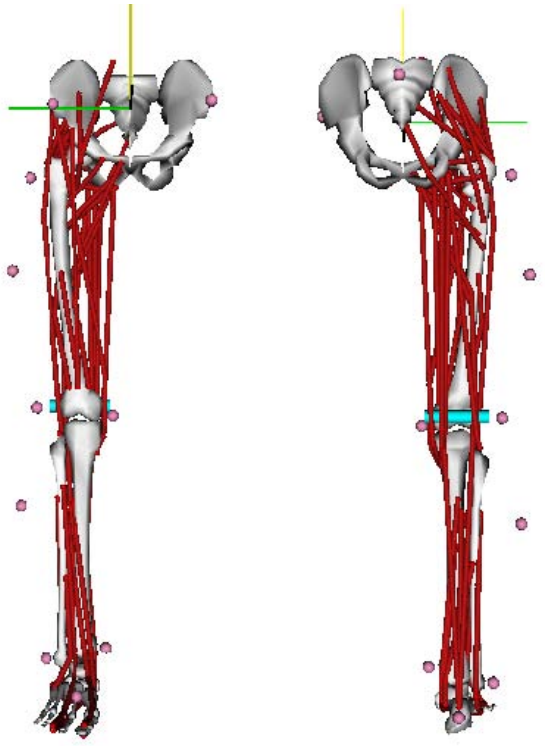

Figure 4.14: Set of markers used for the captures.

Helen Heyes marker protocol:	
L. ASIS	Placed directly over the left anterior superior iliac spine.
R. ASIS	Placed directly over the right anterior superior iliac spine.
Sacrum	Placed on the skin mid-way between the posterior superior iliac spines (PSIS).
R. Femoral Wand	A 4 inch wand placed on the right leg over the lower lateral 1/3 surface of the thigh, just below the swing of the hand.
R. Femoral epicondyle	Placed on the lateral epicondyle of the right knee.
R. Tibial Wand	A 4 inch wand placed over the lower 1/3 of the shank to determine the alignment of the ankle flexion axis.
R. Malleolus	Placed on the lateral malleolus along an imaginary line that passes through the transmalleolar axis.
R. Metatarsal Head II	Placed over the second metatarsal head, on the mid-foot side of the equinus break between fore-foot and mid-foot.
R. Heel	Placed on the calcaneus at the same height above the plantar surface of the foot as the toe marker.

Table 4.7: Description of the positions of the markers of the Helen Heyes protocol.

4.2.2 Protocol of execution of the tests

The tests were executed mainly in order to see what are the differences between the movements performed pre and post vibrations; after the application of the EMG system and the reflecting markers, the subject performed three sidestep cutting movements, with one minute of recovery between each other. After the execution of the three sidestep cutting movements pre-vibrations and five minutes of recovery, the subject made the warming-up with full body mechanical vibrations (VCC) and then performed three more sidestep cutting movements.

A block diagram representing tasks made during the execution of the tests can be seen in Figure 4.15.

All the subjects performed the tests using indoor football shoes during the warming-up and during the sidestep cutting movements.

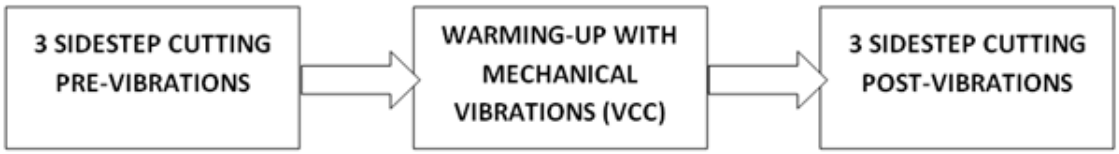

Figure 4.15: Block diagram representing the tasks made during the execution of the tests.

Protocol of the sidestep cutting maneuver:

The execution of the sidestep cutting maneuver in our case took more or less 5 minutes for each session. This kind of movement is particularly problematic for the ACL noncontact injuries, especially according with the mechanism of injury we presented in the previous chapters.

The subject jumped from a step of 30 *cm* and the frontal border of this step was located at a distance equal to 2/3 of the height of the subject from the center of the force platform, landing on the force platform with the dominant leg. This first jump was executed in a longitudinal direction, then the subject made the second part of the jump along a direction inclined at 60° with respect to the longitudinal direction in the side of the non-dominant leg, pushing with the dominant leg. Some frames of the execution of the maneuver and a planar scheme of it can be seen in Figures 4.16 and 4.17.

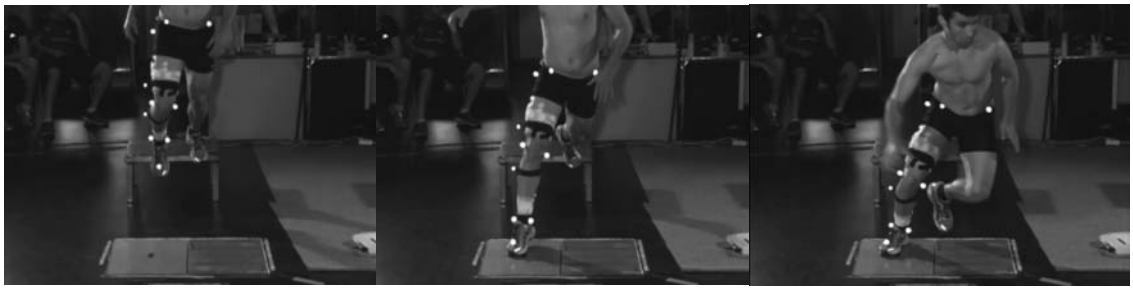

(a) Intitial phase of the movement (b) Landing with the dominant leg (c) Maximum flexion of the knee

(d) End of the contact of the dominant leg (e) Landing with the non-dominant leg

Figure 4.16: The most significant frames of the execution of the sidestep cutting maneuver.

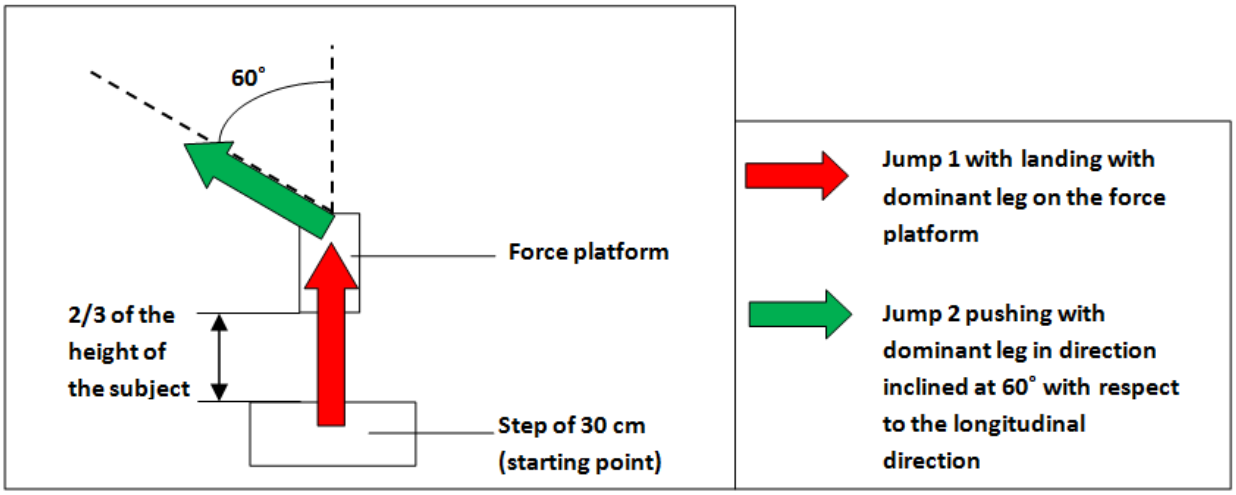

Figure 4.17: Planar scheme (top view) of the execution of a sidestep cutting maneuver.

Protocol of warming-up with mechanical vibrations:

The warming-up with mechanical vibration is an operation that in our case took more or less 15 minutes of time. The warming-up with mechanical vibrations was performed on a vibratory platform with a frequency of vibration of 30 *Hz* and an amplitude of 2 *mm*. These values had been chosen according with a study of Cardinale and Lim 2003 [14] where they explained that with a frequency of 30 *Hz* the EMG activation of the vastus lateralis of the quadriceps is the highest. The same values of frequency and amplitude had been used also in other studies with the application of full body mechanical vibrations.

The warming-up consisted in six series of squats on one leg of 45 seconds each with 60 seconds of recovery between each other; these six series of squats were divided in three series of dynamic squats and three series of static squats as shown in Figure 4.18.

In the three series of dynamic squats the subject performed squats lasting 5 seconds each (three seconds in eccentric action and two seconds in concentric action), with a maximum knee flexion angle of 90°. The time of flexion and extension was controlled using a metronome. In the three series of static squats, the subject maintained the static position of flexion of the knee at 90° (isometric squat).

During the execution of the warming-up the subjects had a rod that helped them to maintain the balance staying on the vibratory platform. In Figure 4.19, we can see how the squats have been performed by two of the analyzed subjects.

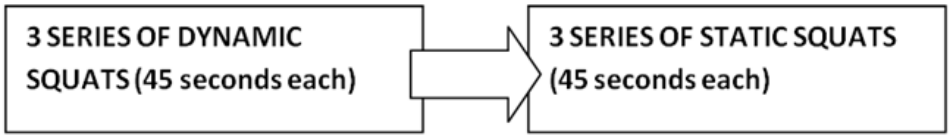

Figure 4.18: Protocol of execution of the six series of squats during the warming-up with mechanical vibrations.

Figure 4.19: Execution of the squats with mechanical vibrations: on the left dynamic squat, on the right static squat.

In the following chapter we will present the numerical part of the work explaining in details the choices made, the problems we find and all the procedure followed during the running of the numerical simulations with OpenSim.

Chapter 5

Numerical methodology

5.1 Presentation of OpenSim

5.1.1 Capabilities of OpenSim

OpenSim [21] is a freely available software package created and certificated by the National Center for Simulation in Rehabilitation Research of the Stanford University that enables users to build, exchange, and analyze computer models of the musculoskeletal system and dynamic simulations of movement.

The core software is written in C++, and the Graphical User Interface (GUI) is written in Java. OpenSim's plugin technology makes possible to develop customized controllers, analyses, contact models, and muscle models among other things. The user can analyze existing models and simulations or develop its own new models and simulations.

According to this idea of the first developers of the Stanford University, there is a community [20] in which it's possible to share for free experiences, models, tutorials, guides, plugins, advices and many other things between the members of the community.

Some of the most useful features of the software include:

- Scaling the size of a musculoskeletal model;
- Performing inverse kinematics analysis to calculate joint angles from marker positions;
- Performing inverse dynamics analysis to calculate joint moments from joint angles and external forces;
- Generating forward dynamics simulations of movement;
- Analyzing dynamic simulations;

- Calculating muscle forces and activations;
- Plotting results of your analysis;
- Taking pictures of musculoskeletal models and making animated movies.

5.1.2 How OpenSim works

To make an analysis with OpenSim first of all we need a model of the musculoskeletal system of the body we want to analyze. There are a lot of models already created in the folder of OpenSim and in the website [20] there are many other models developed by the users ready to be downloaded for free.

The models are made of rigid bodies in the three-dimensional space; each of them has its own reference system and its geometrical and physical properties are described through differential equations. These rigid bodies can't move in the space as they want, but there are some constraint conditions, described through boundary conditions, that definewhich are the movements allowed to each child body with respect to the parent body (conditions on the reference systems). In the model there are also muscles with all their geometrical and physical characteristics described through other differential equations based on the Hill's model.

The data coming from the motion capture system give the instantaneous position of some points attached to each body segment so, since each body is a rigid body in the three-dimensional space, we need at least three conditions for each body to describe completely its position and orientation in the space in every instant. The data coming from the force platform give more boundary conditions to the differential motion equations that have to be solved during the analysis.

5.2 Procedure of the numerical simulation

5.2.1 Preparation of the data

The data coming from the force platform, the motion capture system and the EMG system has been acquired with Vicon Motus software and, after reconstructing the trajectories of each marker, they have been saved in a *.c3d file.

This format of file cannot be read immediately from OpenSim as an input; so it's needed to process the files through Matlab. There are some scripts already created by users that can be

downloaded for free from the OpenSim community [20] and allow the user to create all the data files needed to run the simulations with OpenSim.

In our case, the script for the processing of the force platform data was not compatible with the force platform used. This is because the scripts are made just for a 6 channels force platform, but the force platform used for the project has 8 channels. To solve this problem without spending too much time with Matlab, we decided to save from the Vicon Motus software an *.xls file containing all the data from the force platform already processed, and then converting this file separately in the format needed by OpenSim. The scheme of the data conversion made can be seen in Figure 5.1.

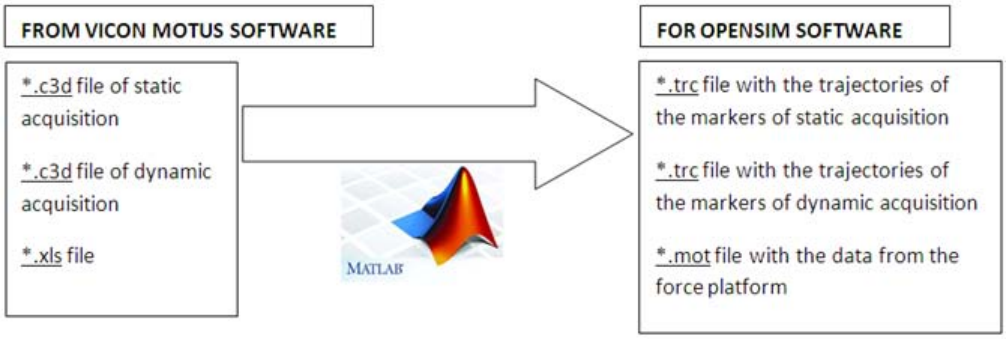

Figure 5.1: Scheme of the conversion of the data to the formats used by OpenSim.

Sometimes it can happen that in the marker trajectories there is a singular point (due to a flickering of the marker) and this could bring to big errors during the execution of the simulations. So, it's better to plot the trajectory of each marker before starting any simulation in order to see if there is any singular point and, in that case, correct manually the value to have a good shape of the curve. To do this, we just replaced the wrong value with the mean of the previous and the following values.

In Figure 5.2 it's possible to see an example of the trajectory of a marker with the problem of singularity and the same curve after replacing the wrong value.

It's not suggested to filter the trajectories of the markers before starting the analysis because this could introduce some problems also in the Inverse Kinematics analysis. Instead of filtering the coordinates of the markers it's possible to filter the results of the Inverse Kinematics analysis in order to remove the high frequency noise.

The data coming from the force platform have been filtered with a Butterworth low pass filter of the third order with a cutting frequency of 15 *Hz*. The frequency of cutting is the same used in another researches about sidestep cutting [4] and it should reduce the noise and

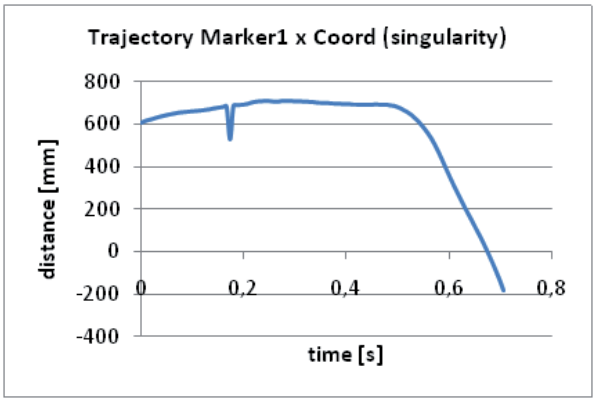

(a) Example of problem of singularity in the trajectory of a marker.

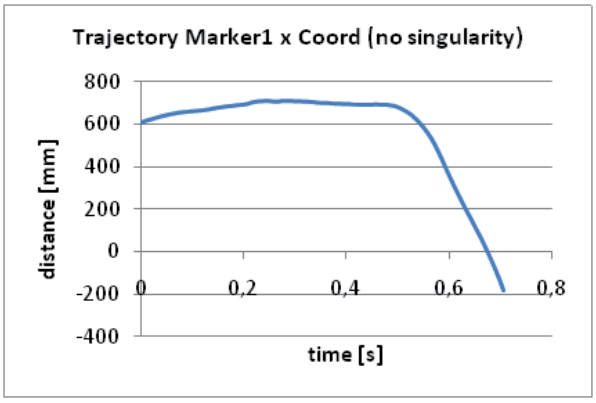

(b) Trajectory of the marker after the manual correction of the signularity.

Figure 5.2: Example of the trajectory of a marker before and after the correction of a singuarity.

the artifacts of impact typical of this kind of movement. It's possible to see an example of the vertical component of the ground reaction force before and after filtering in Figure 5.3. Note the reduction of the peak of the impact, the reduction of the noise and the appearance of negative values.

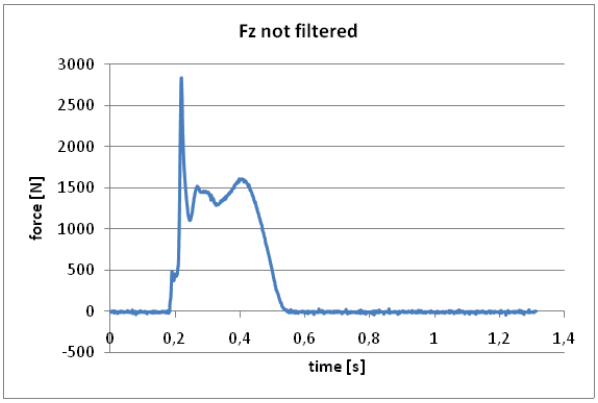

(a) Example of raw vertical force.

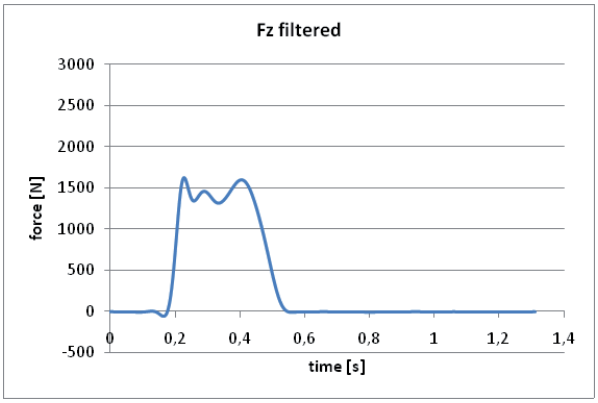

(b) Example of vertical force filtered.

Figure 5.3: Example of vertical component of the ground reaction force before and after filtering.

One important parameter that we wanted to preserve during the analysis was the instant of first contact of the foot with the force platform; this is conventionally considered as the instant when the vertical force is greater than 10 N. For this purpose, we tried to use different orders of filter paying attention to the instant of first contact of the foot with the force platform and we

saw that with the third order filter this parameter was closer to the original one; we can observe it in Figure 5.4.

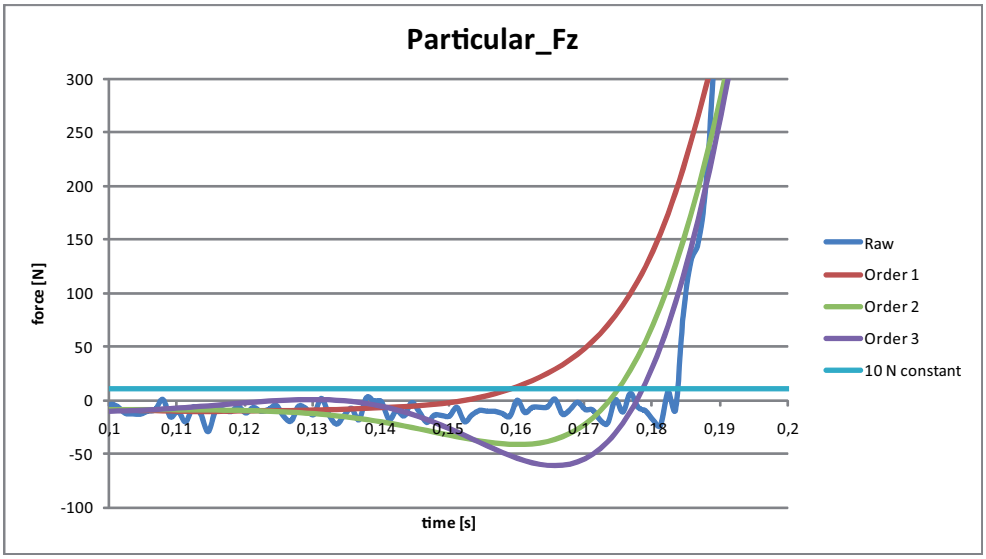

Figure 5.4: Comparison in the zone of first contact, between the raw vertical force and the same data filtered with Butterworth low pass filters with a cut off frequency of 15 *Hz* but with different orders. It can be observed that the instant of first contact with the floor (Fz $\geq$ 10 *N*) in the case of using the third order filter is closer to the one corresponding to the raw data.

This solution brought to a diagram of the vertical force with a negative part before the instant of first contact. Although know that this is not possible in the reality, we accept it because we are not using the forces before the first contact of the foot in our analysis.

5.2.2 Model

The biomechanical model used in the analysis is the "Gait2392_Simbody" (downloadable from [20]) without the torso and the left leg and with 3 degrees of freedom at the knee joint. The model can be seen in Figure 5.5.

The model is described in a code where we can see how the bodies are defined, which are the reference systems, which are the characteristics of the joints, how the muscles are defined and so on. Some small changes to the model can be made using the GUI (Graphical User Interface) but, if more significant changes are needed, then the code that describes the model has to be edited manually using a text editor.

The first change we made to the original code was to delete the bodies not needed (torso and left leg) with all the muscles attached to them. As default settings of the model the knee

Figure 5.5: Biomechanical model used for the analysis coming from the "Gait2392_Simbody" with some changes.

joint had just 1 DOF (flexion), but in our case it was interesting to have some information also about the adduction and the internal rotation, considering which is the mechanism of ACL injury described in the chapter 2. So, in the code we just added the other two degrees of freedom of abduction and internal rotation in order to have the three degrees of freedom at the knee.

A range of motion of 0,8 radians ($+0,4/-0,4$ *radians* each) was given to the motions in order to capture also non-physiologically consistent movements (we can consider as physiologically consistent a maximum abduction angle around 10° and a maximum rotation angle around 15°). Some preliminary simulations were made in parallel with three different models in order to see which of them was realistic enough:

- Model with flexion of the knee (1 DOF);
- Model with flexion and adduction of the knee (2 DOF);
- Model with flexion, adduction and internal rotation of the knee (3 DOF);

The results concerning the internal rotation were not physiologically consistent, but the adduction's ones were good, so at the end it was decided to use the model with two DOF at the knee joint: flexion and adduction.

Even if the angles of the adduction obtained in the preliminary simulations were physiologically consistent, we have to consider that the error that can be made from the motion capture system in determining the angles (around 5° in an acceptable case [12]) is quite big if compared to the range of the adduction movement, so we can think to trust more in the tendency of the adduction instead of in the absolute value of it.

In the preliminary simulations also a muscle analysis was made and it was possible to notice a discontinuity in the lever arm of the lateral and medial gastrocnemius. Since the Static Optimization is quite sensible to discontinuities in the lever arm of the muscles, we decided to create a wrapping surface to be placed under the two gastrocnemius muscles.

A wrapping surface is a surface where some muscles indicated by the user can lean during the movement. These two muscles in the original model were defined in the following way:

- As straight lines between two points in the range of flexion of the knee from 120° to 45°;
- As straight lines passing through three points in the range of flexion of the knee from 45° to −10°.

So when the knee passed through the angle of 45 degrees of flexion the definition of these two muscles changed instantly from a straight line to a broken line, that is why there was the discontinuity on the lever arms.

The wrapping surface created is a portion of cylinder where the muscles can lean when the knee is in the range of flexion from −10° to 45°; the definition of this surface has been introduced in the code where the two muscles are defined. We can see the two muscles before and after adding the wrapping surface in Figure 5.6.

We have moreover to consider that with the set of markers we used, we don't have any information about the movement of the fingers, so the "2^{nd} metatarsal head" marker has been attached to the calcaneus body and the "mtp_angle" has been locked during the simulations.

In the preliminary simulations we also noticed that the Static Optimization couldn't converge to a solution; the problem was due to the fact that in some joints all the muscles acting with their maximum isometric force and their lever arms were not enough to make the total joint moment.

This problem is quite complex and will be presented later in the section dedicated to the Static Optimization. Right now we can say that in order to solve this problem the maximum isometric force of all the muscles was multiplied by 2,5.

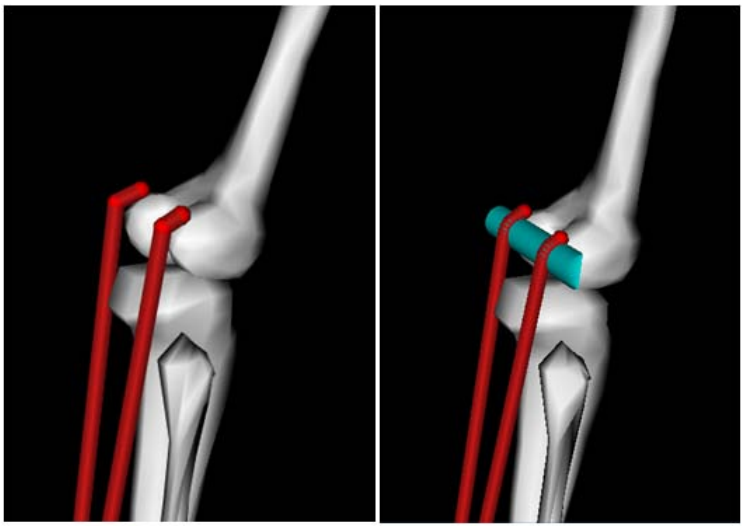

Figure 5.6: The lateral and medial gastrocnemius as defined in the original model on the left and as defined with the wrapping surface on the right.

So, the following list presents the changes made to the original model at the end of the preliminary simulations:

- The torso and the left leg with all the muscles attached to them have been removed;
- Three degrees of freedom have been considered at the knee (flexion, adduction and internal rotation);
- A wrapping surface to solve the discontinuity of lever arm on the lateral and medial gastrocnemius muscles has been adeed;
- The maximum isometric force of all the muscles has been multiplied by a factor 2,5;
- The "knee_rotation" angle and the "mtp_angle" have been locked to the value of zero.

5.2.3 Scaling tool

The scaling is a very important multi step operation in the execution of the simulations. This tool allows the user to:

- Change the dimensions of each body of the virtual model according to the dimension of each body of the real subject;
- Adjust the positions of the most unsure model markers according to the experimental ones from the static acquisition.

To start with the scaling operation, first of all we needed to define a set of markers attached to the model; the positions of these model markers had to be as close as possible to the anatomical landmarks where the experimental markers were attached. Moreover these markers needed to have the same names as the markers in the *.trc file and it had to be specified to which body they belong.

During the scaling operation we needed to set the mass of our model. The anthropometric measurements made before starting the execution of the tests could give us the mass of the full body of each subject, but our model was just composed by the pelvis and one leg.

In order to have an estimation of the model's mass , we used the relations of Zatsiorsky-De Leva illustrated in Figure 5.7 that relate the mass of each segment to the total mass of the subject for males and females.

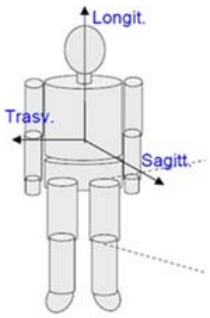

	MASS (%)	
segment	Male	female
Head	6,94	6,68
Trunk	43,46	42,57
Upper Part Trunk	15,96	15,45
Medium Part Trunk	16,33	14,65
Hand	0,61	0,56
Upper arm	2,71	2,55
Forearm	1,62	1,38
Lower Part Trunk	11,17	12,47
Thigh	14,16	14,78
Shank	4,33	4,81
Foot	1,37	1,29

Figure 5.7: Relations of Zatsiorsky-De Leva that relate the mass of each segment of the body with the total mass of the subject. Highlighted in red the segments needed for our model.

It is possible to scale each body with a maximum of three scale factors, putting in relation the distances between pairs of experimental markers from the static acquisition with the same pairs of model markers. The scale factor is just the ratio between these two values and an example of its definition can be seen in Figure 5.8.

The second part of the scaling process was the adjusting of the position of the model markers, according to the position of the experimental ones. This step is essential because the positioning of the experimental markers could be affected by errors. The markers affected by the biggest error were certainly the femoral and tibial wands, because they were not attached to a particular anatomical landmark. So it was difficult to position them in the same place for all the subjects.

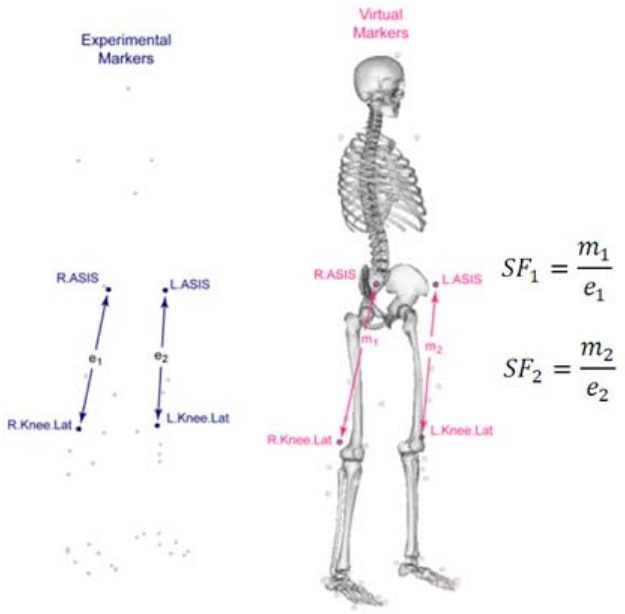

Figure 5.8: Example of the process of scaling of the length of the femurs: the distance between pairs of markers in the model divided by the distance between the same pairs of experimental markers is equal to the scale factor.

The position of all the other markers was referred to a particular landmark of the body, therefore the positioning could be more accurate than the wand's ones.

During this operation it is important to give a weight to each marker: the higher is the weight of a marker, the better the experimental marker should be matching the position of the model marker. Taking into account of this idea, the tibial wand and the femoral wand markers had a very low weight. It is also possible to give some additional conditions on the coordinates of the joints, if we know the precise value that they should have during the static pose.

The scaling is an iterative operation so, after the process of changing the dimension of the bodies and adjusting of the positions of the markers, we had to go on reiterating these two operations until the position's RMS error that describes the quality of the markers' adjustment became close to a couple of millimeters.

5.2.4 Inverse Kinematics

With this tool it is possible to make the model reproducing frame by frame the movement of the markers captured from the motion capture system, as illustrated in Figure 5.9, and to calculate the joint angles.

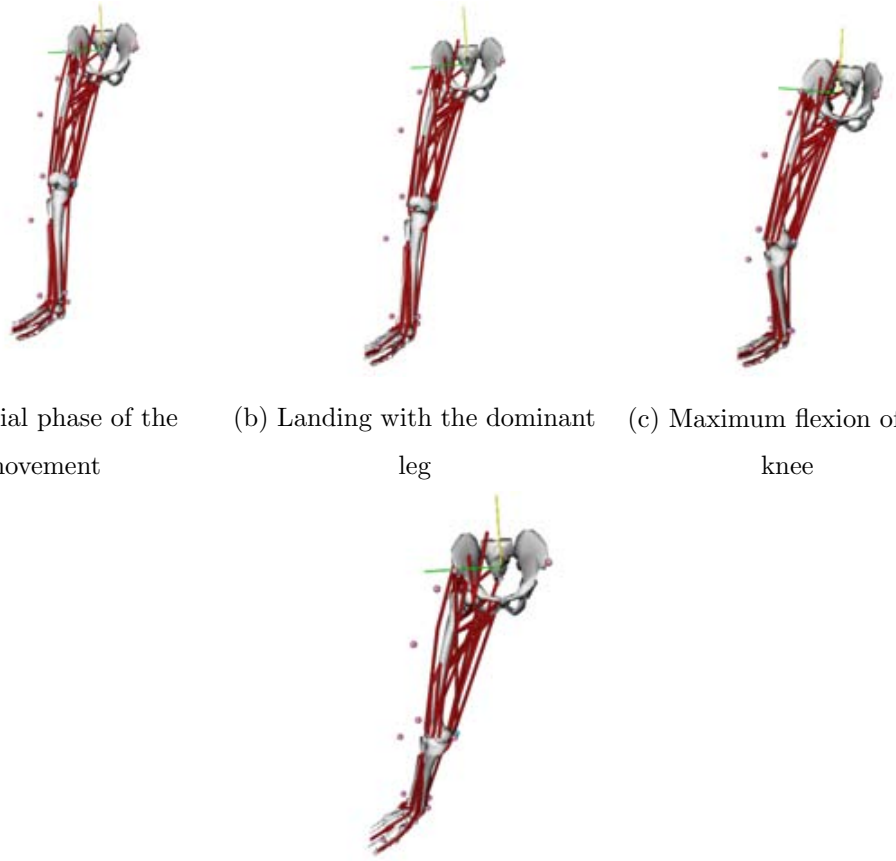

(a) Intitial phase of the movement

(b) Landing with the dominant leg

(c) Maximum flexion of the knee

(d) End of the contact of the dominant leg

Figure 5.9: Model reproducing the movement of the experimental markers: the most significant frames of the execution of the sidestep cutting maneuver of one subject.

It is possible to find frame by frame the model's pose that best matches the position of the experimental markers. The concept of best matching can be expressed as an objective function that has to be minimized as we can see here:

$$min_q \left[\sum_{i \in markers} w_i \| {x_i}^{exp} - x_i(q) \|^2 + \sum_{j \in unprescribed\ coords} \omega_j (q_j^{exp} - q_j)^2 \right] \tag{5.1}$$

$$q_j = q_j^{exp} for\ all\ prescribed\ coordinates\ j$$

where:

$\left[\| {x_i}^{exp} - x_i(q) \|^2 \right]$ is the square error on the position of each marker;

$\left[(q_j^{exp} - q_j)^2 \right]$ is the square error on the determination of each coordinate.

These two components of the objective function have to be weighted setting a weight (w_i

and ω_j), according with how sure we are about the position of each marker or about the value of each coordinate.

In Table 5.1 rimmed in red, we can see how we can classify the quality of the results of an Inverse Kinematics analysis.

Thresholds:	GOOD	OKAY	BAD
MAX Residual Force (N)	0-10 N	10-25N	> 25 N
RMS Residual Force (N)	0-5 N	5-10 N	> 10 N
MAX Residual Moment (Nm)	0-50 Nm	50-75 Nm	>75 Nm
RMS Residual Moment (Nm)	0-30 Nm	30-50 Nm	>50 Nm
MAX pErr (trans, cm)	0-2 cm	2-5 cm	>5 cm
RMS pErr (trans, cm)	0-2 cm	2-4 cm	>4 cm
MAX pErr (rot, deg)	0-2 deg	2-5 deg	> 5 deg
RMS pErr (rot, deg)	0-2 deg	2-5 deg	> 5 deg

Table 5.1: Classification of the quality of the analysis. Adapted from [12].

Since we did not filter the coordinates of the markers given as input to the Inverse Kinematics analysis, before analyzing the results coming from this analysis it's better to save a copy of them and filter them with a Butterworth low pass filter of the third order with a cutting frequency of 15 *Hz* as suggested in [4].

5.2.5 Inverse Dynamics

The Inverse Dynamics tool allows the user to determine the net forces and torques at each joint responsible for a given movement (the moments that can balance the external loads); a simplified example of this analysis can be seen in Figure 5.10.

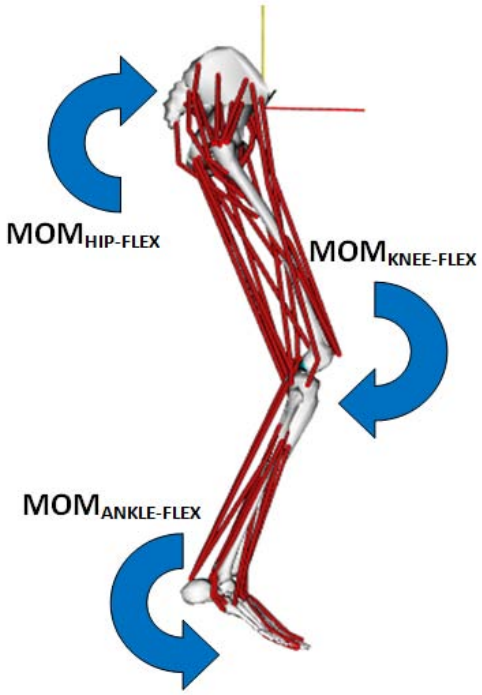

Figure 5.10: Example of some of the equilibrating joint moments that can be find out as result of an Inverse Dynamics analysis.

Given the kinematics describing the movement of a model and the external loads applied to the model, the Inverse Dynamics tool solves the equations of motion for each body:

$$M(q)\ddot{q} + C(q,\dot{q}) + G(q) = \tau \tag{5.2}$$

where:

N is the number of degrees of freedom;

$q, \dot{q}, \ddot{q} \in R^N$ are the vectors of generalized positions, velocities and accelerations;

$M(q) \in R^{N\times N}$ is the system mass matrix;

$C(q,\dot{q}) \in R^N$ is the vector of Coriolis and centrifugal forces;

$G(q) \in R^N$ is the vector of gravitational forces;

$\tau \in R^N$ is the vector of generalized forces, that is the unknown of the problem.

As we said before, the coordinates of the markers had not been filtered before launching the Inverse Kinematics so, in order to launch the Inverse Dynamics we took the results of the Inverse Kinematics analysis (the not filtered ones) and we applied them the filter already implemented in OpenSim with a cutting frequency of 15 *Hz*.

The results file contains, frame by frame, the values of the net moments for each DOF (even

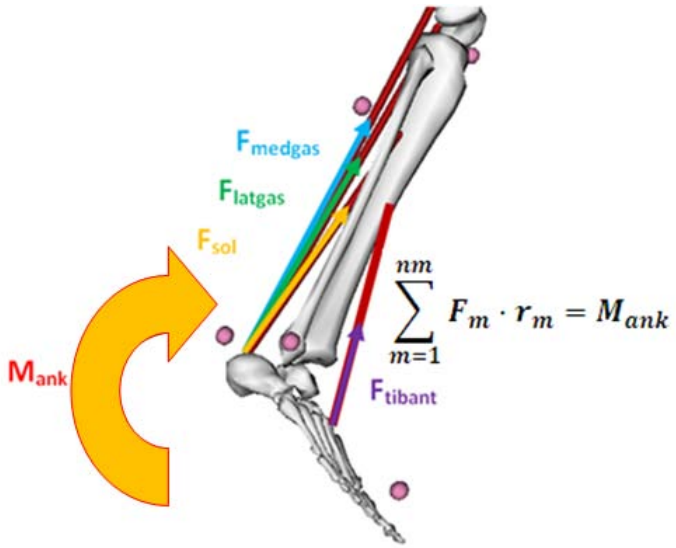

Figure 5.11: Example of force-sharing problem in a simplified model of the ankle. If we don't add any additional condition, this problem has an infinite number of solutions.

if it's locked) and the values of the three moments and the three forces at the pelvis. In our case, the forces and moments at the pelvis are related to the contact between the pelvis and the upper part of the body and between the pelvis and the left leg, which are were included in our system.

5.2.6 Static Optimization

The Static Optimization tool is an extension to Inverse Dynamics that further resolves the net joint moments into individual muscle forces frame by frame. The particularity of this process is that the movement is divided in frames and the problem of muscular distribution is solved in each frame as it would be static.

With the results of the Inverse Dynamics we know the net moment at a precise joint; we know that this net moment has to be given by the sum of the forces of the muscles acting on the joint multiplied by the lever arm of the muscles with respect to the joint.

This kind of problem, known as force-sharing problem has an infinite number of solutions because, for each DOF, there is an equation of equilibrium with nm variables, where nm is the number of muscles acting on that joint according with that DOF considered. An example of this problem of forces repartition can be seen in Figure 5.11.

In order to find a unique solution we need another condition that in our case is an objective function to be minimized. This objective function is represented by the sum of the activation of

the muscles acting on the precise joint we are considering, according to the precise DOF we are looking for, at the power p that can be defined by the user. This is the objective function used by OpenSim:

$$J = \sum_{m=1}^{nm} (a_m)^p \tag{5.3}$$

where a_m is the activation of the m^{th} muscle. The suggestion of minimizing a function dependent on the muscular activation comes from the idea that maybe the human body tries to make the muscles working as less as possible to do a particular movement in order to save energy. We don't know if this is what really happens in the human body, and we can't say that all the subjects are responding to this mechanism of activation. This is just one possible way to solve the muscle force-sharing problem, which is accepted by the scientific community. In our case we used a coefficient p=2 that is the most common value find in literature.

OpenSim gives the possibility to choose between two different muscle models, depending on how much we want the analysis to be accurate.

- Simple model without pennation (ideal actuator) that can be seen in Figure 5.12;
- Model of the contraction dynamics that can be seen in Figure 5.13.

This ideal actuator model is based on these main hypotheses:

- The tendon is infinitely stiff;
- The force produced by the muscle is not dependent on its velocity or length;
- The muscle fibers are acting on the same direction of the tendon.

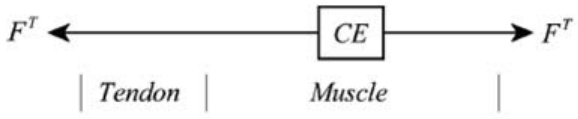

Figure 5.12: Ideal actuator muscle model.

The force of the tendon can be expressed in the following way:

$$F^T = F^{CE} = a(t) \cdot F_0^M \tag{5.4}$$

where:

F^{CE} is the force of the contractile element;

$a(t)$ is the activation of the muscle, found respecting the condition of minimization explained before;

F_0^M is the optimal isometric force of the muscle, found in literature and from studies on cadavers.

The muscle model of the contraction dynamics is the most complete muscle model that is possible to use in OpenSim and it's based in the following hypothesis:

- The tendon is elastic with a linear stress-strain relationship;
- The force produced by the muscle depends non-linearly on its velocity and length;
- The muscle fibers are acting on a direction inclined at an angle with respect to the direction of the tendon (pennation angle).

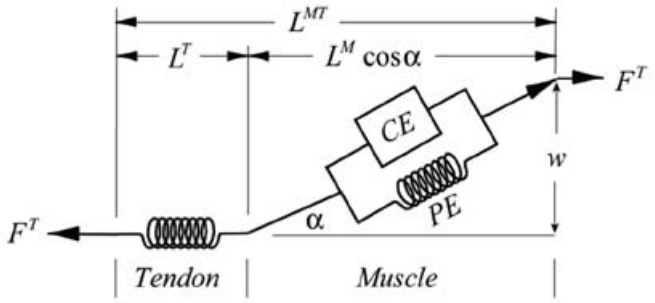

Figure 5.13: Muscle model of the contraction dynamics.

The force of the muscle is a complex function depending on the pennation angle, the maximum isometric force, the velocity of contraction, the length of the fibers, the activation, the elasticity of the tendon and the elasticity of the parallel element.

The equations of equilibrium for each j^{th} DOF are shown below and depending on which model of muscle we want to use to solve the Static Optimization they can be:

For the ideal force generators:

$$\sum_{m=1}^{nm} (a_m F_m^0) r_{m,j} = \tau_j \tag{5.5}$$

For the muscle model of the contraction dynamics:

$$\sum_{m=1}^{nm} \left[a_m f(F_m^0, l_m, v_m) \right] r_{m,j} = \tau_j \tag{5.6}$$

where:

nm is the number of muscles of the model;

a_m is the activation level of the m^{th} muscle at a discrete time step;

F_m^0 is the maximum isometric force of the m^{th} muscle;

l_m is the instantaneous length of the muscle;

v_m is the shortening velocity of the muscle;

$f(F_m^0, l_m, v_m)$ is the relation between force-length-velocity for the muscle;

$r_{m,j}$ is the moment arm of the muscle about the j^{th} joint axis;

τ_j is the torque acting about the j th joint axis.

In our case in the preliminary simulations the Static Optimization using the ideal actuators muscle model and the parameters of the original model "Gait2392_Simbody" could not converge. This happened because the muscles could not produce enough force to balance the joint moments.

This can be seen well in Figure 5.14, an example of comparison between the knee flexion moment coming from the Inverse Dynamics analysis and the maximum knee flexion moment that can be given by the muscles acting with their maximum isometric force and using the ideal actuator model. It's possible to see that in a portion of time the moment at the joint is greater than the maximum moment that can be given by the muscles.

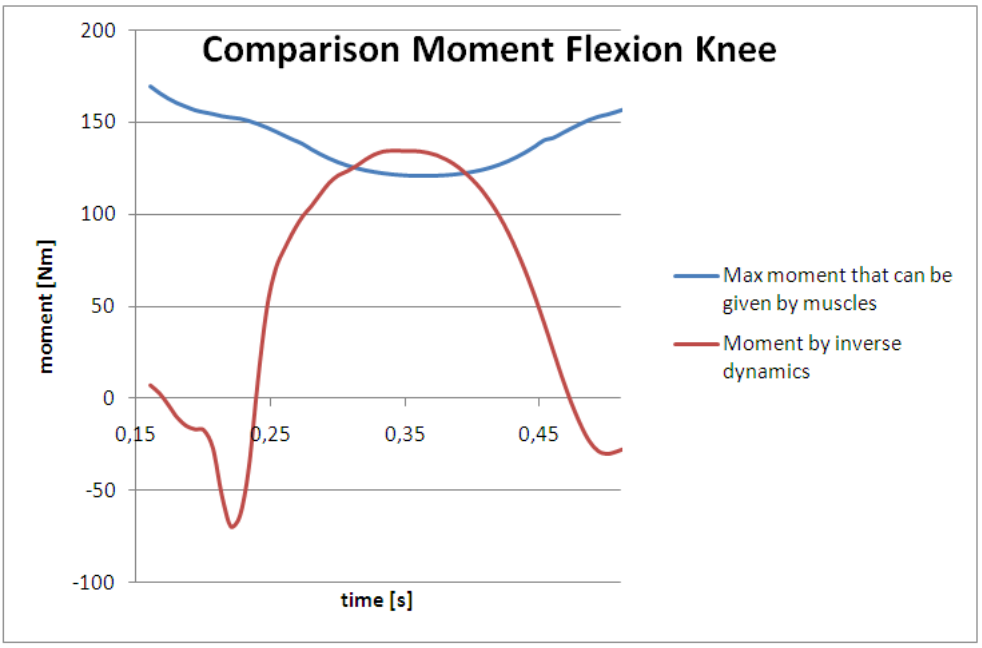

Figure 5.14: Example of a comparison between the moment of flexion at the knee coming from the Inverse Dynamics analysis and the maximum moment of flexion that can be given by the muscles.

We have to take care that the reasoning made here is true just if we consider the ideal muscle model, where the maximum force that can be produced by a muscle is exactly equal to the maximum isometric force (it's like treating each frame of the movement as an instant where we have just isometric action).

If we take into account the dependence of the force on the velocity, the maximum force that a muscle can product is not always the maximum isometric one, but depends on the velocity of shortening/lengthening as it can seen in Figure 5.15. In fact for values of abscissa greater than zero we have eccentric action (lengthening) and the maximum force is greater than the maximum isometric one, for values of abscissa lower than zero we have concentric action (shortening) and the maximum force is lower than the maximum isometric one.

The inconsistency we saw before in Figure 5.14 between the moment at the joint and the maximum moment that can be given by the muscles could be explained in the following way:

- The data used to create the models are taken from cadavers, so we can think that the strength of a dead tissue is lower than a live one;
- The original model "Gait2392_Simbody", as the name says, it's made to analyze the gait, a movement that for sure causes lower stress on the muscles than the sidestep cutting, characterized by a high dynamic and an explosive force action;

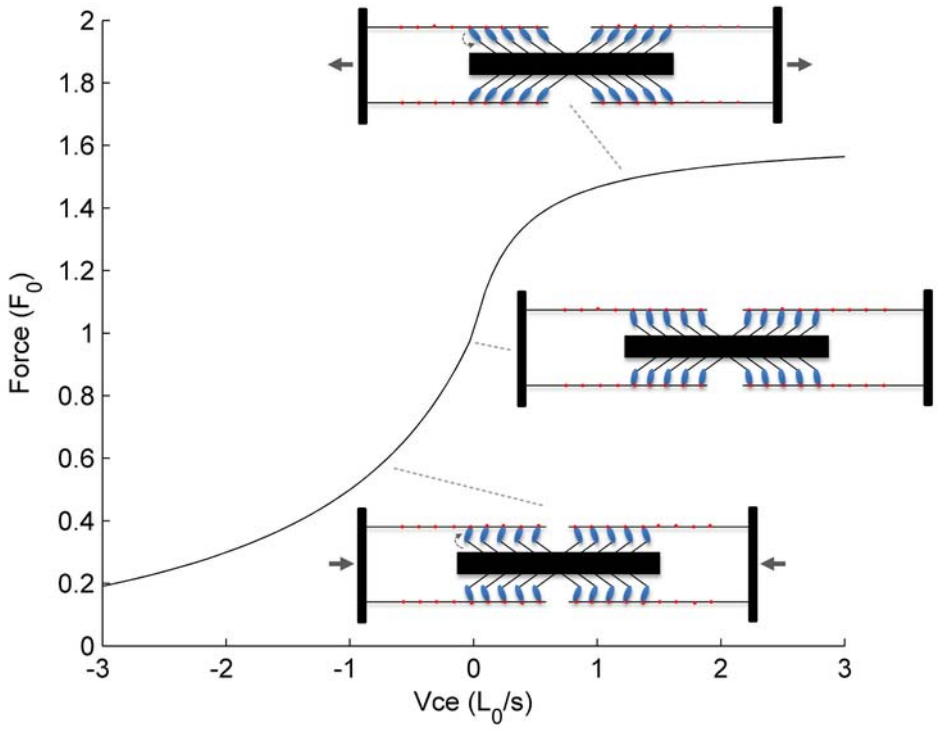

Figure 5.15: Ideal dependence of the force of the muscle on the velocity of extension.

- The model is made to describe the body of a normal person but the subjects used for the tests had a muscle tone greater than a normal person, so probably they can not be well represented by the model.

Considering all these aspects, it was decided to increase the maximum isometric force of all the muscles in the same way. After some simulations, we decided to multiply the maximum isometric forces of all the muscles by 2,5 because this constant could ensure to solve the inconsistency shown in Figure 5.14.

After modifying manually the maximum isometric force of the muscles, the Static Optimization could converge. In this case the process succeeded just using the ideal actuator muscle model, so without considering the dependence between force, length of the fibers and velocity of contraction.

Just increasing the maximum isometric force of the muscles without optimizing the fiber length and other muscular parameters, could bring the muscles to work far from their condition of optimal force (around the peak of the curve shown in Figure 5.16).

For our study the solution obtained with the ideal actuator muscle model can be considered good enough, anyway we also tried to use the muscle model of contraction dynamics optimizing

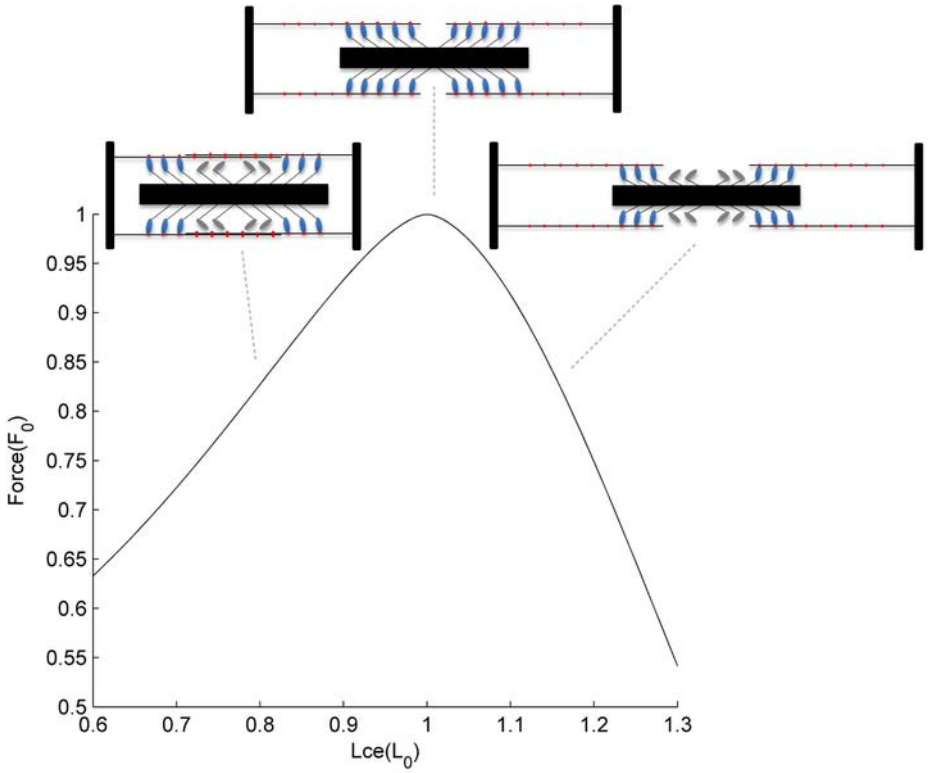

Figure 5.16: Dependence of the force of the muscle (normalized on the maximum isometric force) on the instantaneous length (normalized on the optimal length).

the muscular parameters under the following simplified hypotheses:

- We wanted the muscles to be working around their condition of optimum with respect to the fiber length, this means to be around the peak of the curve shown in Figure 5.16, so where $L^M/L_0^M \sim 1$;

- In order to optimize the optimal length of each muscle we considered a model with rigid tendon and a pennation angle constant during the movement, corresponding to the pennation angle at the optimal length of the muscle α_0.

The length of the muscle and tendon (L^{MT}) has been taken from a Muscle Analysis for one test of one subject, frame by frame for each muscle, the length of the tendon (L^T) has been taken from the scaled model and is a constant (because the tendon is rigid in this model) and also the pennation angle has been taken from the scaled model (it is constant because we decided to take the pennation angle at the optimal length of the muscle).

The length of the muscle (L^M) could be calculated frame by frame in the following way:

$$L^M = \frac{L^{MT} - L^T}{\cos \alpha_0} \tag{5.7}$$

Then, for every muscle, a mean of all the values of L^M calculated at each time step was made, and we considered this equal to the optimal fiber length, according with the first hypothesis made:

$$L_0^M \sim L_{med}^M \tag{5.8}$$

In the model with the maximum isometric forces multiplied by 2,5 the optimal fiber length of all the muscles was changed manually with the L_0^M obtained in this way and the Static Optimization was run using the muscle model of the contraction dynamics.

We have to take care that this approach is an optimization and in the reality the muscles are never working all together in their optimal conditions. We have moreover to consider that this optimization depends on the subject and on the particular kinematic of the test.

From a comparison of the results obtained with the two muscle models, we could see that the two approaches did not give the same results, anyway it is not possible to say that one of the two approaches is better than the other one: they are equally incorrect because they are using simplified hypotheses in order to calculate the muscle forces. The two approaches can be both considered good enough for our pilot study and they would need a comparison with the results of the EMG system in order to verify their reliability. For our simulations we decided to use the ideal actuator muscle model because this is the most time saving approach.

In the following chapter we will present the experimental results obtained and we will discuss them, trying to connect them with the aspects related to the occurrence of ACL non contact injuries.

Chapter 6

Experimental results and discussion

Before starting the quantitative analysis of the results obtained, a qualitative analysis has been done in order to see if there was any significant difference between the subjects. From this preliminary analysis it was possible to see that the techniques of execution of the sidestep cutting maneuver were quite different among the subjects. Looking at the execution of the movement, it was possible to classify the subjects according to the way their dominant foot is touching the ground during the landing phase. Therefore, the subjects have been divided in two classes:

- Forefoot strikers (6 subjects);
- Heel strikers (3 subjects).

The presentation and the discussion of the results will be split in two parallel analyses according with this classification.

In order to focus on the most problematic part of the movement for the risk of occurrence of ACL injuries, we decided to analyze the first part of the movement, in particular the eccentric phase of the sidestep cutting. As we can see in Figure 6.1, the beginning of this phase has been identified as the instant in which the vertical force (already filtered) is greater than 10 N; the ending coincides with the instant of maximum flexion angle of the knee.

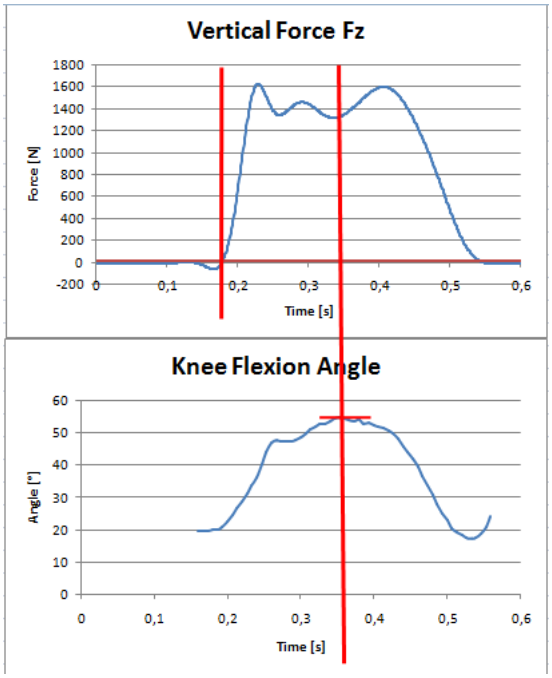

Figure 6.1: Definition of the eccentric phase of the movement.

In our case all the analyses of the results have been made considering for each class (forefoot strikers and heel strikers) if the variables chosen had any difference between the two groups of test (pre and post vibrations). Moreover, where it was possible to appreciate it, any other relevant consideration about differences between forefoot strikers and heel strikers has been highlighted.

6.1 Ground reaction forces

In order to highlight the differences between the trials pre and post vibrations, one of the most significant variables to focus on our attention, seemed the vertical force (filtered) and in particular, the peak value of this variable. The peak value of the vertical force has been calculated as a mean value of the peak of the vertical force of each subject of the class (forefoot strikers or heel strikers).

Since we wanted our analysis to be as much as possible independant from the different subjects, we normalized the values of the force on the body weights of the subjects, in order to have dimensionless values of the vertical force.

We can see the comparison of the vertical force pre and post vibrations for the different forefoot strikers in Figure 6.2 and for the different heel strikers in Figure 6.3; these curves are

representative of the whole eccentric phase of the sidestep cutting maneuver.

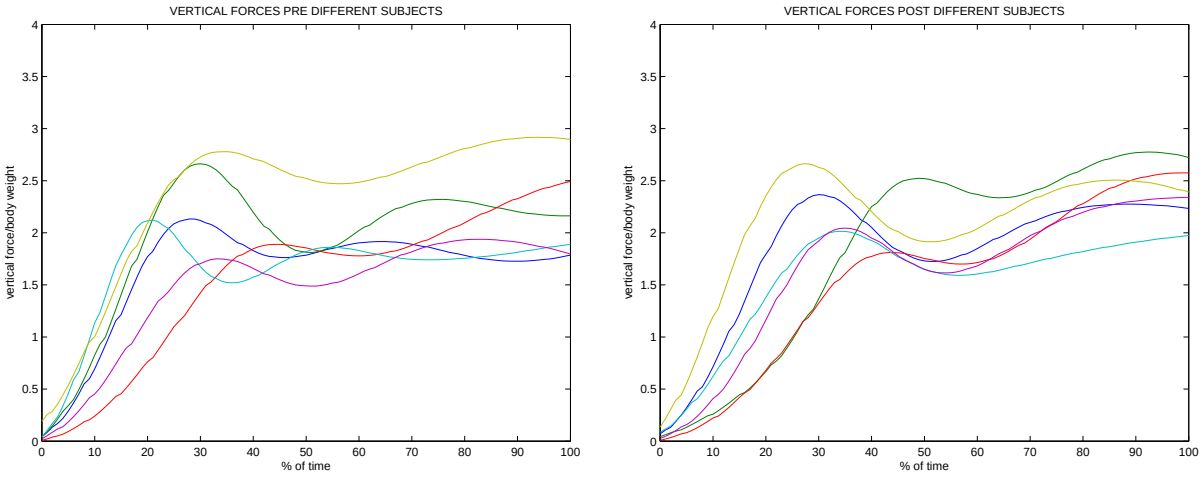

Figure 6.2: Comparison of the vertical force of the different forefoot strikers pre vibrations (on the left) and post vibrations (on the right).

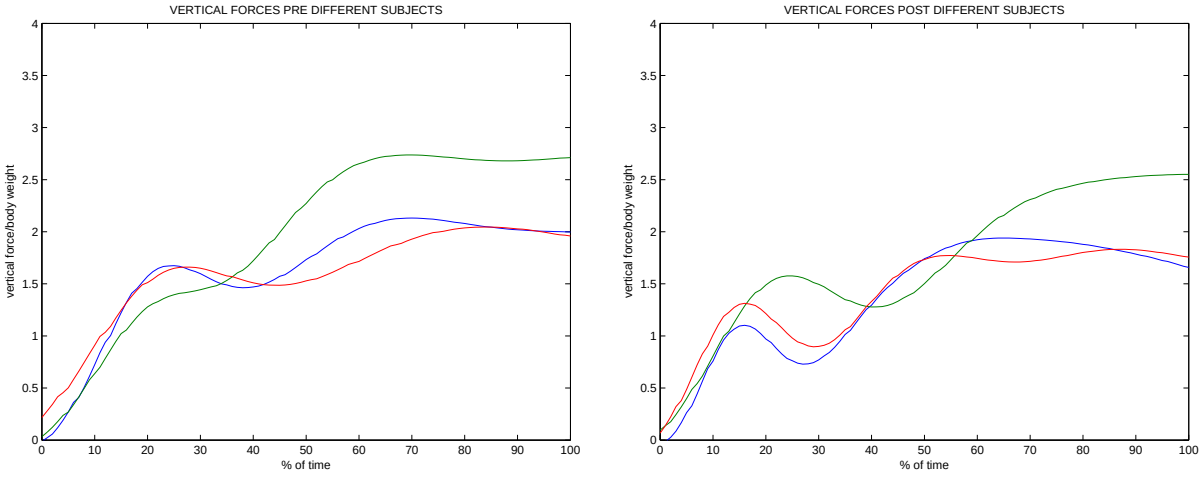

Figure 6.3: Comparison of the vertical force of the different heel strikers pre vibrations (on the left) and post vibrations (on the right).

As we can see in Figure 6.4, for the forefoot strikers it is possible to appreciate an increase on the mean value of the peak of the vertical force between pre and post vibrations but, since the value of "p" of the t-test is high (0,453), this result is not statistically significant. A decrease of the 9% between pre and post vibrations can be appreciated for the heel strikers, as we can see in figure 6.5 and, since the value of "p" of the t-test is low (0,002), this result can be considered

as statistically significant.

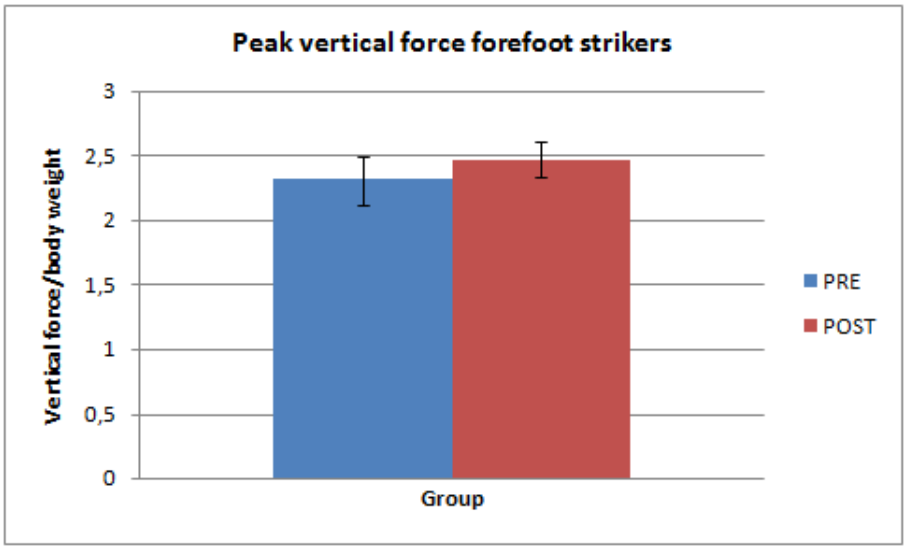

Figure 6.4: Comparison between pre and post vibrations of the peak value of the vertical force for the forefoot strikers.

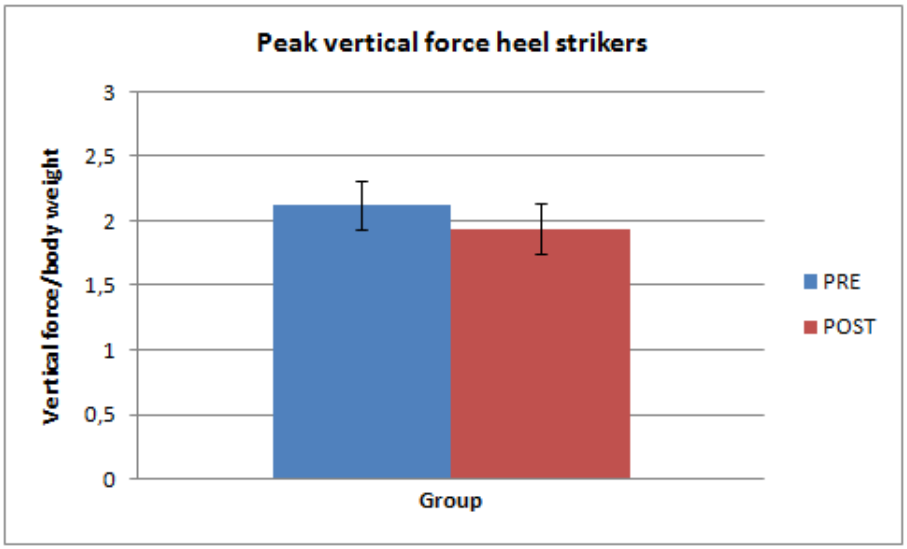

Figure 6.5: Comparison between pre and post vibrations of the peak value of the vertical force for the heel strikers.

It is moreover possible to observe that the mean values of the peaks of the vertical force for the heel strikers are lower than the forefoot strikers' ones. This aspect seems in disaccordance with the common sense that the amount of the force of impact of a heel striker is lower than the forefoot striker's one; it is important to observe that the heel strikers are landing with a knee

flexion angle lower than the forefoot strikers, as we can see in Figures 7.1 and 7.2, so they can dampen more the force of impact with the knee extensor muscles.

In Figure 6.6 we can see a summary table of the analysis of the peak of the vertical forces (mean values and standard deviations), with the values of "p" obtained from the t-test.

		FOREFOOT STRIKERS		HEEL STRIKERS	
		PRE	POST	PRE	POST
PEAK VERTICAL FORCE	mean value	2.313	2.471	2.132	1.940
	SD	0.375	0.274	0.377	0.388
	p	0.453		0.002	

Figure 6.6: Summary table of the analysis of the peak of the vertical forces and the "p" values.

From the analysis of the peak vertical force we can conclude that for the heel strikers it is possible to appreciate a statistically significant reduction of the peak of the vertical force. This result does not seem in line with an increase of the risk of occurrence of ACL injuries between pre and post vibrations, because a lower peak of the vertical force seems to bring to lower stress for the knee. This is not real at all if we do not have any information about the kinematics of the movement, so at this level of analysis it is difficult to relate this result with a possible increase of the risk of occurrence of ACL injuries.

6.2 Kinematics

Most of the kinematic analysis has been done feeding OpenSim with the trajectories of the experimental markers and analyzing the results obtained from the Inverse Kinematics tool, so these results will be presented in the following chapter.

The only kinematic variable we analyzed without OpenSim were:

- Time of duration of the cycle: this variable can be representative of variations in the control of the movement. The idea is that, if the capacity of controlling the lower limb is lower, the time of duration of the cycle should be higher because of the feeling of the subjects of lack of control and safety during the execution of the movement.

- Load rising speed: this variable is espressed in $[s^{-1}]$ and represents the speed of increasing of the vertical force when the foot touches the ground. This variable is calculated as the difference between the peak of the vertical force and the value of the vertical force at the

first contact of the foot with the ground, divided by the time needed to reach the peak of the vertical force from the initial contact.

6.2.1 Time of duration of the cycle

In the forefoot strikers class, as we can see in Figure 6.7 there is no significant difference between the mean value of the time of duration of the cycle between the trials pre and post vibrations and the "p" value of the t-test is very high (0,626), so this result is not statistically significant.

The standard deviation for the pre group is greater than for the post group, this means that the dispersion of the data has decreased between the two groups.

In the heel strikers class as we can observe in Figure 6.8, there is an evident increase of the mean value of the time of duration of the cycle between the trials pre and post vibrations (∼40 *ms*); this could be considered as a direct consequence of the reduction of control of the knee due to the mechanical vibrations warming-up, but the "p" value of the t-test is high (0,212), so this result is not statistically significant.

Anyway we cannot observe a reduction of the standard deviation (and so of the dispersion of the data) between pre and post vibrations.

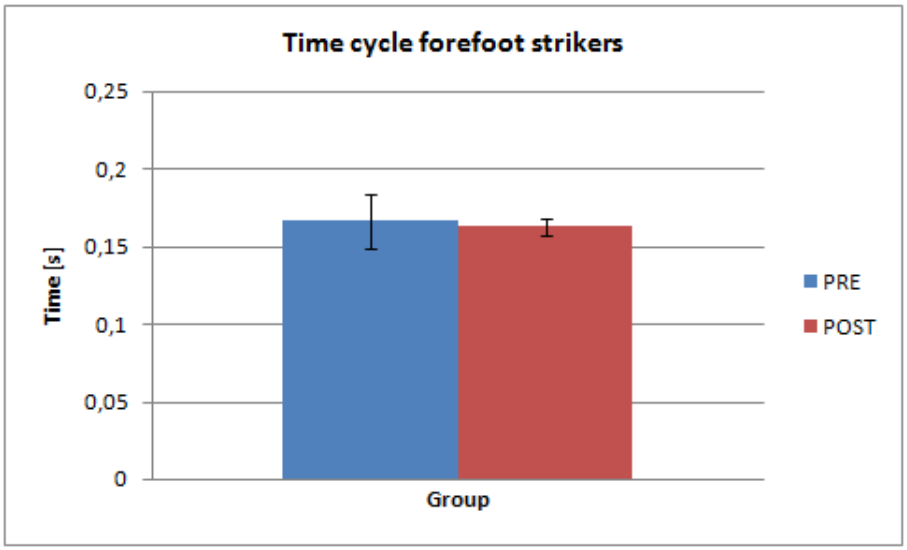

Figure 6.7: Time of duration of the cycle for forefoot strikers.

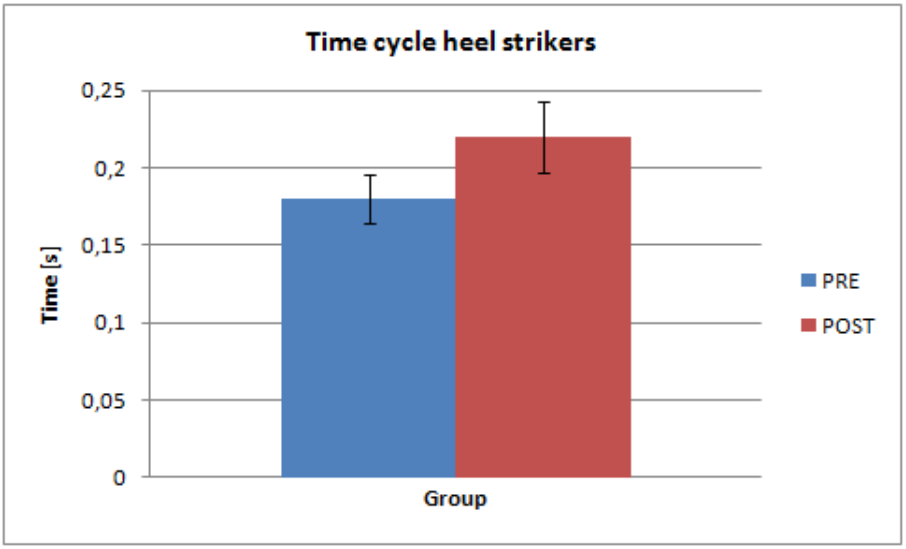

Figure 6.8: Time of duration of the cycle for heel strikers.

In Figure 6.9 we can see a summary table of the analysis of the time of duration of the cycle (mean values and standard deviations), with the values of "p" obtained from the t-test.

		FOREFOOT STRIKERS		HEEL STRIKERS	
		PRE	POST	PRE	POST
TIME DURATION CYCLE	mean value	0.167	0.163	0.180	0.220
	SD	0.035	0.012	0.031	0.047
	p	0.626		0.212	

Figure 6.9: Summary table of the analysis of the time of duration of the cycle and the "p" values.

6.2.2 Load rising rate

This variable is representative of the speed of increasing of the vertical force in the initial part of the landing of the subject. Since the subjects are landing from a jump, the initial part of the contact should be the most impulsive one and the higher is the slope of the graph of the vertical force in this phase, the most dangerous is the landing phase.

In our case we decided to define the load rising rate variable as the slope (normalized on the body weight of the subject) of the streight line connecting the point of initial contact with the ground (vertical force greater than 10 N) with the first peak reached. In Figure 6.10 we can see an example of the plot of the vertical component of the not filtered ground reaction force, with the definition of load rising rate.

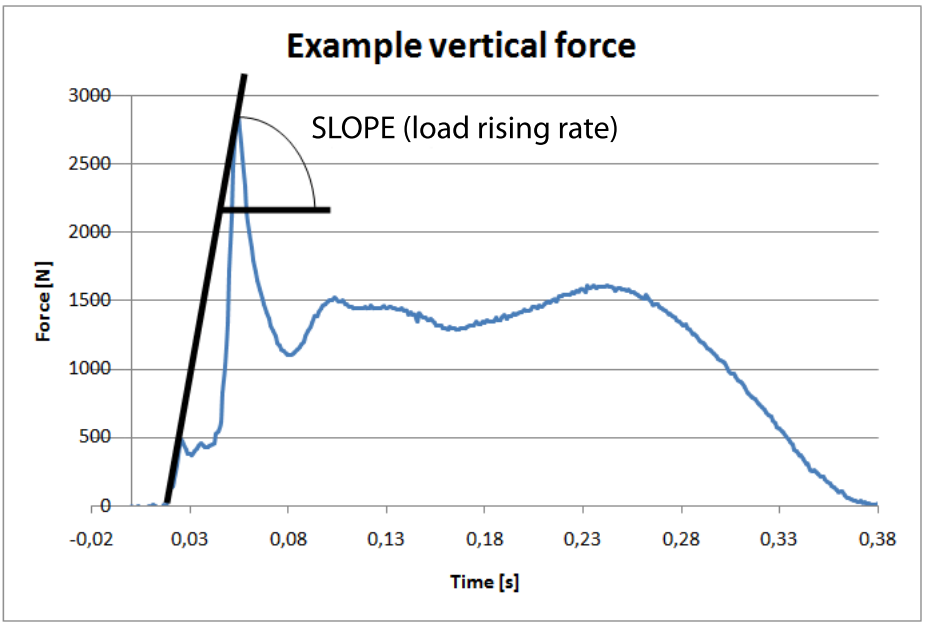

Figure 6.10: Exemple of the vertical force of one subject with the definition of load rising rate.

From the analysis of the mean values of the load rising rate as we can see in Figure 6.11, we can highlight for the forefoot strikers a decrease of the 40% between pre and post vibrations with a level of confidence of the 72%. This result is not in line with an increase of the risk of occurence of ACL injuries.

For the heel strikers as we can see in Figure 6.12 there is not any important variation between pre and post vibrations and we can say this with a level of confidence of the 90%.

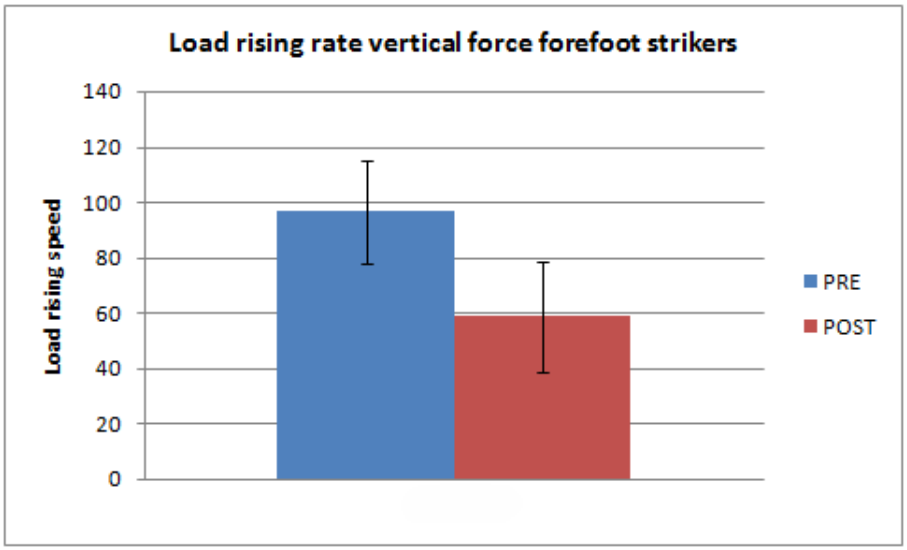

Figure 6.11: Mean values of the load rising rate for the forefoot strikers.

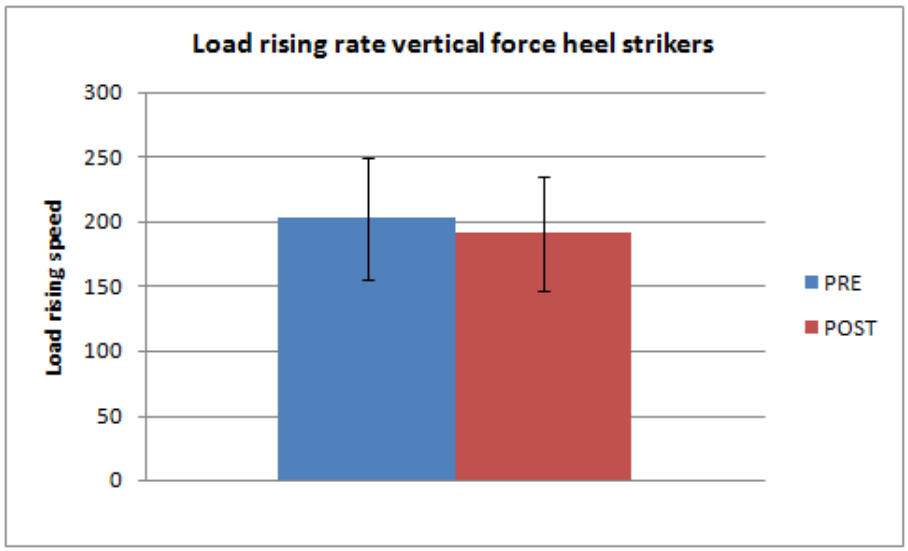

Figure 6.12: Mean values of the load rising rate for the heel strikers.

In Figure 6.13 we can see a summary table of the analysis of the load rising rate (mean values and standard deviations), with the values of "p" obtained from the t-test.

		FOREFOOT STRIKERS		HEEL STRIKERS	
		PRE	POST	PRE	POST
LOAD	mean	96.557	58.563	202.849	190.867
RISING	SD	37.349	40.245	93.671	87.364
RATE	p	0.275		0.100	

Figure 6.13: Summary table of the analysis of the load rising rate and the "p" values.

6.3 EMG

Unfortunately the quality of the EMG signals was not very good, so in our analysis an evaluation of the experimental activations of the muscles was not possible. These data would have been interesting in order to evaluate the reliability of the numerical simulation (that will be presented in the following chapter), comparing the experimental activations of the muscles (coming from the EMG system) with the estimated activations of the muscles (coming from OpenSim).

6.4 Conclusions

The experimental results could bring to the following conclusions:

- It was possible to highlight with a statistical significance a reduction of the peak of the vertical force between pre and post vibrations for the heel strikers;
- With a level of confidence of the 90% it was possible to say that there are not particular differences in the load rising speed between pre and post vibrations for the heel strikers;
- The not statistical significant results can be considered important as a guideline of the possible tendencies of the variables for a more focused and efficient future study.

An increase of the time of duration of the cycle seems compatible with a decrease of the peak of the vertical force and a decrease of the load rising speed.

The connection between the analysis of the experimental results and the aspects related to the risk of occurrence of ACL injuries is not very clear since we miss the main informations of the kinematic of the movement so, in order to have more interpretable results, it is necessary to go deeper in details with the analysis of the numerical results that will be presented in the following chapter.

Chapter 7

Numerical results and discussion

As we did for the analysis of the experimental results, also for the analysis of the numerical results the subjects have been split in the two classes (forefoot strikers and heel strikers) according with the technique of execution of the movement, and two parallel analyses have been done.

7.1 Kinematics

Before starting the treatment of the Inverse Kinematics results coming from OpenSim, these data have been filtered with a Butterworth low-pass filter of the third order with a cutoff frequency of 15 *Hz*.

Let's present the variables we decided to focus on in order to highlight the possible effects of the mechanical vibrations on the kinematics of the subjects:

- Maximum knee flexion angle: we expect that if the control on the knee is lower, the angle of maximum flexion of the knee should be higher.

- Range of motion of knee flexion: we expect that, the worse is the capacity of controlling the movement of the knee the higher should be this variable. In the literature, this variable has been identified as directly related to the risk of occurrence of ACL injuries [7].

- Maximum knee abduction angle: this variable corresponds to the minimum negative value of the knee adduction angle (valgus). The loading in valgus position is the main condition that brings to ACL injuries, as explained by Koga et al. [9].

7.1.1 Maximum knee flexion angle

We can see a comparison of the results of the knee flexion angles for the different subjects in Figure 7.1 for the forefoot strikers (pre on the left and post on the right) and in Figure 7.2 for the heel strikers (pre on the left and post on the right).

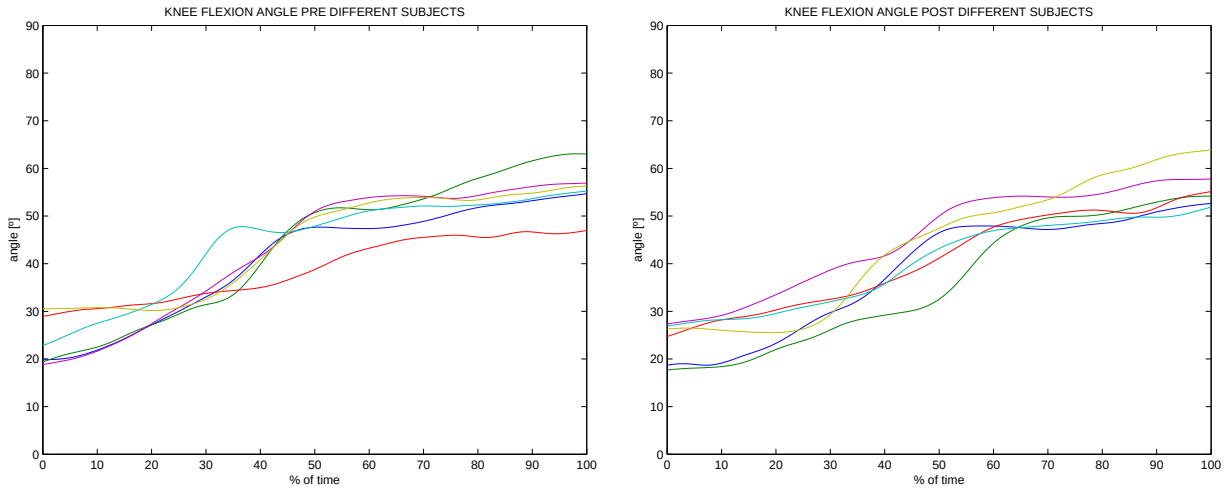

Figure 7.1: Example of comparison of the knee flexion angles of different subjects for forefoot strikers pre vibrations (on the left) and post vibrations (on the right).

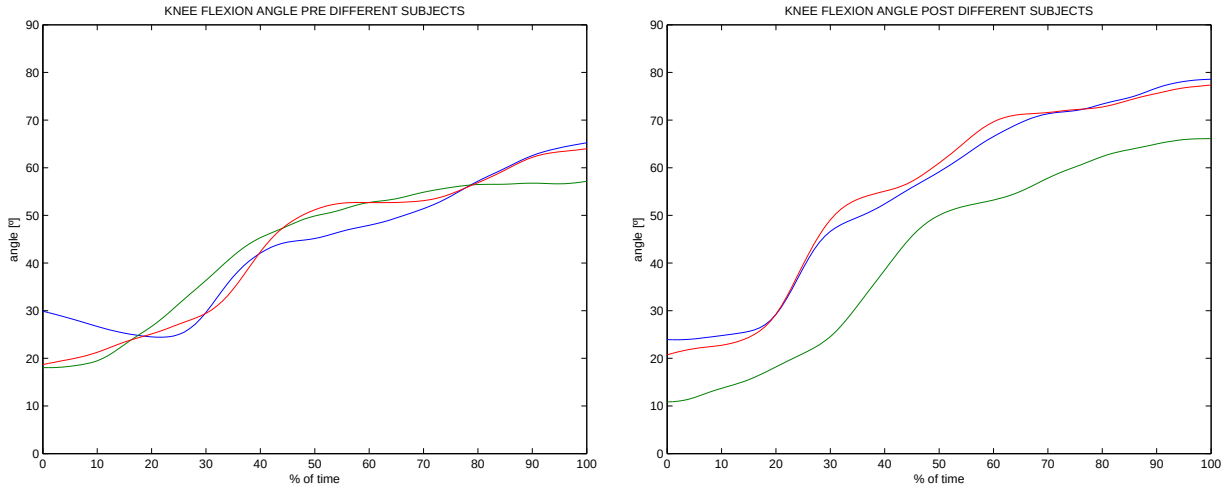

Figure 7.2: Example of comparison of the knee flexion angles of different subjects for heel strikers pre vibrations (on the left) and post vibrations (on the right).

In the forefoot strikers class, as we can see in Figure 7.3, there is no significant difference

between the mean values of the maximum flexion angle between pre and post vibrations, anyway the "p" value of the t-test is very high (0,893), so this result is not statistically significant.

In the heel strikers class there is an evident increase ($\sim 13°$) of the mean value of the maximum knee flexion angle between pre and post groups, as we can see in Figure 7.4. Since the "p" value of the t-test is low (0,015) this result is statistically significant and can be considerd as an evident consequence of the loose of control due to the mechanical vibrations warming-up.

The standard deviation is similar both between the groups (pre and post) and between the classes (forefoot strikers and heel strikers).

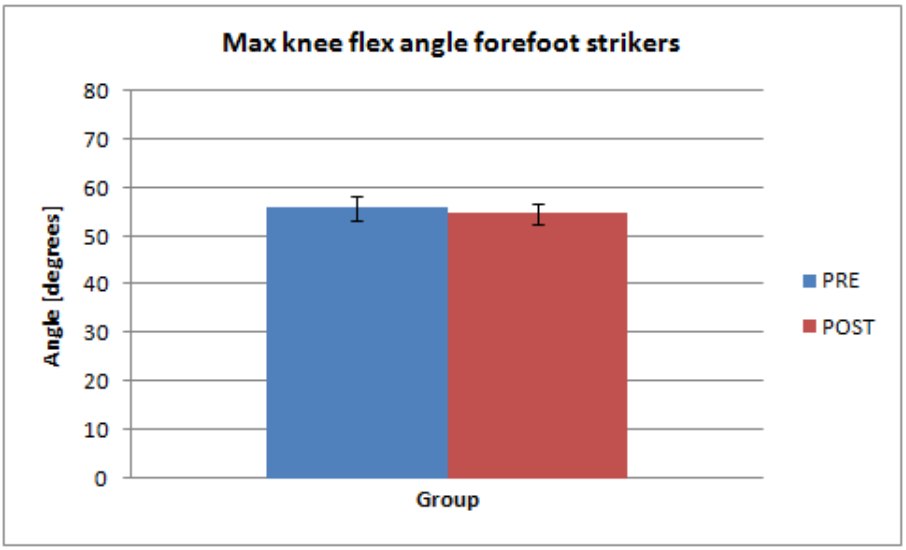

Figure 7.3: Maximum knee flexion angle for forefoot strikers.

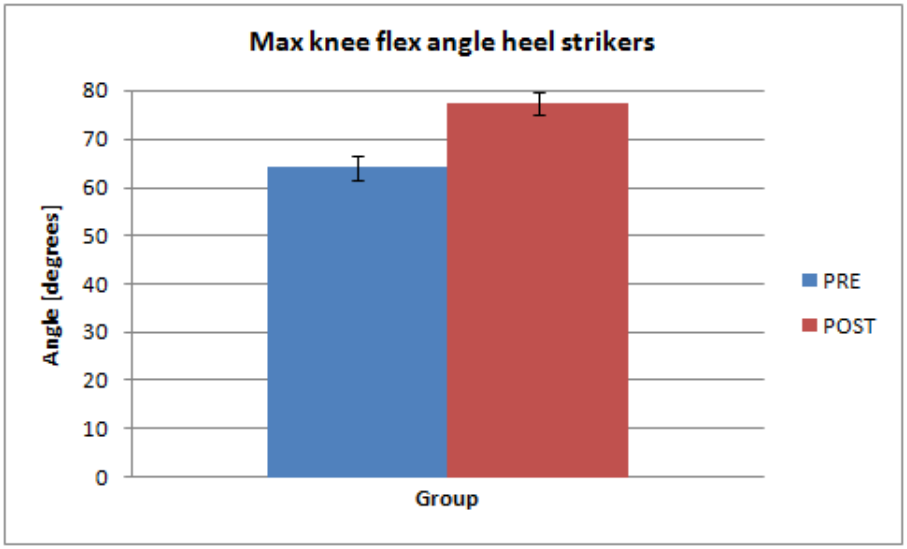

Figure 7.4: Maximum knee flexion angle for heel strikers.

7.1.2 Range of motion of the knee flexion

In the forefoot strikers class, as we can see in Figure 7.5, there is no important difference between the mean values of the range of motion of the flexion angle between pre and post vibrations and, since the value of "p" from the t-test is very high (0,959), this result is not statistically significant.

In the heel strikers class, there is an evident increase (∼14°) in the mean value of the range of motion of the knee flexion angle between the pre and the post vibrations trials as we can see in Figure 6.6. Since the "p" value is very low (0,010), this result is statistically significant and can be considered as a direct consequence of the loose of control of the knee due to the mechanical vibrations warming up. We can moreover observe a reduction of the standard deviation between the pre and the post group, a tendency similar to the one showed for the time of duration of the cycle.

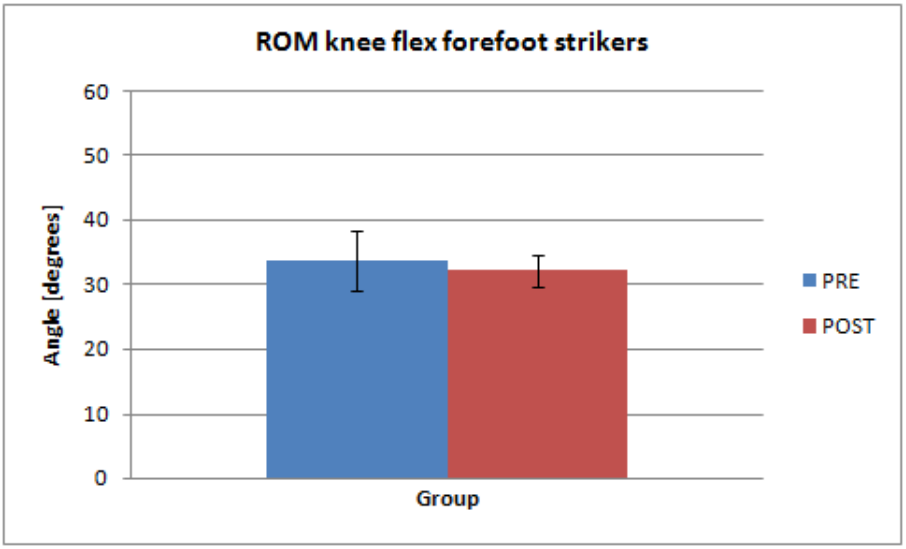

Figure 7.5: Range of motion of the knee flexion angle for forefoot strikers.

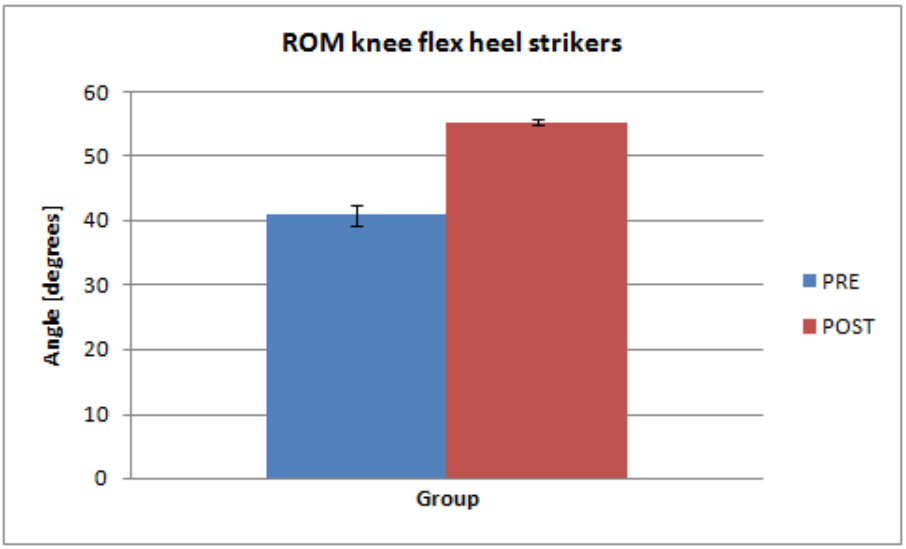

Figure 7.6: Range of motion of the knee flexion angle for heel strikers.

7.1.3 Maximum knee abduction angle

We can see a comparison of the results of the knee abduction angles for the different subjects in Figure 7.7 for the forefoot strikers (pre on the left and post on the right) and in Figure 7.8 for the heel strikers (pre on the left and post on the right).

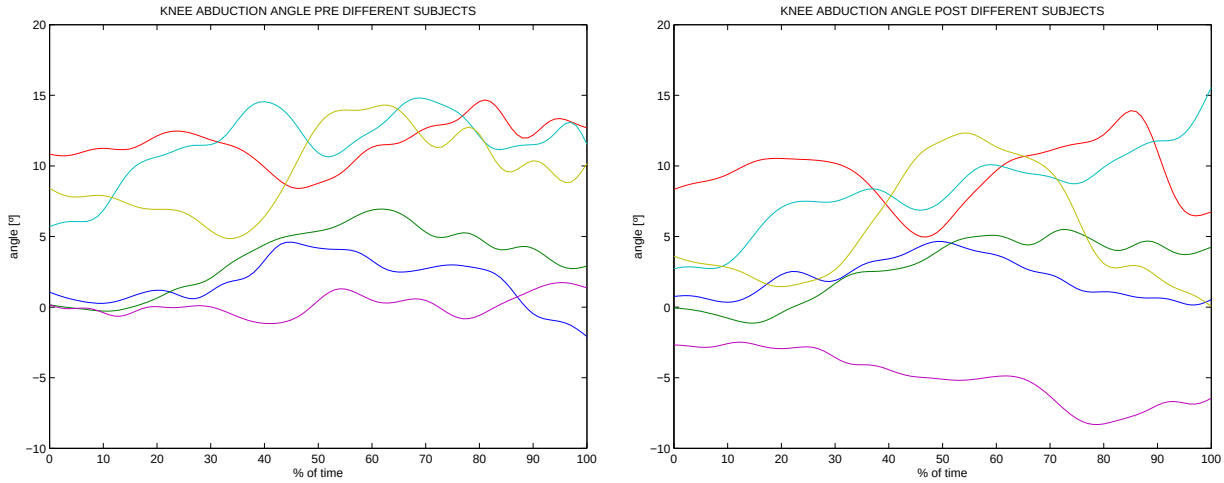

Figure 7.7: Example of comparison of the knee abduction angles of different subjects for forefoot strikers pre vibrations (on the left) and post vibrations (on the right).

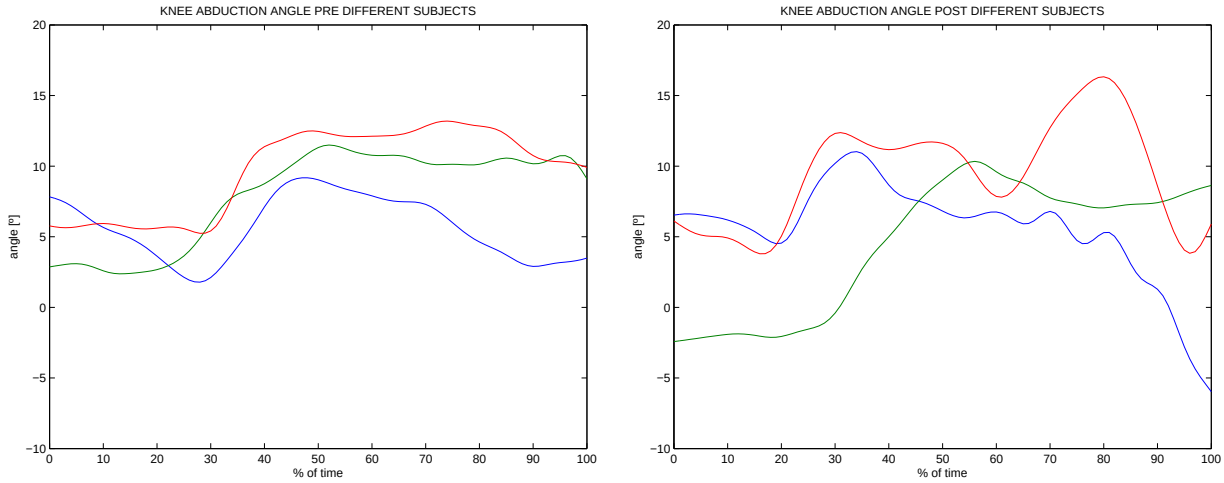

Figure 7.8: Example of comparison of the knee abduction angles of different subjects for heel strikers pre vibrations (on the left) and post vibrations (on the right).

For the forefoot strikers class, as we can see in Figure 7.9, in the pre group the abduction was not reached so, according with the convention of sign adopted, the mean value of the maximum abduction angle is negative. In the post group it is possible to observe a very small value of abduction; this is not important in absolute terms but it is significant if compared to the value obtained in the pre vibrations group. The "p" value of the t-test is not very high (0,085) so this result can be considered statistically significant with a level of confidence of the 91%.

For the heel strikers class in the pre group there was not abduction. In the post vibrations group we can observe the appearance of an evident abduction as we can see in Figure 7.10. These results are in line with the observation made on the results of the forefoot strikers but the value of "p" of the t-test (0,124) is not compatible with a statistical significance of these results.

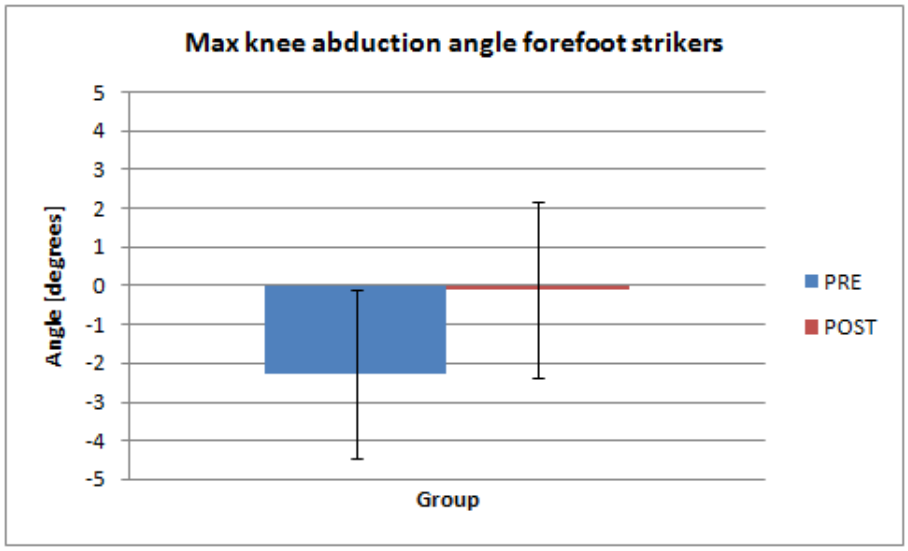

Figure 7.9: Maximum knee abduction angle for forefoot strikers.

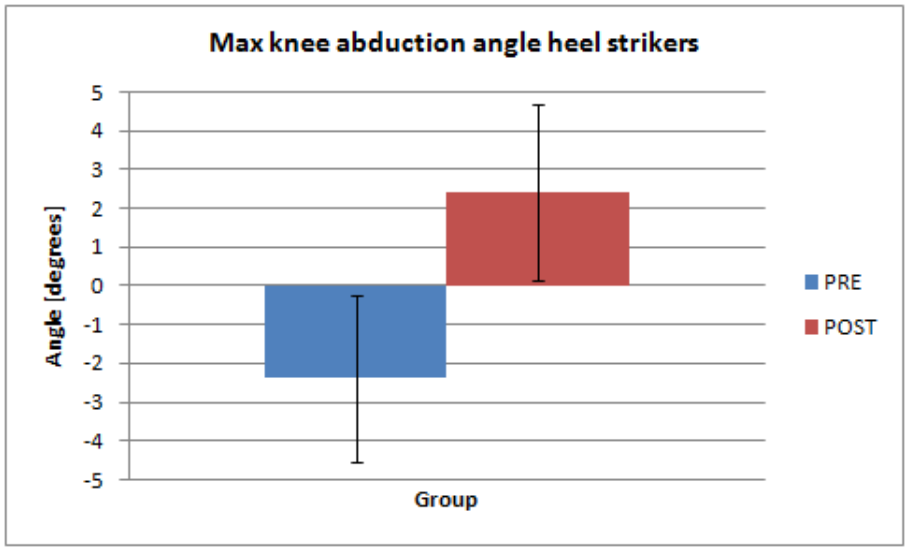

Figure 7.10: Maximum knee abduction angle for heel strikers.

7.1.4 Conclusions

In Figure 7.11 we can see a summary table of the results obtained (mean values and standard deviations), with the values of "p" obtained from the t-tests.

		FOREFOOT STRIKERS		HEEL STRIKERS	
		PRE	POST	PRE	POST
MAXIMUM KNEE FLEXION ANGLE	mean value	55.787	54.655	63.985	77.369
	SD	5.167	4.413	4.354	6.871
	p	0.893		0.015	
ROM KNEE FLEXION	mean value	33.668	32.192	40.822	55.274
	SD	9.070	4.851	3.196	0.997
	p	0.959		0.010	
MAXIMUM KNEE ABDUCTION ANGLE	mean value	-2.284	-0.096	-2.375	2.426
	SD	4.310	4.519	1.851	4.944
	p	0.085		0.124	

Figure 7.11: Summary table of the kinematics results and the "p" values.

Since the number of subjects analyzed was not big enough, the results obtained have a low level of statistical significance, except for two of the results of the heel strikers (with a level of confidence greater than 95%) and one of the results of the forefoot strikers (with a level of confidence greater than 90%) anyway, since this was just a pilot study, even if the other results do not have a statistical significance, we can comment the tendencies of the mean values of the variables in order to give a possible guideline for future studies. Summarizing, from the analysis of the kinematics results we can say that:

- It is possible to highlight with a statistical significance that a decrease of the capacity of control of the knee can be observed for the heel strikers class from an increase of the maximum knee flexion angle and of the range of motion of the knee flexion;
- With a lower level of confidence, we could highlight an increase of the maximum knee abduction angle between pre and post vibrations for the forefoot strikers;
- Even if there is no statistical significance, it was possible to highlight an increase of the maximum abduction angle between pre and post vibrations for the heel strikers and very small variations on the maximum knee flexion angle and on the range of the knee flexion for the forefoot strikers. These results are significant as a guideline of the possible tendency of the variable for a more focused and efficient future study.

- The results regarding the heel strikers class seem more affected by variations between pre and post than the ones related to the forefoot strikers class. This could bring to think that maybe the technique of execution of the movement of the heel strikers is more sensible to the mechanical vibrations compared to the forefoot strikers' one;

- In general, there is a lower dispersion in the data for the heel strikers compared to the forefoot strikers as we could observe in Figures 7.1 and 7.2. This result suggets that maybe the heel strikers have a more similar technique of execution of the movement than the forefoot strikers.

7.2 Dynamics

Before starting any kind of evaluation of the results obtained, we remember that all the joint torques coming from the Inverse Dynamics analysis made with OpenSim are the moments needed to balance the external loads.

Let's present the variables we decided to focus on in order to highlight the effects of the mechanical vibrations on the joint moments of the subjects. All these results have been normalized with respect to the body mass of the subjects, so they are expressed in $[Nm/kg]$:

- Minimum negative moment of flexion of the knee: considering the mechanism of ACL injury presented in chapter 3, the action of the quadriceps muscle has a fundamental role in the occurrence of the injury and considering that the quadriceps is an extensor of the knee, we could relate the possibility of occurrence of ACL injuries with the maximum value of the knee extension moment (minimum of the knee flexion moment with the convention of sign used);

- Minimum negative moment of adduction of the knee: a high valgus loading is recognized as a risk factor for the occurrence of ACL injuries [7], [9]. According with the convention of signs used, the maximum value of valgus (or abduction) loading corresponds to the minimum negative value of the knee adduction moment;

- Range of the moment of flexion of the ankle: since the mechanical vibrations are coming from the foot-ground contact, it seemed interesting to see if those can affect in any way also the ankle dynamics, in particular the range of the ankle flexion moment.

The conventions on the sign of the joint moments presented above are consistent with the conventions on the sign of the joint angles and are presented in Figure 7.12.

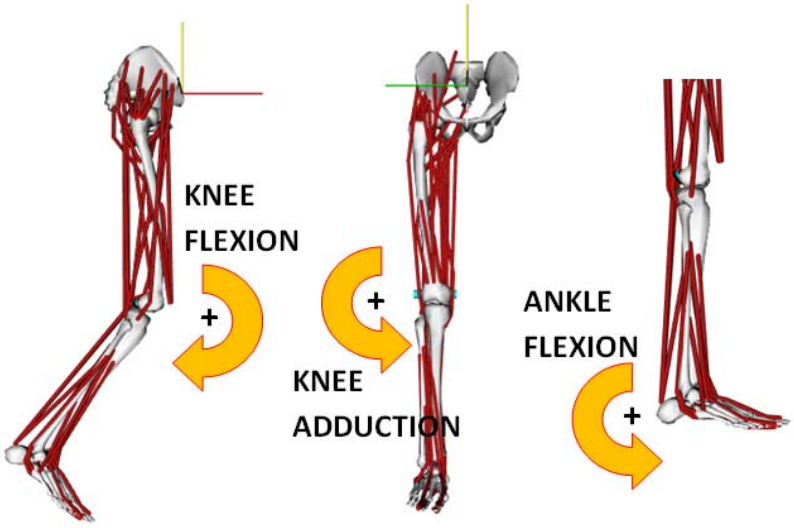

Figure 7.12: Convention on the definition of the signs of the knee flexion moment (on the left), of the knee adduction moment (in the middle) and of ankle flexion moment (on the right).

7.2.1 Minimum negative knee flexion moment

In Figure 7.13 we can see an example of plot of the knee flexion moment, in order to clarify the convention of sign adopted and the meaning of the different peaks highlighted.

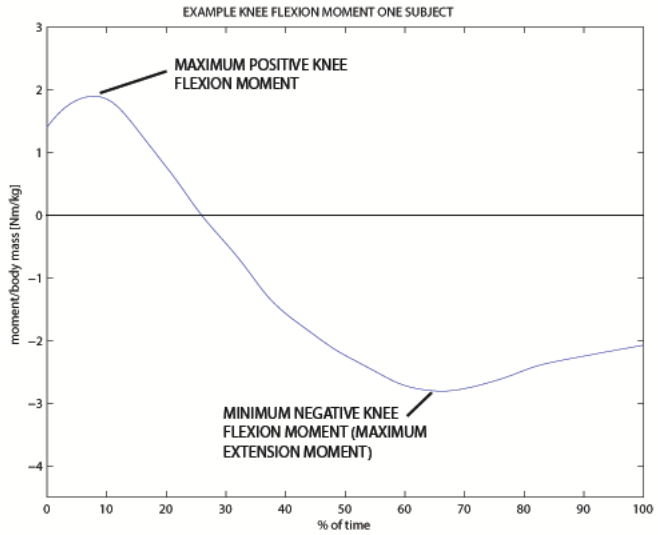

Figure 7.13: Example of knee flexion moment with the convention of sign adopted and the meaning of the peaks.

We can see a comparison of the results of the knee flexion moment for the different subjects in Figure 7.14 for the forefoot strikers (pre on the left and post on the right) and in Figure 7.15

for the heel strikers (pre on the left and post on the right).

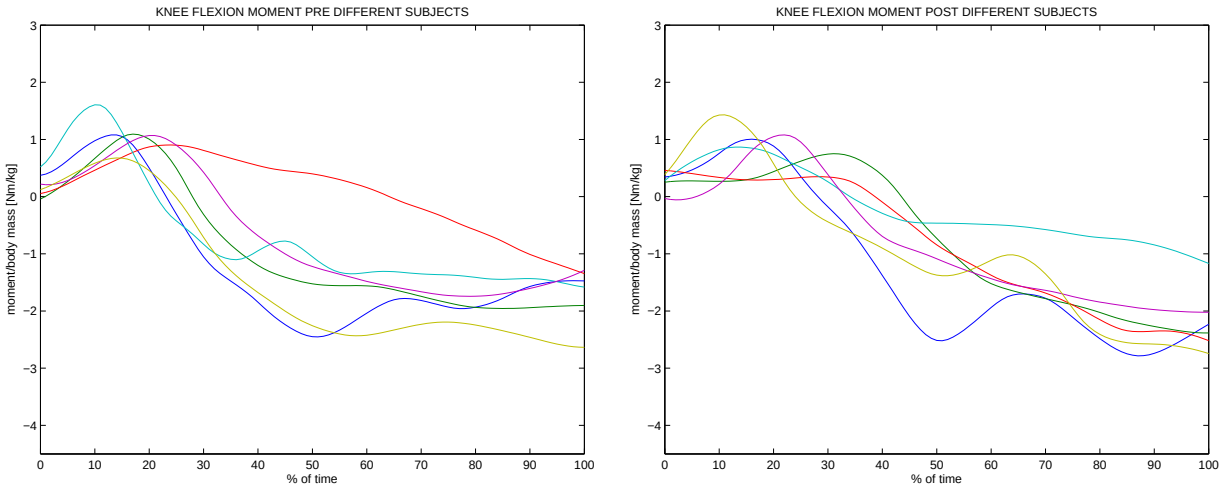

Figure 7.14: Comparison of the knee flexion moments of different subjects for forefoot strikers pre vibrations (on the left) and post vibrations (on the right).

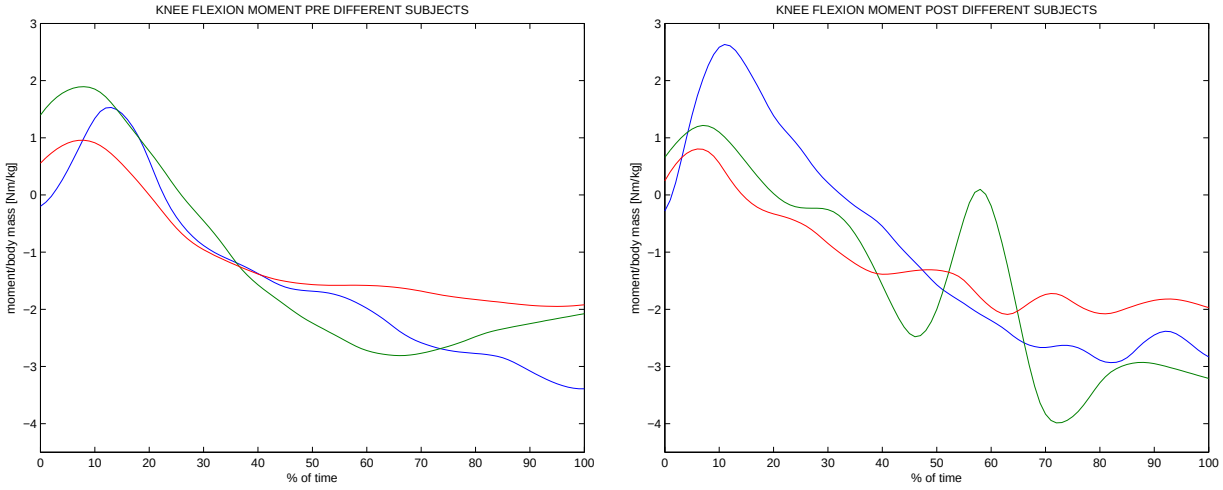

Figure 7.15: Comparison of the knee flexion moments of different subjects for heel strikers pre vibrations (on the left) and post vibrations (on the right).

For the forefoot strikers, as we can see in Figure 7.16 there is an important decrease (around 30%) of the mean value of the minimum knee flexion moment between pre and post vibrations. For the heel strikers, as we can see in Figure 7.17, it is not possible to appreciate any particularvariation of the mean value of the minimum knee flexion moment between pre and post vibrations. For both the classes the value of "p" of the t-test is high (0,191 for the forefoot

strikers and 0,610 for the heel strikers) so the results are not statistically significant.

The tendency for the forefoot strikers is in line with an increase of the risk of occurrence of ACL injuries, but we do not have the statistical significance of the results.

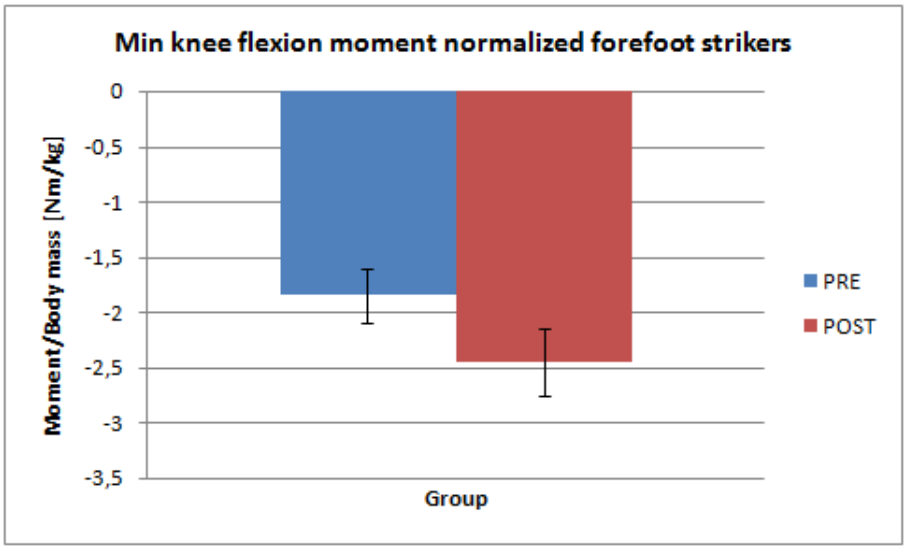

Figure 7.16: Minimum knee flexion moment for forefoot strikers.

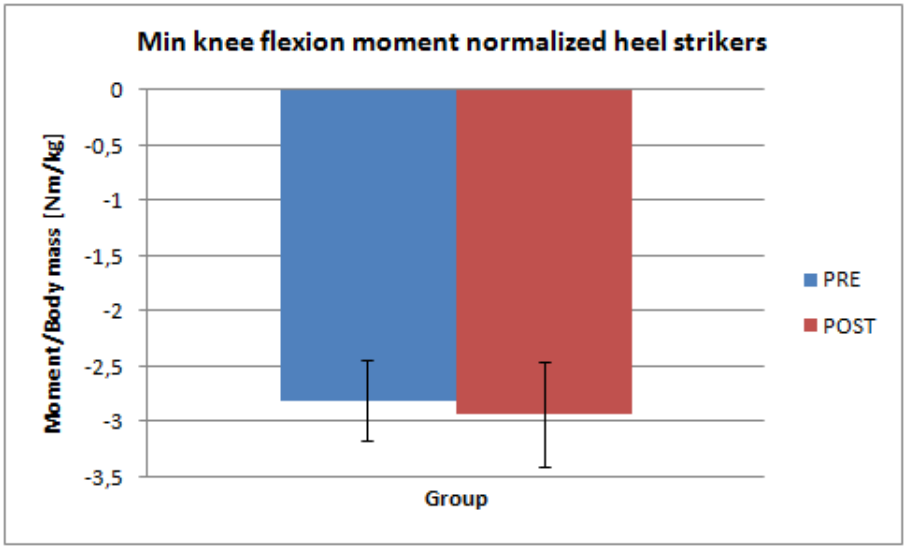

Figure 7.17: Minimum knee flexion moment for heel strikers.

The standard deviation between forefoot strikers and heel strikers for both the classes is similar, so the dispersion of the data is quite similar for this variable, as we could see in Figures 7.14 and 7.15.

7.2.2 Minimum negative knee adduction moment

In Figure 7.18 we can see an example of plot of the knee adduction moment, in order to clarify the convention of sign adopted and the meaning of the different peaks highlighted.

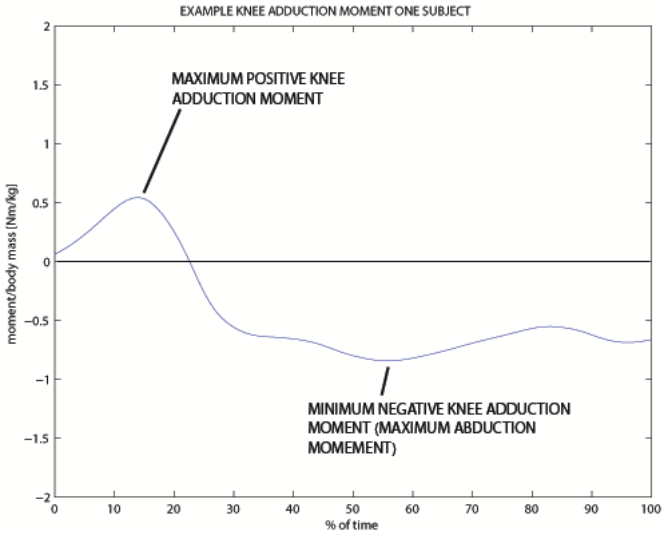

Figure 7.18: Example of knee adduction moment with the convention of sign adopted and the meaning of the peaks.

We can see a comparison of the results of the knee adduction moment for the different subjects in Figure 7.19 for the forefoot strikers (pre on the left and post on the right) and in Figure 7.20 for the heel strikers (pre on the left and post on the right).

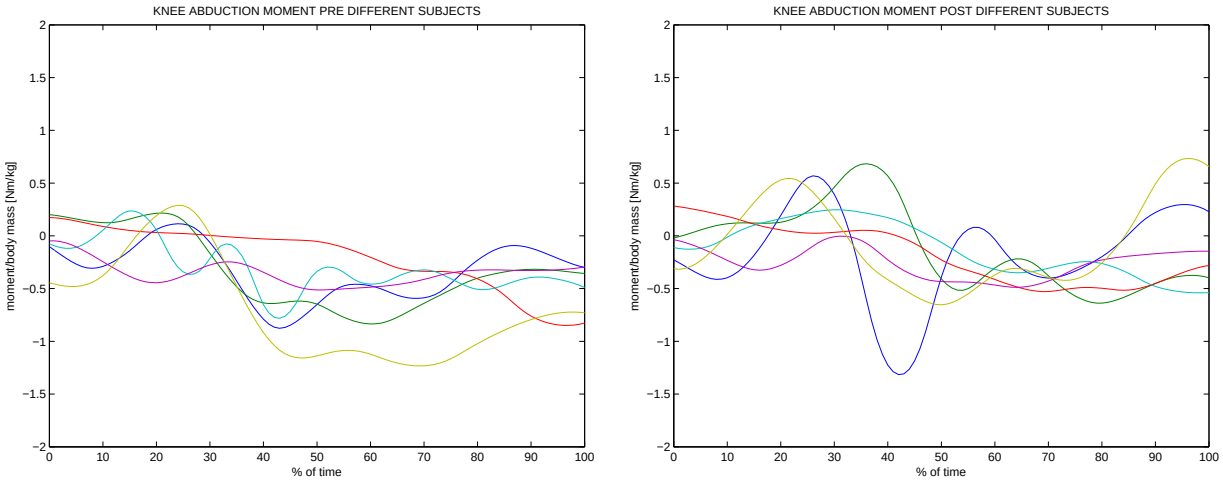

Figure 7.19: Comparison of the knee adduction moments of different subjects for forefoot strikers pre vibrations (on the left) and post vibrations (on the right).

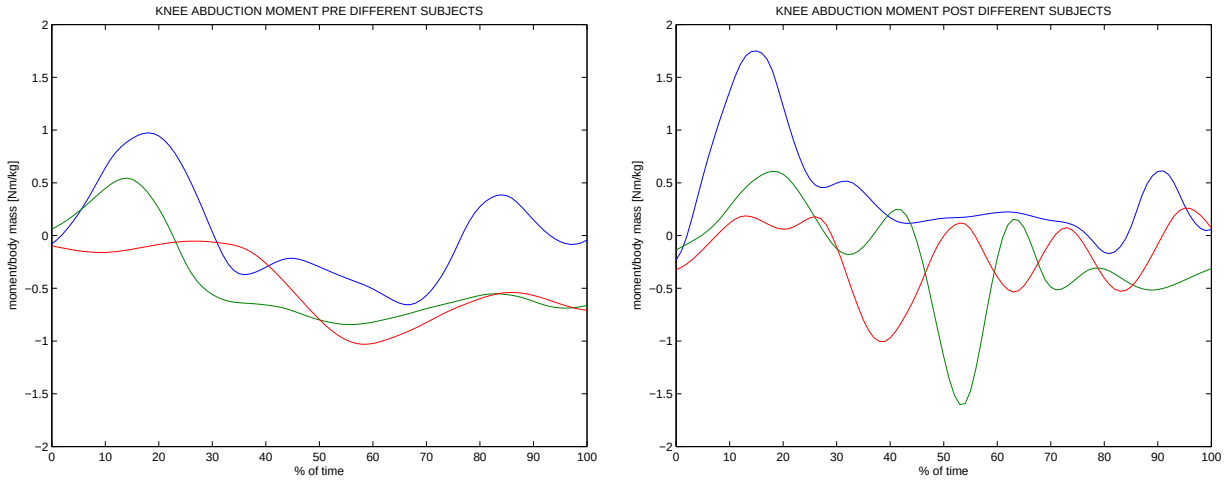

Figure 7.20: Comparison of the knee adduction moments of different subjects for heel strikers pre vibrations (on the left) and post vibrations (on the right).

For the forefoot strikers, as we can see in Figure 7.21, we can observe an important increase of the mean value of the minimum knee adduction moment (around 30%) between pre and post vibrations. This result is not in line with an increase of the risk of occurrence of ACL injuries.

For the heel strikers, as we can see in Figures 7.22, there is an important decrease (around 20%) of the mean value of the minimum knee flexion moment between pre and post vibrations. This result seems in line with an increase of the risk of occurrence of ACL injuries.

For both the classes the value of "p" of the t-test is high (0,322 for the forefoot strikers and 0,796 for the heel strikers) so the results are not statistically significant.

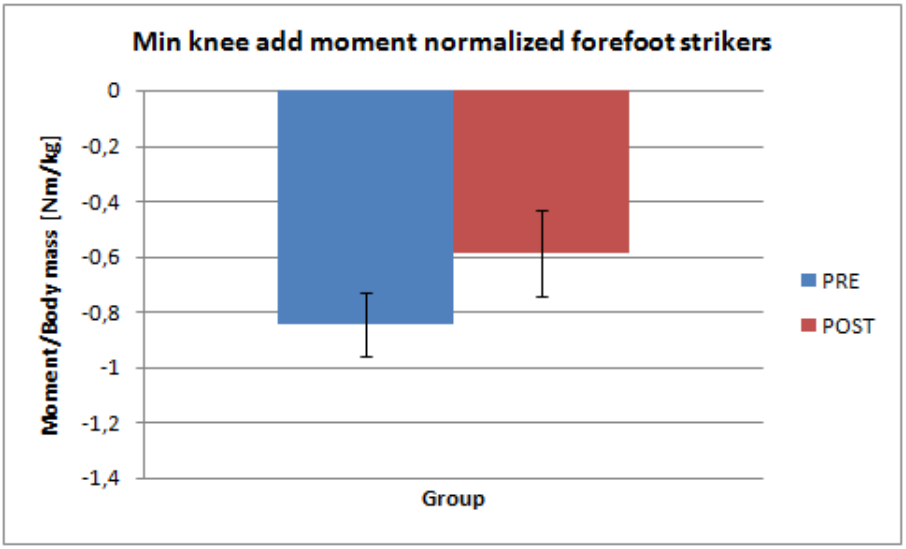

Figure 7.21: Minimum knee adduction moment for forefoot strikers.

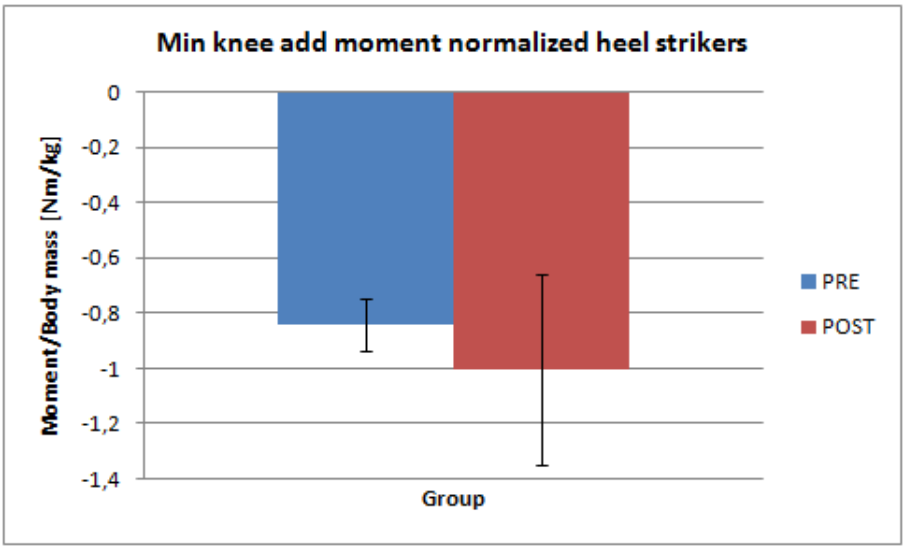

Figure 7.22: Minimum knee adduction moment for heel strikers.

7.2.3 Range of the moment of flexion of the ankle

We can see a comparison of the results of the ankle flexion moment for the different subjects in Figure 7.23 for the forefoot strikers (pre on the left and post on the right) and in Figure 7.24 for the heel strikers (pre on the left and post on the right).

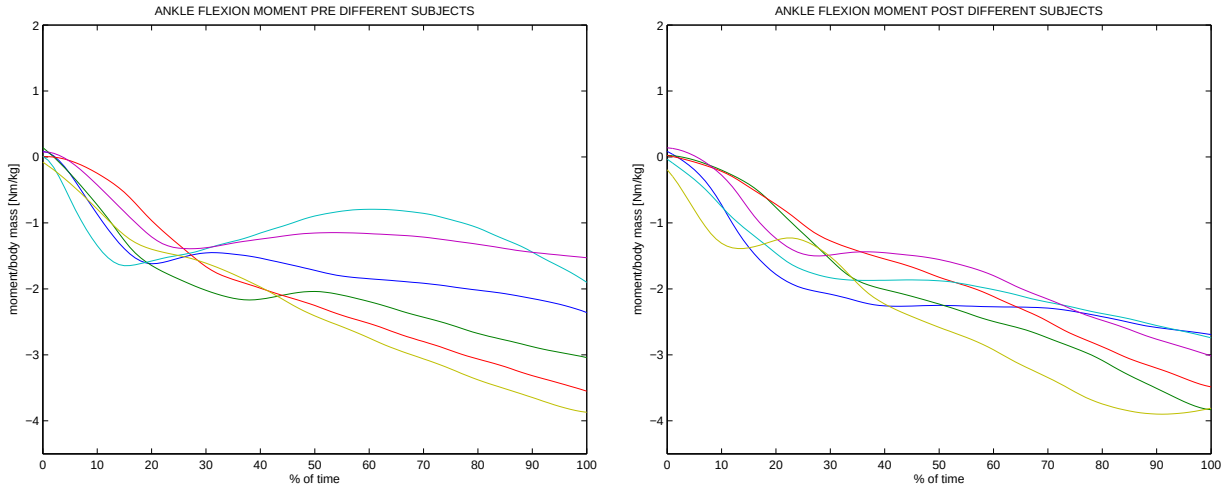

Figure 7.23: Comparison of the ankle flexion moments of different subjects for forefoot strikers pre vibrations (on the left) and post vibrations (on the right).

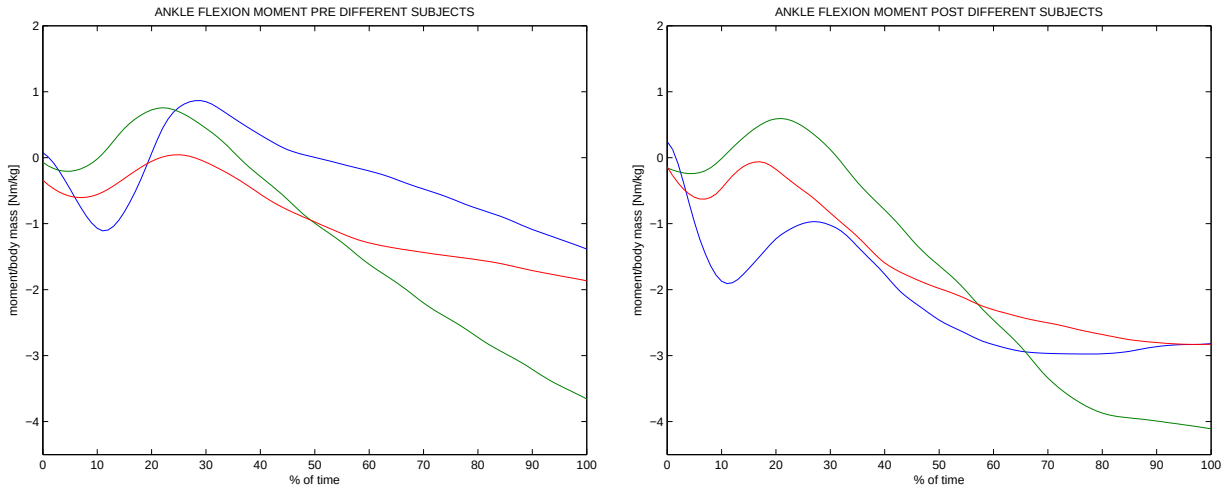

Figure 7.24: Comparison of the ankle flexion moments of different subjects for heel strikers pre vibrations (on the left) and post vibrations (on the right).

For the forefoot strikers class, as we can see in Figure 7.25, the range of the ankle flexion moment increased of more or less the 20% between pre and post. This could be considered as an evident effect of the mechanical vibrations warming-up on the ankle flexion dynamics.

In the heel strikers class as we can see in Figure 7.26, the range of the ankle flexion moment increased of more or less the 40% between pre and post. This could be considered as an evident effect of the mechanical vibrations warming-up on the ankle flexion dynamics.

The values of "p" calculated trough the t-test are lower than 0,1 (0,085 for the forefoot strikers and 0,079 for the heel strikers), so the statistical reliability of the comparisons is good with a level of confidence greater than 90%.

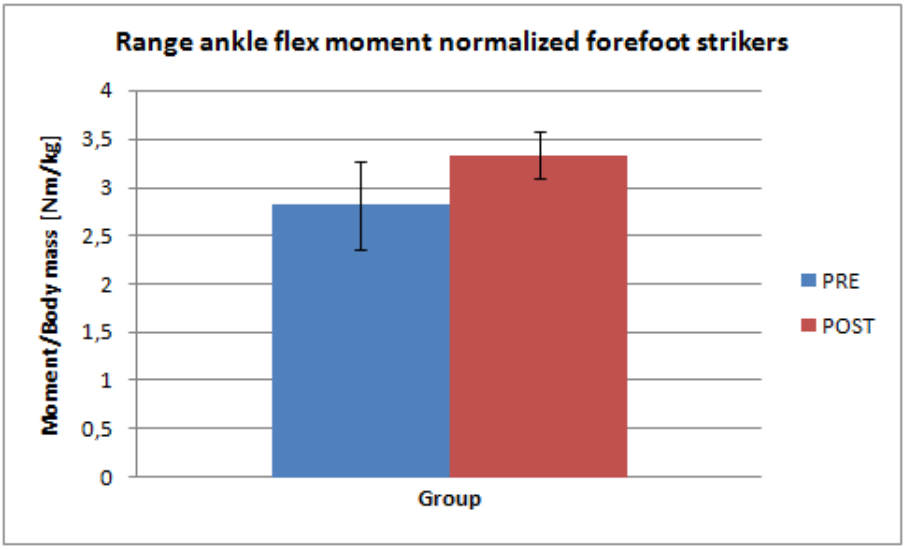

Figure 7.25: Range of the ankle flexion moment for forefoot strikers.

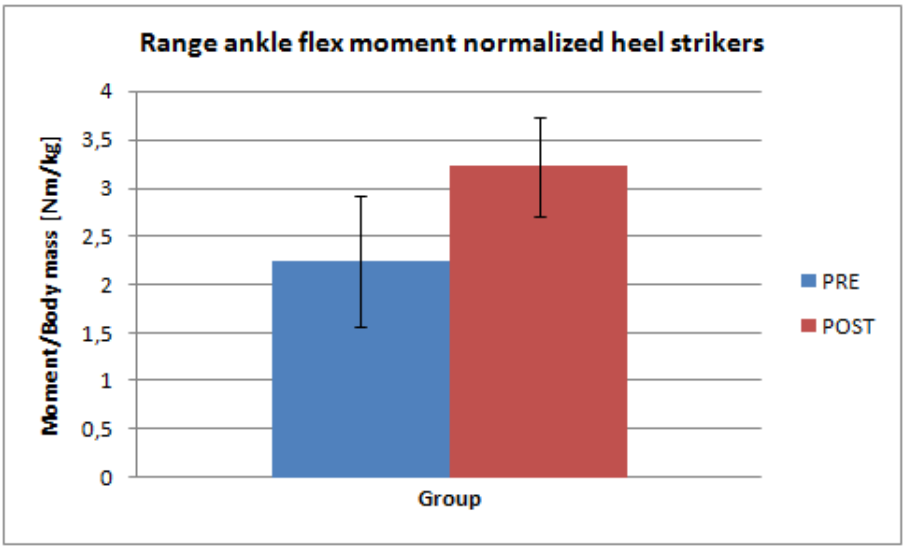

Figure 7.26: Range of the ankle flexion moment for heel strikers.

7.2.4 Conclusions

In Figure 7.27 we can see a summary table of the results obtained (mean values and standard deviations), with the values of "p" obtained from the t-tests.

		FOREFOOT STRIKERS		HEEL STRIKERS	
		PRE	POST	PRE	POST
MIN KNEE FLEXION MOMENT	Mean value	-1.849	-2.451	-2.810	-2.933
	SD	0.504	0.606	0.726	0.951
	p	0.191		0.610	
MIN KNEE ADDUCTION MOMENT	Mean value	-0.842	-0.589	-0.844	-1.004
	SD	0.231	0.311	0.188	0.688
	p	0.322		0.796	
RANGE ANKLE FLEXION MOMENT	Mean value	2.812	3.332	2.250	3.221
	SD	0.899	0.482	1.358	1.012
	p	0.085		0.079	

Figure 7.27: Summary table of the kinematics results and the "p" values.

Since the number of subjects analyzed was not big enough, the results obtained have a low level of statistical significance, except for the results of the range of the ankle flexion moment (with a level of confidence greater than 90% for both the classes) anyway, since this was just a pilot study, even if the other results do not have a statistical significance, we can comment the tendencies of the mean values of the variables. Summarizing, from the analysis of the dynamics results we can say that:

- Between pre and post both for the forefoot strikers and for the heel strikers, it is possible to observe an evident increase on the range of the ankle flexion moment, with a level of confidence greater than the 90%. This can be considered as an effect of the mechanical vibrations warming-up on the ankle flexion dynamics, but it is difficult to relate this with the risk of occurrence of ACL injuries;

- Even if there is no statistical significance, for the heel strikers it is possible to appreciate a relevant decrease of the mean value of the minimum negative knee flexion moment between pre and post. As we said previously a decrease of the minimum knee flexion moment can be related to the action of the knee extensor muscles that have a fundamental role in the mechanism of ACL non contact injury. This result can be a guideline for more focused and efficient future studies.

7.3 Muscular activations

The Static Optimization analysis gave as output the muscular forces and activations estimated by OpenSim sharing the joint moments in the contributions of the different muscles.

The comparison has been made between the muscular activations estimated for the trials pre and post vibrations in order to see if it was possible to highlight any interesting effect due to the mechanical vibrations warming-up. Two different kind of analysis have been made:

- A qualitative analysis looking at the shape of the curves and the peak values;
- A quantitative analysis looking at the value of the integral of the curve of the activation of the muscle.

The integral of the curve of activation of a muscle represents the total amount of energy generated during the execution of the movement and it is proportional to the average level of activation of the muscle. The value of the integral of the curve has been calculated with Matlab using the trapezoidal numerical integration with a resolution of 1%; since the two axes are expressed in percentage, the integral is dimensionless and always lower than 10000. In Figure 7.28 we can see the graphical definition of the integral of a curve of activation of a muscle.

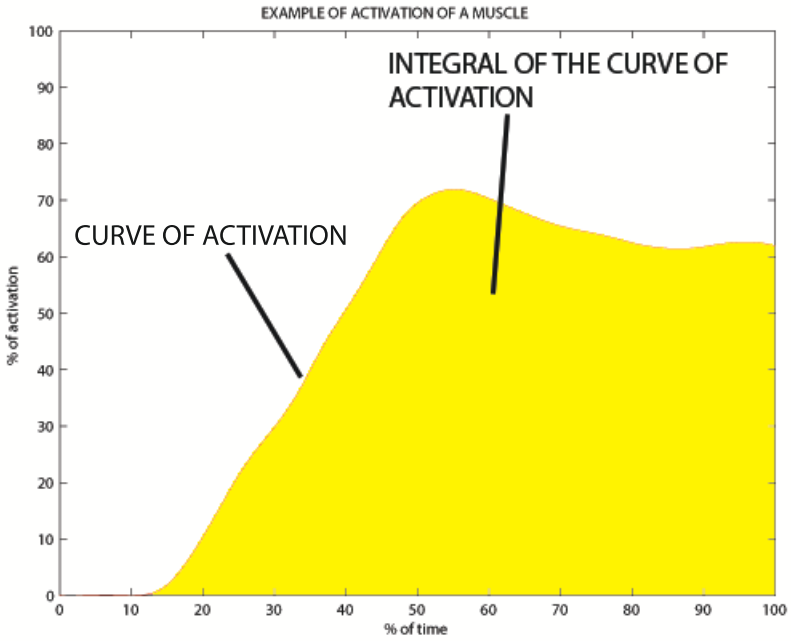

Figure 7.28: Graphical definition of the integral of a curve of activation of a muscle.

The muscles we decided to analyze are the same muscles collected with the EMG system (vastus lateralis, biceps femoris, rectus anterior, semitendinosus and soleus). In this way, in future, it will be possible to make a parallel analysis based on the activations coming from the EMG data and see if it is possible to validate the simulations.

Soleus:

This is one of the main plantar flexors of the ankle. The activation of this muscle presents the most evident differences between pre and post vibrations. For all the subjects it is possible to observe an increase of the maximum value of activation between the pre and the post group. This result is perfectly in accordance with the results of the Inverse Dynamics analysis: in fact a reduction of the minimum ankle flexion moment was highlighted between pre and post vibrations and this suggests an increase of the activity of the muscles responsible of the plantar flexion of the ankle. The trend of the activation is always growing in the time for all the subjects and for all the trials, with the peak of activation very close to the ending of the eccentric phase of the movement.

For the heel strikers we can observe a flat zone on the activation of the soleus near the initial contact of the foot with the floor. Since these subjects are landing with the heel, in the first part of the movement the moment of plantar flexion of the ankle is smaller than for the forefoot strikers, since the toe is not touching the ground yet.

In Figure 7.36 we can observe the curves of the activation of this muscle for the forefoot strikers and for the heel strikers.

The analysis of the integrals of the plots highlighted an increase of the area under the plots between pre and post vibrations both for the forefoot strikers (with a level of confidence of the 97%) and for the heel strikers (with a level of confidence of the 75%). The area under the plots is representative of the level of activation of the muscle during the execution of the movement, so the soleus is more activated post vibrations than pre. The mean values, standard deviations and "p" values coming from the t-test for the soleus can be seen in Figure 7.29.

		FOREFOOT STRIKERS		HEEL STRIKERS	
		PRE	POST	PRE	POST
INTEGRAL SOLEUS	mean	2996.055	3348.548	1323.238	3265.463
	SD	882.008	555.848	522.462	1306.540
	p	0.032381343		0.14697476	

Figure 7.29: Summary table of the integral analysis of the activation of the soleus.

Long head of the biceps femoris:

This is a bi-articular muscle, responsible mainly for the flexion of the knee and for the extension of the hip. For this muscle it is possible to observe a reduction of the maximum values

of activation between pre and post vibrations, as we can see in Figure 7.37.

The shape of most of the activation plots of this muscle, follows a wave with two main peaks and two main valleys.

The analysis of the integrals of the plots highlighted a decrease of the area under the plots between pre and post vibrations both for the forefoot strikers (with a level of confidence of the 99%) and for the heel strikers (with a level of confidence of the 88%). The area under the plots is representative of the level of activation of the muscle during the execution of the movement, so the long head of the biceps femoris is less activated post vibrations than pre. The mean values, standard deviations and "p" values coming from the t-test for the long head of the biceps femoris can be seen in Figure 7.30.

		FOREFOOT STRIKERS		HEEL STRIKERS	
		PRE	POST	PRE	POST
INTEGRAL	mean	4134.980	2561.900	3574.868	2125.516
BICEPS FEMORIS	SD	990.547	884.003	962.318	405.594
LONG HEAD	p	0.006590165		0.130856728	

Figure 7.30: Summary table of the integral analysis of the activation of the long head of the biceps femoris.

Short head of the biceps femoris:

This is a muscle responsible for the flexion of the knee. As we can see in Figure 7.38, in the activation of this muscle it is not possible to observe a unique trend of variation beetween pre and post vibrations.

We can observe that the average level of activation of this muscle is always lower than the one of the long head of the biceps femoris.

The analysis of the integrals of the plots highlighted a decrease of the area under the plots between pre and post vibrations both for the forefoot strikers (with a level of confidence of the 93%) and for the heel strikers (with a level of confidence of the 93%). The area under the plots is representative of the level of activation of the muscle during the execution of the movement, so the short head of the biceps femoris is less activated post vibrations than pre. The mean values, standard deviations and "p" values coming from the t-test for the short head of the biceps femoris can be seen in Figure 7.31.

		FOREFOOT STRIKERS		HEEL STRIKERS	
		PRE	POST	PRE	POST
INTEGRAL BICEPS FEMORIS SHORT HEAD	mean	794.390	409.569	878.519	536.204
	SD	373.622	301.877	428.660	294.162
	p	0.065199368		0.061666112	

Figure 7.31: Summary table of the integral analysis of the activation of the short head of the biceps femoris.

Semitendinosus:

This is a biarticular muscle responsible mainly for the flexion of the knee. For most of the subjects, it is possible to observe an increase on the maximum value of activation of this muscle between pre and post vibrations.

The maximum values of activation reached for two of the three heel strikers, are higher than the ones reached by the forefoot strikers. This suggests that maybe the technique of execution of the movement of the heel strikers requires a more important contribution of this muscle.

The plots for comparing the activation of the semitendinosus muscle among the trials can be seen in Figure 7.39.

As we can observe in Figure 7.32 it is not possible to observe any common tendency of the integral of the activation of this muscle and the level of confidence of these results is very low.

		FOREFOOT STRIKERS		HEEL STRIKERS	
		PRE	POST	PRE	POST
INTEGRAL SEMITENDINOSUS	mean	490.558	514.540	944.520	748.609
	SD	368.965	243.281	484.843	594.380
	p	0.825371941		0.383168249	

Figure 7.32: Summary table of the integral analysis of the activation of semitendinosus.

Vastus lateralis: This muscle is responsible for the extension of the knee. As we can see in Figure 7.40, the maximum value of the activation of this muscle, decreases or stays more or less constant between pre and post vibrations for all the subjects, maintaining also a very similar shape of the curves.

The plots of the activation of this muscle present almost for all the subjects, a flat zone at the beginning, a ramp-up and than another almost flat zone at the end of the cycle. This suggests that the different way of execution of the movement between forefoot strikers and heel

strikers, does not affect significantly the activation patten of this muscle.

The analysis of the integrals of the plots highlighted a decrease of the area under the plots between pre and post vibrations both for the forefoot strikers (with a level of confidence of the 93%) and for the heel strikers (with a level of confidence of the 91%). The area under the plots is representative of the level of activation of the muscle during the execution of the movement, so the vastus lateralis is less activated post vibrations than pre. The mean values, standard deviations and "p" values coming from the t-test for the vastus lateralis can be seen in Figure 7.33.

		FOREFOOT STRIKERS		HEEL STRIKERS	
		PRE	POST	PRE	POST
INTEGRAL	mean	3208.767	2539.553	3975.061	3220.732
VASTUS	SD	969.652	389.981	313.147	230.252
LATERALIS	p	0.062410476		0.085992443	

Figure 7.33: Summary table of the integral analysis of the activation of the vastus lateralis.

Rectus anterior:

This is a biarticular muscle responsible for the extension of the knee. The activation of this muscle, both in the pre and in the post vibrations, is very low for almost all the subjects analyzed as we can see in Figure 7.41. This could seem in disaccordance with the results of the Inverse Dynamics analysis, where we could see a quite low minimum in the knee flexion moments (high knee extension moments).

In order to clarify this question, in Figure 7.35 we can see in red the total knee flexion moment and in other colours the contribution of each muscle to this moment (calculated as force of the muscle multiplied by its lever arm). We can see that the contribution of the rectus anterior to the extension moment is negligible if compared with the contribution of the vastus lateralis (in violet). So we can conclude that the activation of the rectus anterior is very low because the cknee extension moment is exerted mainly by the vastus lateralis.

The analysis of the integrals of the plots highlighted an increase of the area under the plots between pre and post vibrations both for the forefoot strikers and for the heel strikers but with a very low level of confidence (lower than the 60%). The area under the plots is representative of the level of activation of the muscle during the execution of the movement, so the rectus anterior is more activated post vibrations than pre. The mean values, standard deviations and "p" values coming from the t-test for the rectus anterior can be seen in Figure 7.34.

		FOREFOOT STRIKERS		HEEL STRIKERS	
		PRE	POST	PRE	POST
INTEGRAL	mean	12.466	15.185	34.938	81.836
RACTUS	SD	182.087	515.170	26.300	687.141
ANTERIOR	p	0.457001925		0.410345421	

Figure 7.34: Summary table of the integral analysis of the activation of the rectus anterior.

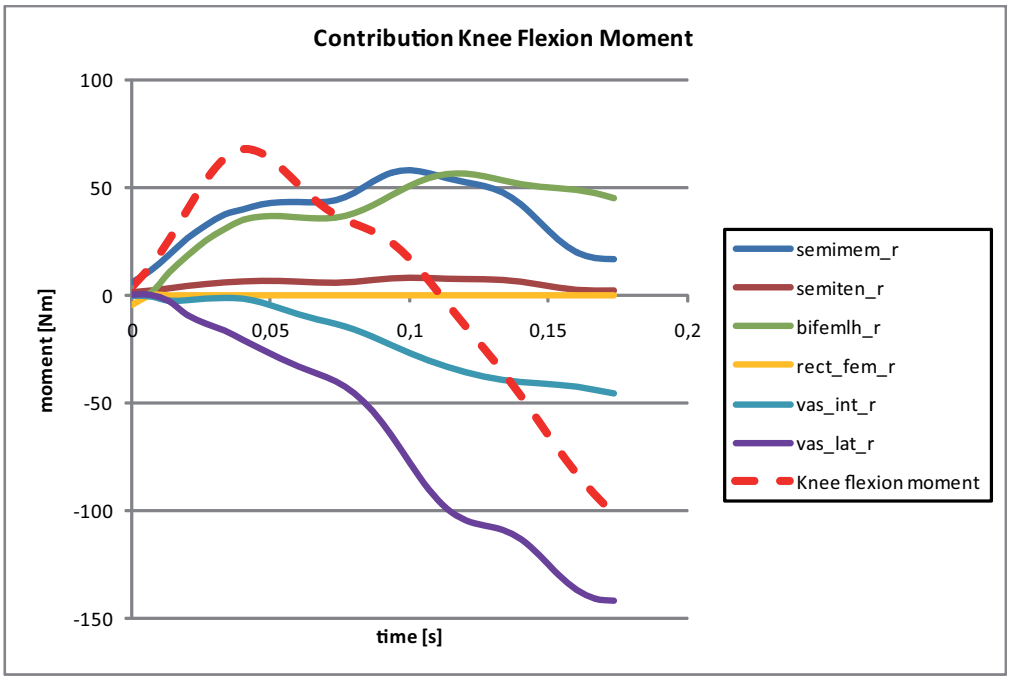

Figure 7.35: Example of the contribution of each muscle to the knee flexion moment for one of the forefoot strikers.

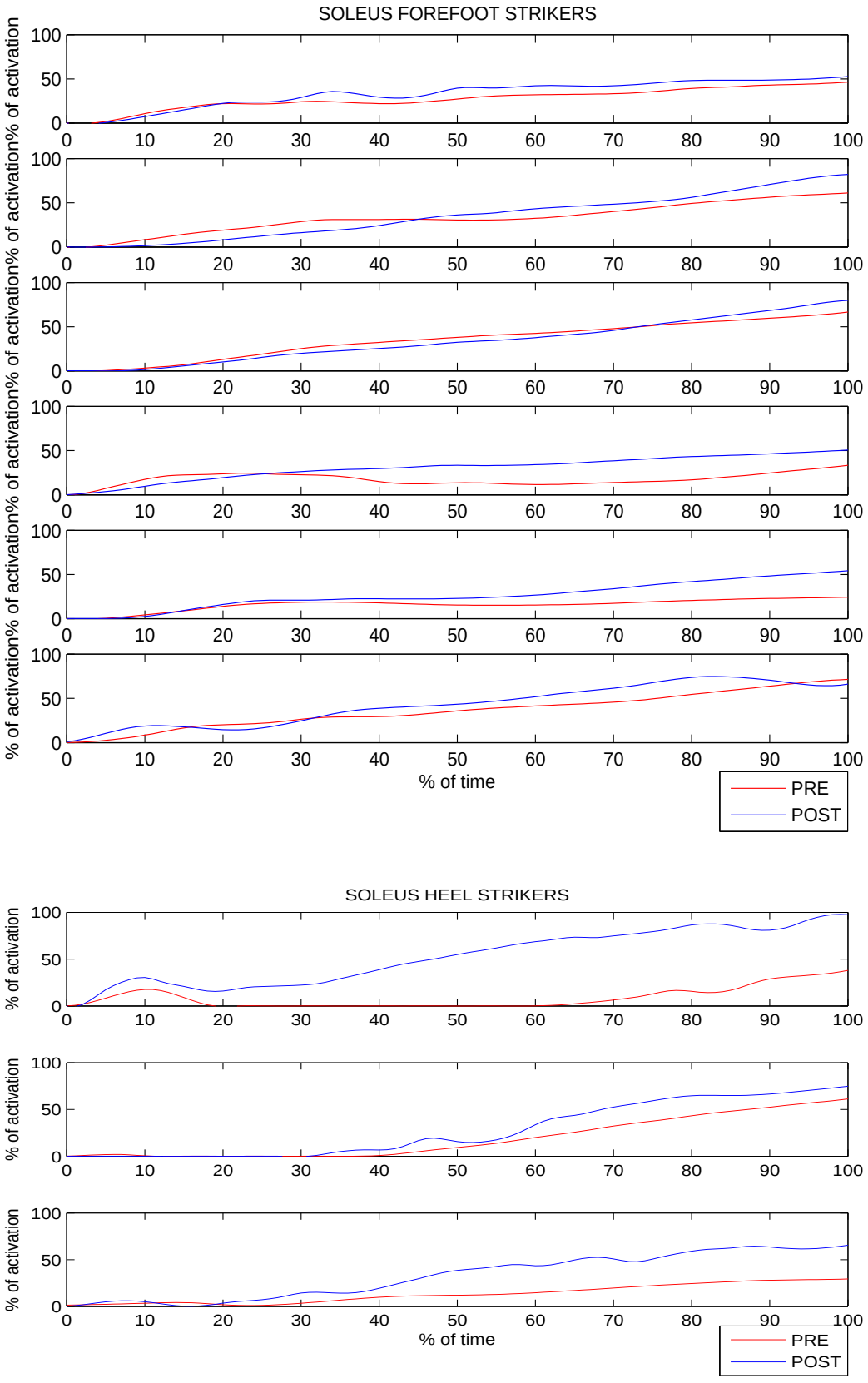

Figure 7.36: Comparison of the activation of the soleus for forefoot strikers (above) and heel strikers (below) pre vibrations and post vibrations.

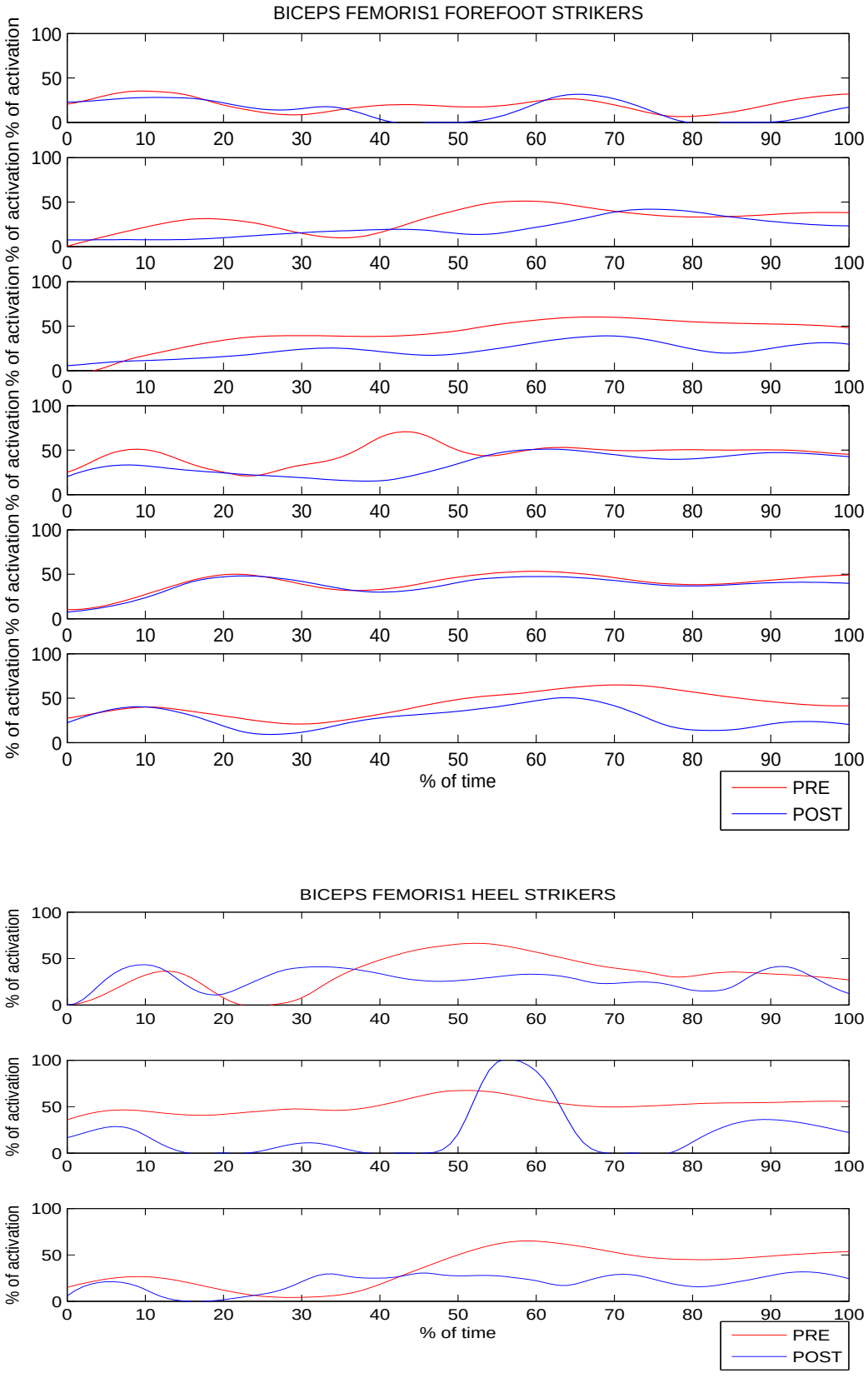

Figure 7.37: Comparison of the activation of the long head of the biceps femoris for forefoot strikers (above) and heel strikers (below) pre vibrations and post vibrations.

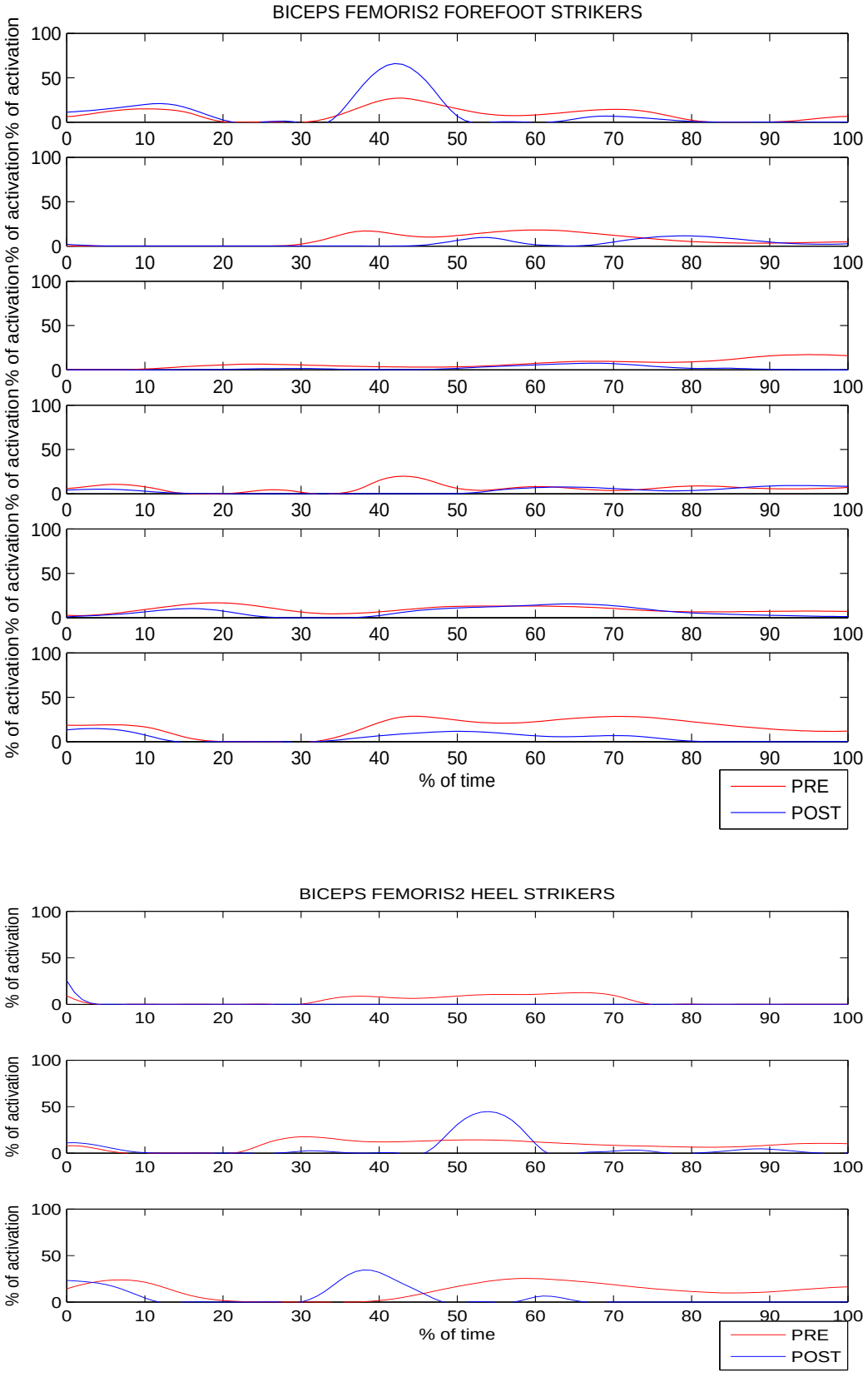

Figure 7.38: Comparison of the activation of the short head of the biceps femoris for forefoot strikers (above) and heel strikers (below) pre vibrations and post vibrations.

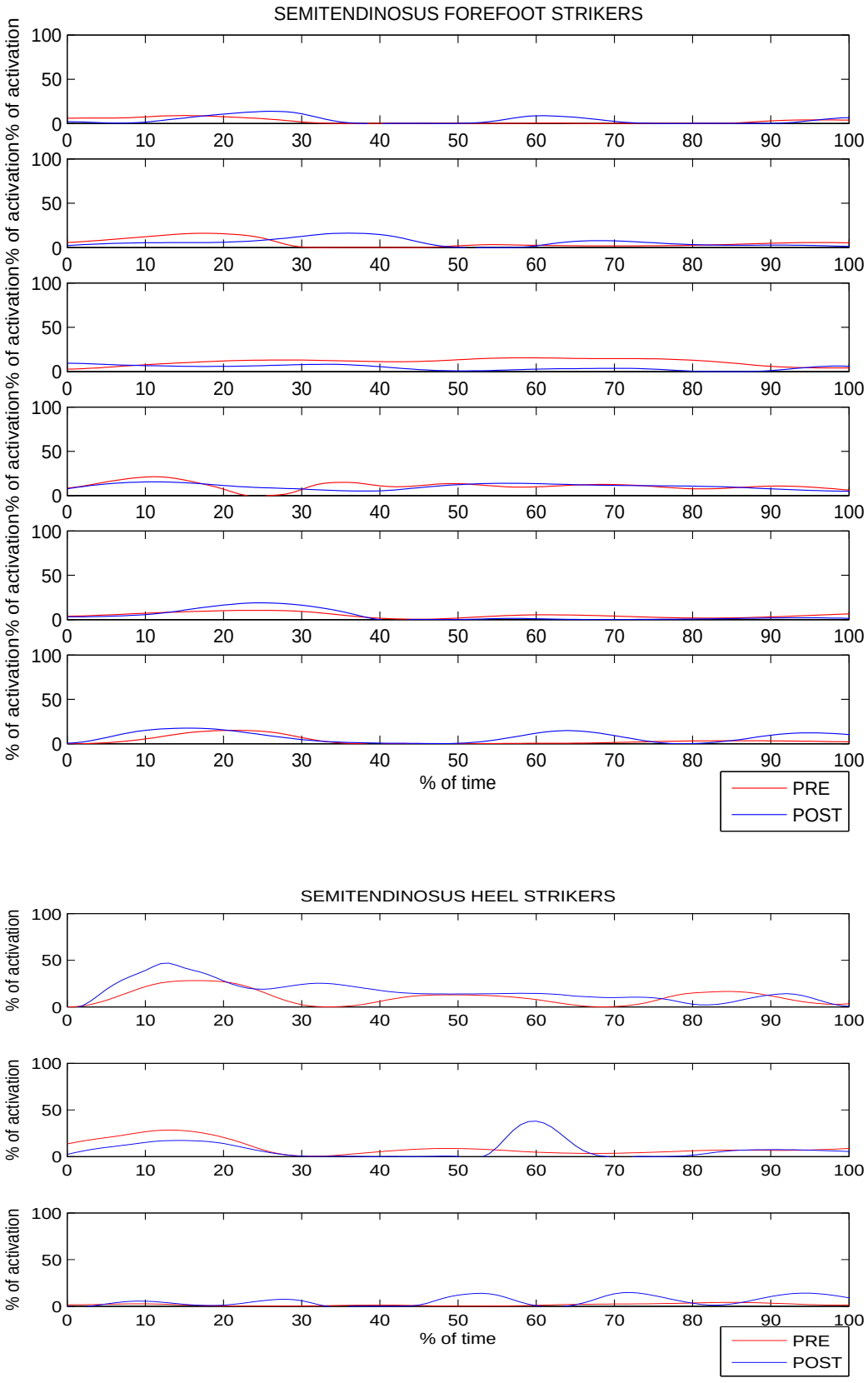

Figure 7.39: Comparison of the activation of the semitendinosus for forefoot strikers (above) and heel strikers (below) pre vibrations and post vibrations.

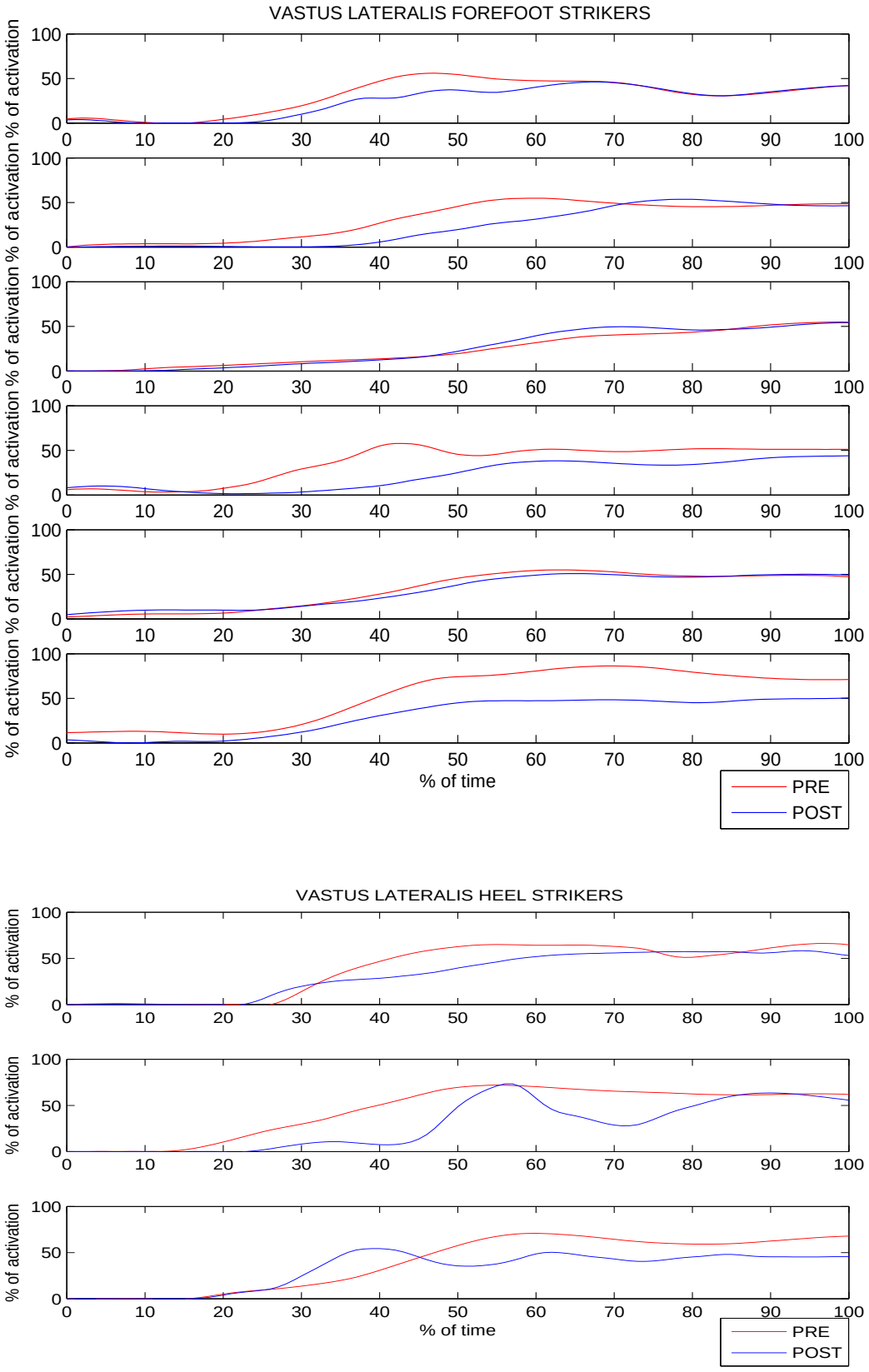

Figure 7.40: Comparison of the activation of the vastus lateralis for forefoot strikers (above) and heel strikers (below) pre vibrations and post vibrations.

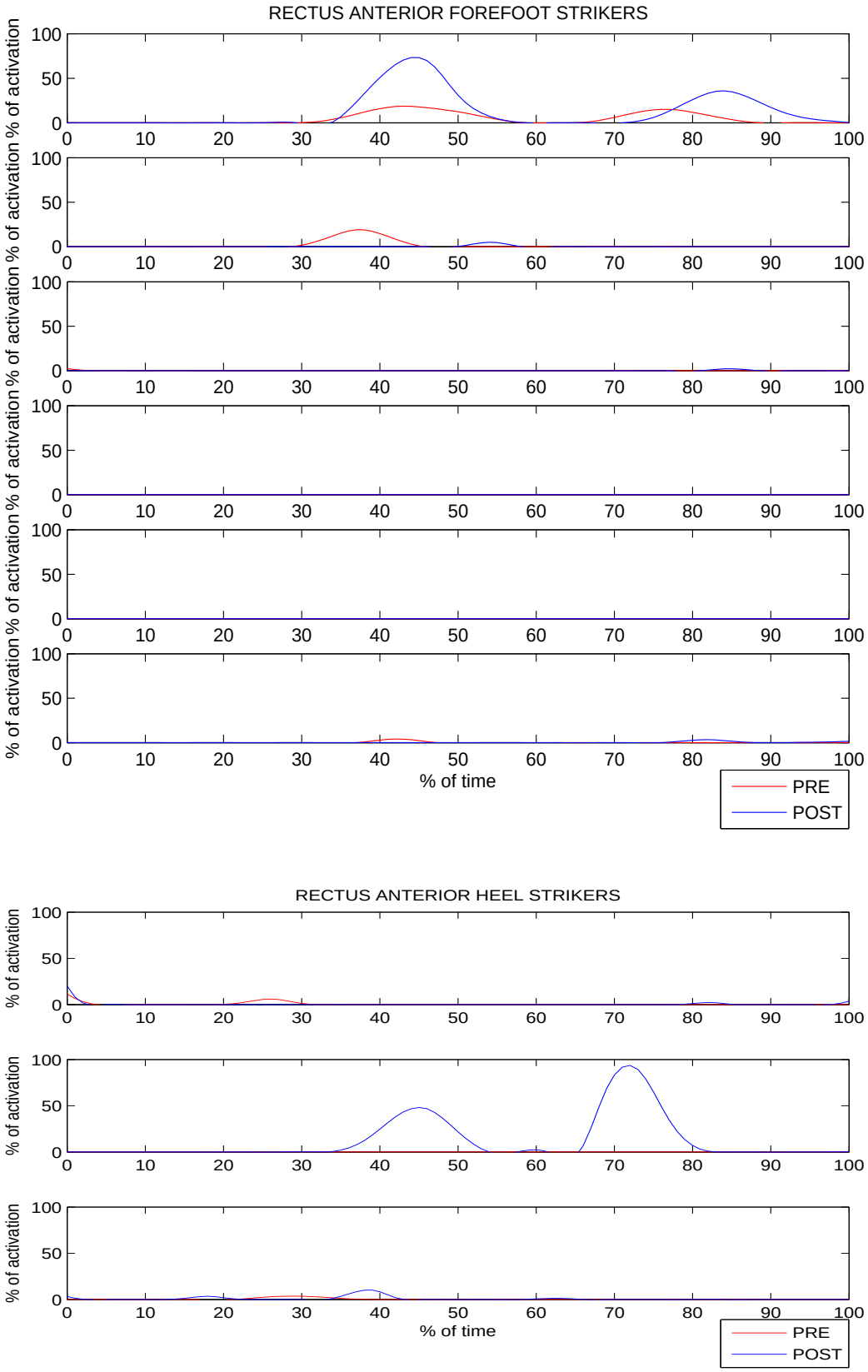

Figure 7.41: Comparison of the activation of the rectus anterior for forefoot strikers (above) and heel strikers (below) pre vibrations and post vibrations.

A summary table with mean values, standard deviations and "p" values of the integral of the muscular activations can be seen in Fugure 7.42.

		FOREFOOT STRIKERS		HEEL STRIKERS	
		PRE	POST	PRE	POST
INTEGRAL SOLEUS	mean	2996.055	3348.548	1323.238	3265.463
	SD	882.008	555.848	522.462	1306.540
	p	0.032		0.147	
INTEGRAL BICEPS FEMORIS LONG HEAD	mean	4134.980	2561.900	3574.868	2125.516
	SD	990.547	884.003	962.318	405.594
	p	0.007		0.131	
INTEGRAL BICEPS FEMORIS SHORT HEAD	mean	794.390	409.569	878.519	536.204
	SD	373.622	301.877	428.660	294.162
	p	0.065		0.062	
INTEGRAL SEMITENDINOSUS	mean	490.558	514.540	944.520	748.609
	SD	368.965	243.281	484.843	594.380
	p	0.825		0.383	
INTEGRAL VASTUS LATERALIS	mean	3208.767	2539.553	3975.061	3220.732
	SD	969.652	389.981	313.147	230.252
	p	0.062		0.086	
INTEGRAL RECTUS ANTERIOR	mean	12.466	15.185	34.938	81.836
	SD	182.087	515.170	26.300	687.141
	p	0.457		0.410	

Figure 7.42: Summary table of the integral analysis of the activation of the muscles analyzed.

In the following chapter we will analyze the economic and environmental aspects related to this project of thesis; in particular the economic cost of the project, its environmental impact and the aspects related to the social cost of the ACL injuries.

Chapter 8

Economic and environmental aspects

8.1 Economic cost of the project

The economic cost of this project is mainly represented by:

- The depreciation of the instrumentation and the software used during the project;
- The cost of the time of working of all the people involved in it;
- The cost of the consumable material.

The equipment used during the project is composed by:

- The instrumentation of the laboratory of the CAR composed by the motion capture system (including the computer and the software licenses), the force platform, the EMG system and the mechanical vibrations machine;
- The computer of the office of the ETSEIB used by the student.

For the instrumentation of the laboratory of the CAR we can estimate an average operating life of 8 years, considering a utilization of 45 weeks per year and for a weekly use of 10 hours. The total number of operating hours of the equipment is 3600 hours.

For the computer of the ETSEIB we can estimate an average operating life of 5 years, considering a utilization of 45 weeks per year and a weekly use of 50 hours. The total number of operating hours of the computer is 11250.

The effective use of the lab equipment to make 9 motion captures has been 18 hours. Since the motion capture system is a visible light video system and not an infrared video system, the

process of reconstruction of the trajectories of the markers and preparation of the data to feed OpenSim have been quite long and can be estimated in 2 hours for each subject yielding a total of 18 hours.

The student spent 630 hours working with the computer of the office in order to find information and bibliography, to study the operation of the software used, to process the data, to analyze the results and to write the final report of the master thesis. The calculation of the depreciation of the equipment is resumed in Table 7.1 and the total cost of depreciation is 363,90 €.

Considering the cost of working of the people involved in the project we have to distinguish between the work of the student and the work of the people at the laboratory.

The execution of the tests has been made by four people, two of them were students and two of them were internal employees of the CAR. The salary recommended by the ETSEIB for an engineering student is of 8 €/h and the salary of an employee of the CAR is 16 €/h. The total cost of the work of the people involved in the execution of the tests can be quantified in:

$$8€/h \cdot 18h + 16€/h \cdot 18h = 432€ \tag{8.1}$$

The preparation of the data to feed OpenSim has been made by one student and the cost of his work can be quantified in:

$$8€/h \cdot 18h = 144€ \tag{8.2}$$

For the total time of 630 hours, the cost of the work of the student can be quantified in:

$$8€/h \cdot 630h = 5040€ \tag{8.3}$$

So, the total labor cost is:

$$432€ + 144€ + 5040€ = 5616€ \tag{8.4}$$

We decided to neglect the cost due to the electricity consumption, because the use of electricity hasn't involved any significant increase on the consumption at CAR and ETSEIB.

We have to consider also the cost of the consumable material used during the execution of the tests (double side tape, disposable electrodes, material for preparing the skin for the EMG, etc.) that can be quantified in 60 €.

Equipment	Total cost [€]	Operating life [h]	Depreciation per hour [€/h]	Time of use [h]	Cost of depreciation [€]
Motion capture system Peak Motus 9.2.0 + computer	16000	3600	4,4	36	160,00
Force platform Kistler 9281B	12000	3600	3,33	18	60,00
EMG system Mega WBA	16200	3600	4,5	18	81,00
Mechanical vibrations machine ViBalance	2500	3600	0,69	18	12,50
Computer	900	11250	0,08	630	50,40
					TOTAL [€]
					363,90

Table 7.1: Calculation of the depreciation of the equipment.

Summing all the contributions of cost, we can say that the total cost of the execution of the project has been:

$$363,90€ + 5616€ + 60€ = 6039,90€ \tag{8.5}$$

8.2 Environmental impact of the project

The environmental impact of this project is reduced because no significant waste has been generated during it. The only waste we can talk about is the double side tape used to attach the markers on the skin and the disposable electrodes. We can quantify the double side tape consummate in 3 *cm* for each marker for 12 markers for each subject and for 10 subjects for a total of 360 *cm* of tape. The number of disposable electrodes used during the execution of the test is around 150.

Regarding the waste coming from the instrumentation at the end of its life cycle we know that the treatment of each of its components has to be respectful with the European Directive UE 2002/96/CE.

8.3 Aspects related to the social cost of ACL injuries

Each year just in the United States there are up to 100000 cases of ACL injuries. It's difficult to quantify which could be the real social cost of an ACL injury, because there are many things that have to be considered and that should be analyzed in each case. Anyway we can identify generally and list which are these costs. The treatment of a patient with ACL injury implies a long procedure. Depending on the kind of life of the patient, the patient can decide to go on a conservative treatment or on a surgery reconstruction.

The conservative treatment is suggested to people that do not need to re-obtain a full functionality of the knee. This kind of treatment provides the rehabilitation with the aim of increasing the tone of some muscles and making some postural changes. The shear force that cannot be absorbed by the ACL has to be absorbed principally by the tendon of the quadriceps but without an active action of it, because the action of this muscle is responsible of an anterior translation of the tibia respect to the femur (that is not constrained because the ACL is broken) Instead the biceps, the semitendinosus and the semimembranous are stabilizers of the knee and their active action is important in order to reduce the anterior translation of the tibia with respect to the femur. After the rehabilitation most of the patients have to go on using orthopaedic braces in

order to maintain a better stability of the joint. The time of conservative treatment can change a lot between different patients but it is more or less of 2-3 months.

The surgery reconstruction is suggested to people that want to re-obtain a full functionality of the knee. The surgery consists on the reconstruction of the ligament using natural tissues (parts of tendons coming from the patient himself or ligaments coming from cadavers), synthetic tissues (polyethylene terephthalate PET or polytetrafluoroethylene PTFE) or synthetic matrices where the tissue can be regenerated from the organism. After the surgery there is a long period of rehabilitation before re-obtaining the full functionality of the knee; the lasting of this period can change from 4 to 6 months depending on the kind of surgery, the kind of rehabilitation and the kind of patient.

In both options, the rehabilitation of the patient lasts some months and during this period the rehabilitation facilities and staff have to be paid by the community if the National Health Service provides the treatment. The same thing holds for the surgery and the hospital stay in the case of surgery.

Another social cost that has to be considered is the economic support to the patient during the period of convalescence.

In the following chapter we will summarize the most significant results obtained from this work and we will give some recommedations for a future continuation and deepening of the work.

Chapter 9

Conclusions and recommendations

This thesis is part of a collaborative project between the UPC, the CAR of Sant Cugat and the University of Lleida in order to investigate which is the influence of a mechanical vibrations warming up on the capacity of control of the lower limb movement.

The aim of the present work was mainly to contribute to the whole project with the part of biomechanical analysis using the OpenSim software.

A customized biomechanical model of the right leg and the pelvis was created starting from the original musculoskeletal model "Gait2392_Simbody" freely available with the software OpenSim version 3.1.

Starting from the data collected at the Biomechanics Laboratory at CAR, it was possible to make a scaling of the models based on the anthropometry of the subjects and perform:

- An Inverse Kinematics analysis in order to obtain information about the joint angles;
- An Inverse Dynamics analysis in order to obtain information about the joint moments;
- A Static Optimization in order to obtain information about the muscle activations and forces.

For the analysis of the obtained results we had to split the subjects in two classes: heel strikers and forefoot strikers, according with the way the subjects landed from the jump onto the ground.

The analysis of the data was focused on finding significant differences in the considered variables between the trials pre and post mechanical vibrations warming-up. It was possible to appreciate some relevant differences between pre and post vibrations in the kinematics and in the dynamics.

From the analysis of the experimental results it was possible to highlight between pre and post vibrations the following results:

- A decrease of the 9% on the peak of the vertical force for the heel strikers with a level of confidence of the 98%;
- Not very important variations on the load rising rate for the heel strikers with a level of confidence of the 90%;
- An increase of the 22% on the time of duration of the cycle for the heel strikers with a level of confidence of the 78%;
- Since the statistical significance of the other experimental results was not very high, these can be considered as guidelines for future studies with a higher number of subjects.

From the analysis of the kinematics and dynamics numerical results it was possible to highlight between pre and post vibrations the following results:

- An increase of 13° on the maximum knee flexion angle for the heel strikers with a level of confidence of the 98,5%;
- An increase of 14° on the range of motion of the knee flexion for the heel strikers of the 99%;
- An increase on the maximum knee abduction angle of 2,2° for the forefoot strikers with a level of confidence of the 91,5% and an increase of 4,8° for the heel strikers with a level of confidence of the 87,6%;
- An increase on the range of the ankle flexion moment of the 18% for the forefoot strikers with a level of confidence of the 91,5% and an increase of the 43% for the heel strikers with a level of confidence of the 92,1%;
- An decrease of the 32% on the minimum negative knee flexion moment for the forefoot strikers with a level of confidence of the 81%.

From the analysis of the numerical results of the integral of the activations of the muscles it was possible to highlight between pre and post vibrations the following results:

- For the soleus an increase of the 11% for the forefoot strikers with a level of confidence of the 97% and an increase of the 146% for the heel strikers with a level of confidence of the 75%;

- For the long head of the biceps femoris a decrease of the 38% for the forefoot strikers with a level of confidence of the 99% and a decrease of the 40% for the heel strikers with a level of confidence of the 88%;
- For the short head of the biceps femoris a decrease of the 48% for the forefoot strikers with a level of confidence of the 93% and a decrease of the 38% for the heel strikers with a level of confidence of the 94%;
- For the vastus lateralis a decrease of the 20% for the forefoot strikers with a level of confidence of the 93% and a decrease of the 18% for the heel strikers with a level of confidence of the 91%.

The study made for this thesis can be considered as an adequate pilot study in order to have an idea of the trends of the variables, to highlight the limits of the protocols used during the project and to give some suggestions for a more efficient and targeted future study.

In what follows, some recommendations for future work are given. First of all, a higher number of subjects could make it possible to obtain a statistical evaluation of the results. Moreover, a higher number of markers could increase the level of precision of the movement analysis.

The use of a visible light motion capture system allows to make captures in particular environmental conditions. However, in our case, since the tests were made in laboratory conditions, it would have been better to use an infrared motion capture system because the process of markers trajectory detection and reconstruction would have been easier and less time consuming.

As we said previously, it would be interesting to make an evaluation of the reliability of the muscular model used, comparing the results obtained for the estimation of the muscular activations with the EMG data. In order to normalize the activations coming from the EMG system, it would be useful to make the exercises of maximum voluntary contraction for each subject.

The experience of working abroad for a project of thesis was very interesting and helped me to grow both professionally and as person. Certainly the organization of a project in collaboration among different partners is more challenging than a project organized and done by the same partner, but it allows to learn more about different ways of working and solving problems.

Chapter 10

Appendix

10.1 Model parameters

Starting from the original "Gait2392_Simbody" model, some changes have been made in order to make the model useful for our analysis.

Deleting the torso and the left leg, the bodies left in our model were the ones described in Table 10.1:

Bodies of the model:
ground
pelvis
femur_r
tibia_r
talus_r
calcn_r
toes_r

Table 10.1: Bodies of our modified model.

Since we wanted the knee to have 3 degrees of freedom, we added manually in the code that describes all the characteristics of the model, the two missing degrees of freedom. In the part of the code that describes the "tibia_r" there is a section called "Joint" where we can find the definition of the "knee_r". In this part the coordinates of the joint are described and the modified part is the following:

```
<CoordinateSet>
        <objects>
                <Coordinate name="knee_flexion_r">
                        <!--Coordinate can describe rotational,
                            translational, or coupled motion. Defaults
                             to rotational.-->
                        <motion_type>rotational</motion_type>
                        <!--The value of this coordinate before any
                            value has been set. Rotational coordinate
                            value is in radians and Translational in
                            meters.-->
                        <default_value>0</default_value>
                        <!--The speed value of this coordinate before
                             any value has been set. Rotational
                            coordinate value is in rad/s and
                            Translational in m/s.-->
                        <default_speed_value>0</default_speed_value>
                        <!--The minimum and maximum values that the
                            coordinate can range between. Rotational
                            coordinate range in radians and
                            Translational in meters.-->
                        <range>-2.0943951 0.17453293</range>
                        <!--Flag indicating whether or not the values
                             of the coordinates should be limited to
                            the range, above.-->
                        <clamped>false</clamped>
                        <!--Flag indicating whether or not the values
                             of the coordinates should be constrained
```

```
                to the current (e.g. default) value, above
                .-->
            <locked>false</locked>
            <!--If specified, the coordinate can be
                prescribed by a function of time. It can
                be any OpenSim Function with valid second
                order derivatives.-->
            <prescribed_function />
            <!--Flag indicating whether or not the values
                 of the coordinates should be prescribed
                according to the function above. It is
                ignored if the no prescribed function is
                specified.-->
            <prescribed>false</prescribed>
        </Coordinate>
        <Coordinate name="knee_rotation_r">
            <!--Coordinate can describe rotational,
                translational, or coupled motion. Defaults
                 to rotational.-->
            <motion_type>rotational</motion_type>
            <!--The value of this coordinate before any
                value has been set. Rotational coordinate
                value is in radians and Translational in
                meters.-->
            <default_value>0</default_value>
            <!--The speed value of this coordinate before
                 any value has been set. Rotational
                coordinate value is in rad/s and
                Translational in m/s.-->
            <default_speed_value>0</default_speed_value>
            <!--The minimum and maximum values that the
                coordinate can range between. Rotational
                coordinate range in radians and
```

```
            Translational in meters.-->
        <range>-0.4 0.4</range>
        <!--Flag indicating whether or not the values
            of the coordinates should be limited to
            the range, above.-->
        <clamped>false</clamped>
        <!--Flag indicating whether or not the values
            of the coordinates should be constrained
            to the current (e.g. default) value, above
            .-->
        <locked>true</locked>
        <!--If specified, the coordinate can be
            prescribed by a function of time. It can
            be any OpenSim Function with valid second
            order derivatives.-->
        <prescribed_function />
        <!--Flag indicating whether or not the values
            of the coordinates should be prescribed
            according to the function above. It is
            ignored if the no prescribed function is
            specified.-->
        <prescribed>false</prescribed>
    </Coordinate>
    <Coordinate name="knee_abduction_r">
        <!--Coordinate can describe rotational,
            translational, or coupled motion. Defaults
            to rotational.-->
        <motion_type>rotational</motion_type>
        <!--The value of this coordinate before any
            value has been set. Rotational coordinate
            value is in radians and Translational in
            meters.-->
        <default_value>0</default_value>
```

```
                <!--The speed value of this coordinate before
                    any value has been set. Rotational
                    coordinate value is in rad/s and
                    Translational in m/s.-->
                <default_speed_value>0</default_speed_value>
                <!--The minimum and maximum values that the
                    coordinate can range between. Rotational
                    coordinate range in radians and
                    Translational in meters.-->
                <range>-0.4 0.4</range>
                <!--Flag indicating whether or not the values
                    of the coordinates should be limited to
                    the range, above.-->
                <clamped>false</clamped>
                <!--Flag indicating whether or not the values
                    of the coordinates should be constrained
                    to the current (e.g. default) value, above
                    .-->
                <locked>true</locked>
                <!--If specified, the coordinate can be
                    prescribed by a function of time. It can
                    be any OpenSim Function with valid second
                    order derivatives.-->
                <prescribed_function />
                <!--Flag indicating whether or not the values
                    of the coordinates should be prescribed
                    according to the function above. It is
                    ignored if the no prescribed function is
                    specified.-->
                <prescribed>false</prescribed>
            </Coordinate>
        </objects>
        <groups />
```

```
</CoordinateSet>
<!--Whether the joint transform defines parent->child or child->
    parent.-->
<reverse>false</reverse>
<!--Defines how the child body moves with respect to the parent as a
    function of the generalized coordinates.-->
<SpatialTransform>
        <!--3 Axes for rotations are listed first.-->
        <TransformAxis name="rotation1">
                <!--Names of the coordinates that serve as the
                    independent variables          of the transform
                    function.-->
                <coordinates>knee_flexion_r</coordinates>
                <!--Rotation or translation axis for the transform
                    .-->
                <axis>0 0 1</axis>
                <!--Transform function of the generalized coordinates
                     used to         represent the amount of
                    transformation along a specified axis.-->
                <function>
                        <LinearFunction>
                                <coefficients> 1 0</coefficients>
                        </LinearFunction>
                </function>
        </TransformAxis>
        <TransformAxis name="rotation2">
                <!--Names of the coordinates that serve as the
                    independent variables          of the transform
                    function.-->
                <coordinates>knee_rotation_r</coordinates>
                <!--Rotation or translation axis for the transform
                    .-->
                <axis>0 1 0</axis>
```

```
            <!--Transform function of the generalized coordinates
                used to represent the amount of
                transformation along a specified axis.-->
            <function>
                <LinearFunction>
                    <coefficients> 1 0</coefficients>
                </LinearFunction>
            </function>
        </TransformAxis>
        <TransformAxis name="rotation3">
            <!--Names of the coordinates that serve as the
                independent variables of the transform
                function.-->
            <coordinates>knee_abduction_r</coordinates>
            <!--Rotation or translation axis for the transform
                .-->
            <axis>1 0 0</axis>
            <!--Transform function of the generalized coordinates
                used to represent the amount of
                transformation along a specified axis.-->
            <function>
                <LinearFunction>
                    <coefficients> 1 0</coefficients>
                </LinearFunction>
            </function>
        </TransformAxis>
```

The wrapping surface added to correct the discontinuity on the lever arm of the lateral and medial gastrocnemius muscles is a portion of cylinder and its geometry is described in the section of the code where the "femur_r" is defined. The definition of this wrapping surface is the following:

```
<WrapObjectSet>
        <objects>
                <WrapCylinder name="TRI">
                        <!--Display Pref. 0:Hide 1:Wire 3:Flat 4:
                            Shaded-->
                        <display_preference>4</display_preference>
                        <xyz_body_rotation> 0 0 0</xyz_body_rotation>
                        <translation> -0.0205 -0.406 0</translation>
                        <active>true</active>
                        <quadrant>-x</quadrant>
                        <VisibleObject>
                                <!--Set of geometry files and
                                    associated attributes, allow .vtp,
                                     .stl, .obj-->
                                <GeometrySet>
                                        <objects />
                                        <groups />
                                </GeometrySet>
                                <!--Three scale factors for display
                                    purposes: scaleX scaleY scaleZ-->
                                <scale_factors> 1 1 1</scale_factors>
                                <!--transform relative to owner
                                    specified as 3 rotations (rad)
                                    followed by 3 translations rX rY
                                    rZ tx ty tz-->
                                <transform> 0 0 0 -0.0205 -0.406 0</
                                    transform>
                                <!--Whether to show a coordinate
                                    frame-->
```

```
                                    <show_axes>false</show_axes>
                                    <!--Display Pref. 0:Hide 1:Wire 3:
                                        Flat 4:Shaded Can be overriden for
                                         individual geometries-->
                                    <display_preference>4</
                                        display_preference>
                            </VisibleObject>
                            <radius>0.01</radius>
                            <length>0.1</length>
                    </WrapCylinder>
            </objects>
            <groups />
</WrapObjectSet>
```

In order to make the two muscles to lean on the wrapping surface, in the definition of the "med_gas_r" and of the "lat_gas_r", the following part of code has been added:

```
<PathWrapSet>
        <objects>
                <PathWrap>
                        <wrap_object>TRI</wrap_object>
                        <method>hybrid</method>
                        <range> -1 -1</range>
                </PathWrap>
        </objects>
        <groups />
</PathWrapSet>
```

The values of the maximum isometric force of the musclesof the original model and of the modified model can be seen in Table 10.2:

Name muscle	Original model "Gait2392_Simbody	Modified model	Name muscle	Original model "Gait2392_Simbody	Modified model	Name muscle	Original model "Gait2392_Simbody	Modified model
glut_med1_r	819	2047.5	add_mag3_r	488	1220	vas_lat_r	1871	4677.5
glut_med2_r	573	1432.5	tfl_r	233	582.5	med_gas_r	1558	3895
glut_med3_r	653	1632.5	pect_r	266	665	lat_gas_r	683	1707.5
glut_min1_r	270	675	grac_r	162	405	soleus_r	3549	8872.5
glut_min2_r	285	712.5	glut_max1_r	573	1432.5	tib_post_r	1588	3970
glut_min3_r	323	807.5	glut_max2_r	819	2047.5	flex_dig_r	310	775
semimem_r	1288	3220	glut_max3_r	552	1380	flex_hal_r	322	805
semiten_r	410	1025	iliacus_r	1073	2682.5	tib_ant_r	905	2262.5
bifem_lh_r	896	2240	psoas_r	1113	2782.5	per_brev_r	435	1087.5
bifem_sh_r	804	2010	quad_fem_r	381	952.5	per_long_r	943	2357.5
sar_r	156	390	gem_r	164	410	per_tert_r	180	450
add_long_r	627	1567.5	peri_r	444	1110	ext_dig_r	512	1280
add_brev_r	429	1072.5	rect_fem_r	1169	2922.5	ext_hal_r	162	405
add_mag1_r	381	952.5	vas_med_r	1294	3235			
add_mag2_r	343	857.5	vas_int_r	1365	3412.5			

Table 10.2: Maximum isometric force of the muscles of the original model and of the modified model.

The names and the coordinates of the 12 markers used for our captures can be seen in Table 10.3:

Markers coordinates (relative):				
marker	body	X	Y	Z
R_ASIS	pelvis	0.00953097	0.00737548	0.127414
L_ASIS	pelvis	0.00953097	0.00737548	-0.127414
R_Trocanther	femur_r	-0.0165688	-0.0263671	0.0701751
R_Knee_Joint_Line	femur_r	0.0019855	-0.403705	0.0480504
R_Knee_Medial	femur_r	0.012203	-0.401151	-0.0473211
R_Lat_Mal	talus_r	-0.00746779	0.0177978	0.052069
R_Ankle_Medial	tibia_r	0.0103784	-0.389954	-0.0343424
R_Heel	calcn_r	-0.0174386	0.00816477	-0.00627294
R_2nd_Meta_Head	calcn_r	0.178825	0.0178367	0.0014048
R_Tibial_Wand	tibia_r	0.00525186	-0.232169	0.065348
R_Femoral_Wand	femur_r	0.0202031	-0.235957	0.079839
Sacrum	pelvis	-0.141564	0.0986655	0.00165085

Table 10.3: Names and coordinates of the markers.

10.2 Scaling parameters

The mass of the real model used in the first part of the scaling has been estimated with the relations of Zatsiorsky-DeLeva that relate the mass of each body segment to the total mass of the subject; these relations can be seen in Table 10.4:

Zatsiorsky-DeLeva relations:		
	MASS (%)	
segment	female	male
Head	6.68	6.94
Trunk	42.57	43.46
UPT	15.45	15.96
MPT	14.65	16.33
LPT	12.47	11.17
Upper arm	2.55	2.71
Forearm	1.38	1.62
Hand	0.56	0.61
Thigh	14.78	14.16
Shank	4.81	4.33
Foot	1.29	1.37

Table 10.4: Relations of ZatsiorskyDeLeva.

The set of measurement defined to run the first step of the scaling can be seen in Figure 10.1:

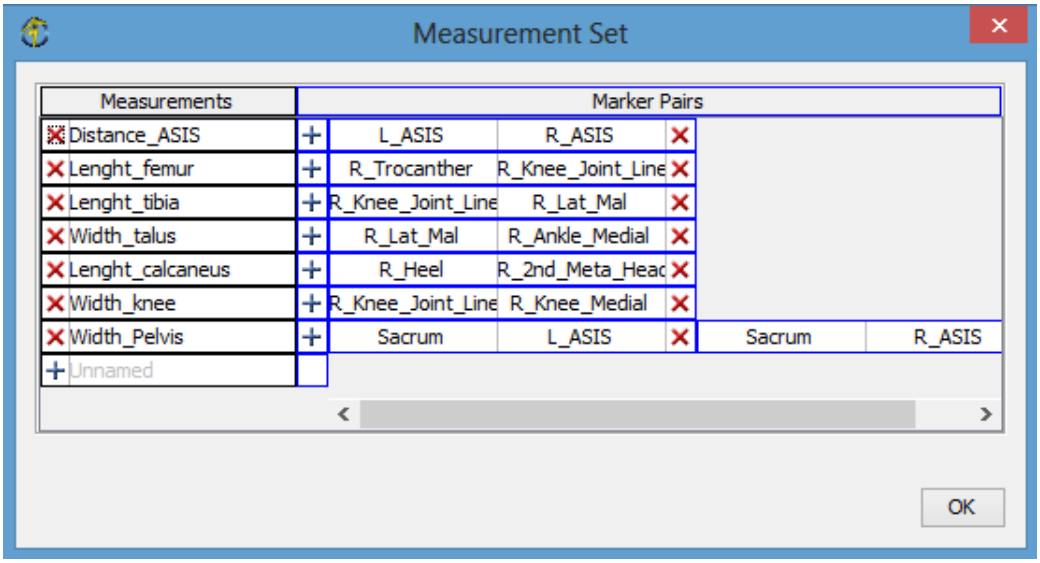

Figure 10.1: Set of measurement defined for the scaling.

The definition of the scale factors used to scale the model can be seen in the central column of Figure 10.2, in the column at the right an example of the particular values of the scale factors of one of the subjects:

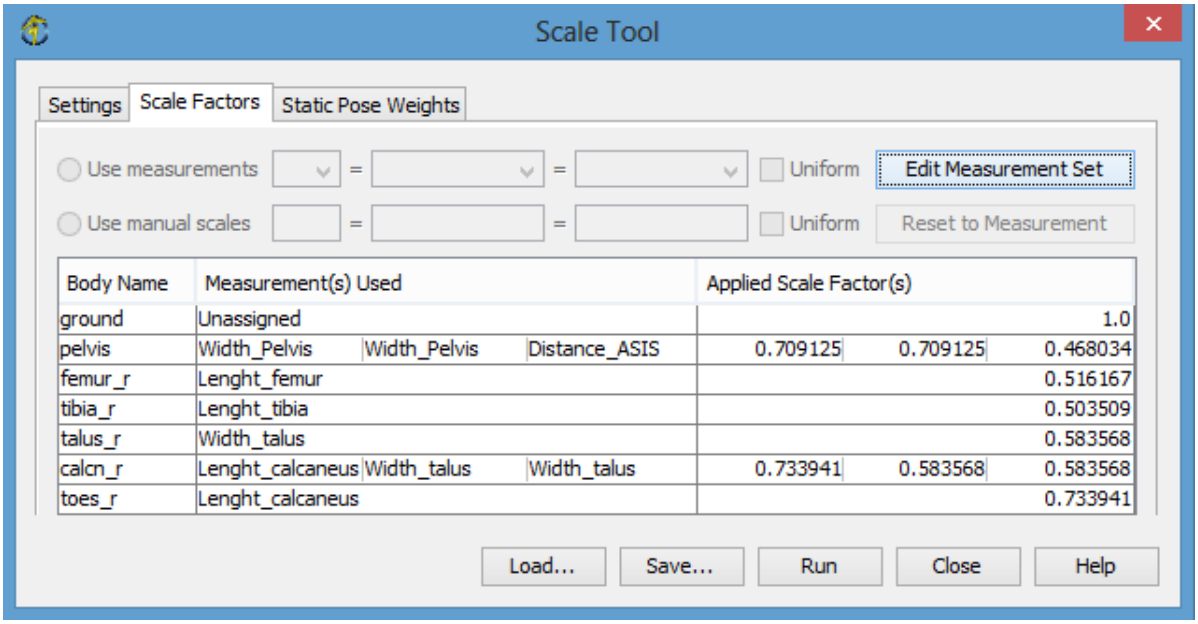

Figure 10.2: Scale factors used for the Scaling.

The set of weights used for the second step of the Scaling can be seen in Figure 10.3. In the first part the weights of the markers, on the second part the weights on the coordinates with the desired values.

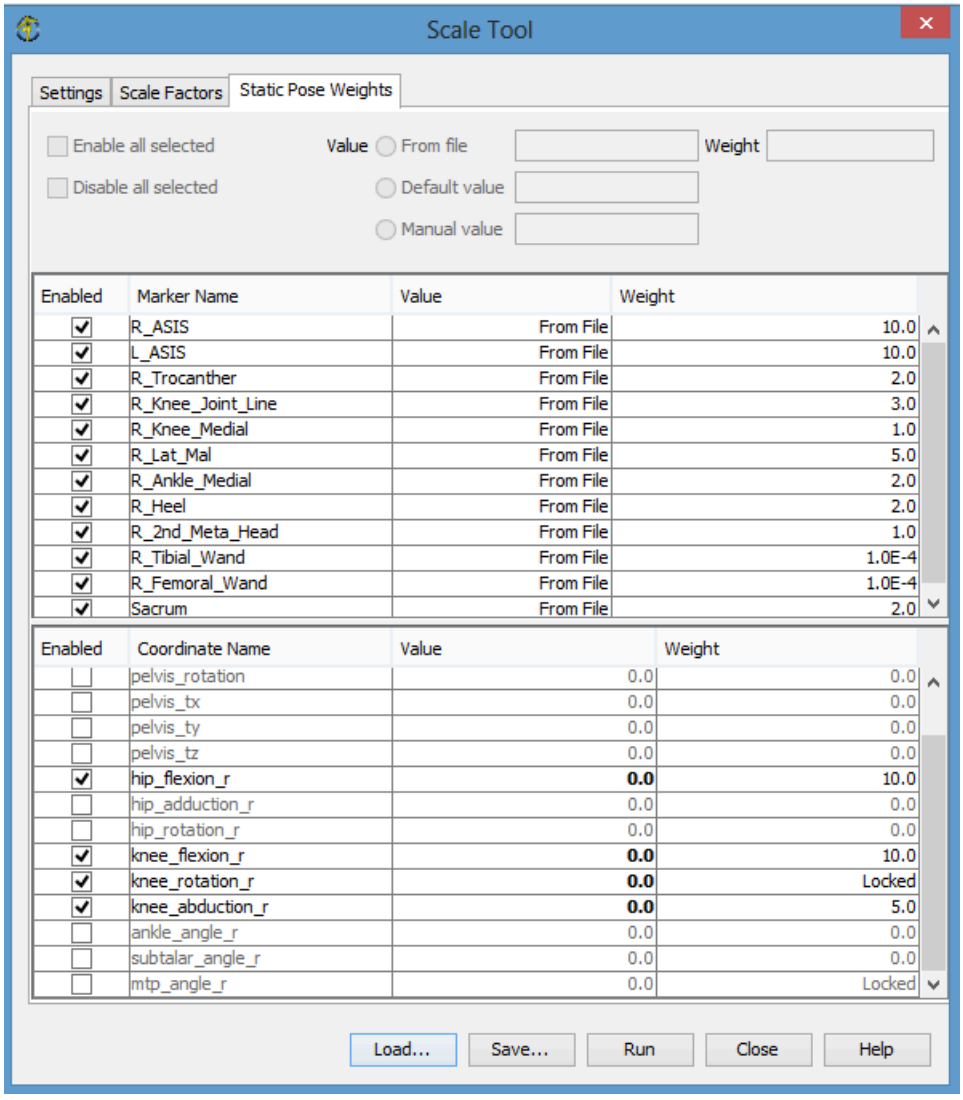

Figure 10.3: Weights used for the Scaling.

10.3 Inverse Kinematics parameters

The set of weights used for the Inverse Kinematics analysis can be seen in Figure 10.4. In the first part the weights of the markers, in the second part the weights on the coordinates with the desired values.

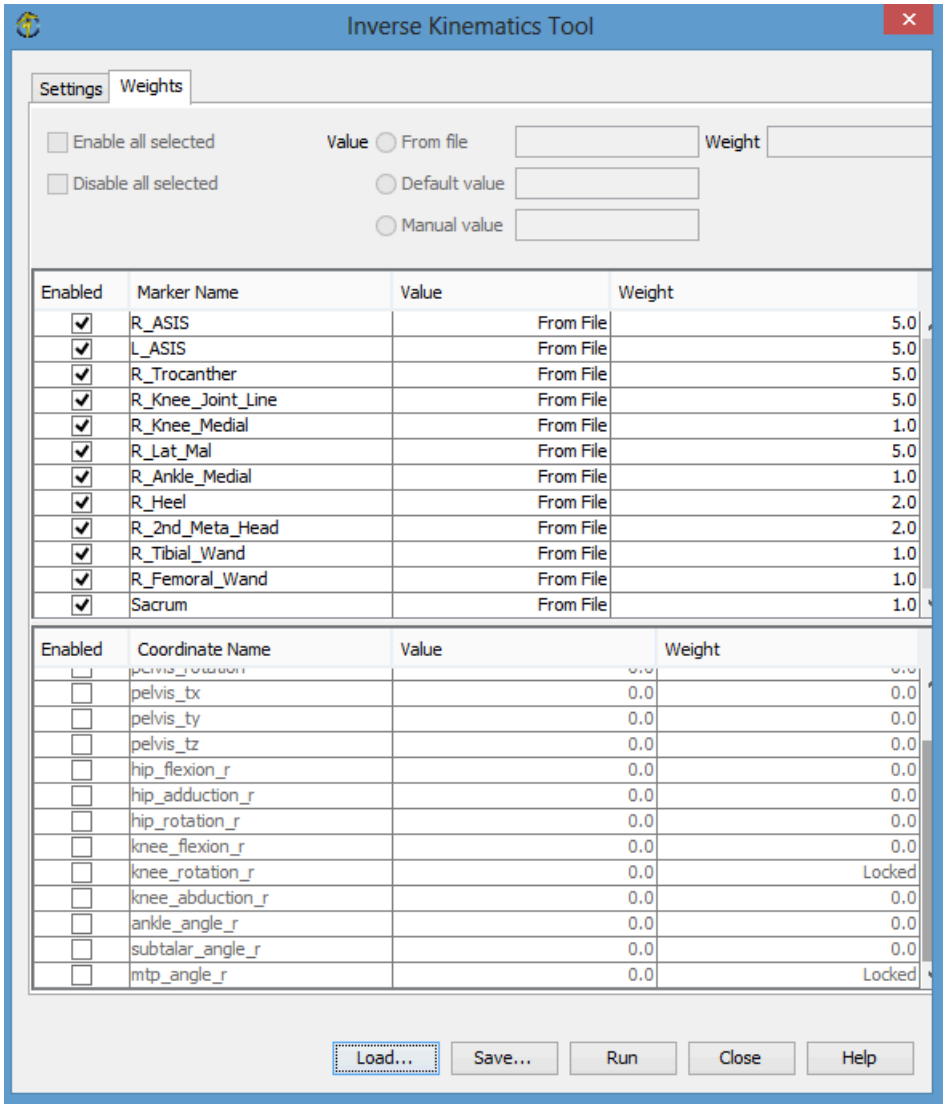

Figure 10.4: Weights used for the Inverse Kinematics analysis.

10.4 Inverse Dynamics parameters

The main settings used to run the Inverse Dynamics analysis can be seen in Figure 10.5. Let's notice that the results of the Inverse Kinematics analysis have been used as input, filtering them at 15 Hz; the time range and the output folder were different for each trial.

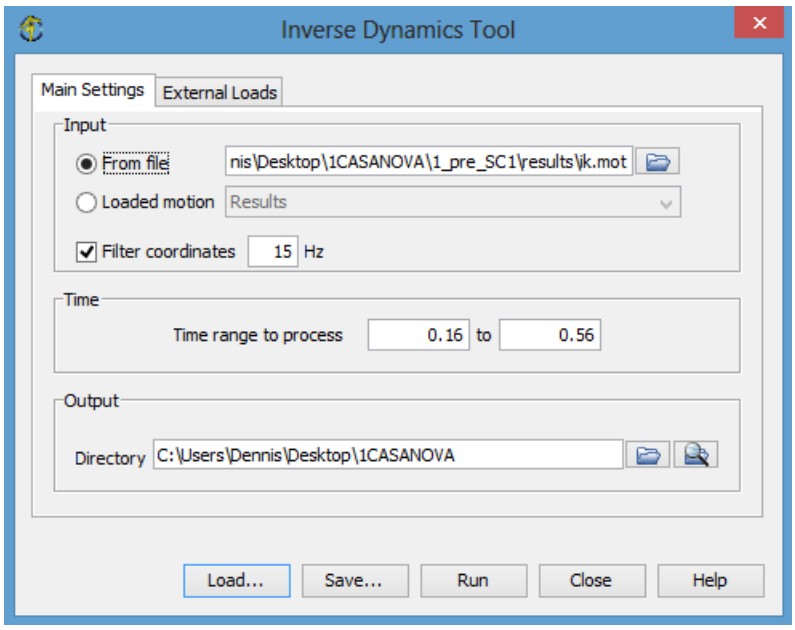

Figure 10.5: Main settings used for the Inverse Dynamics analysis.

The specification of the external loads used to run the Inverse Dynamics analysis can be seen in Figure 10.6:

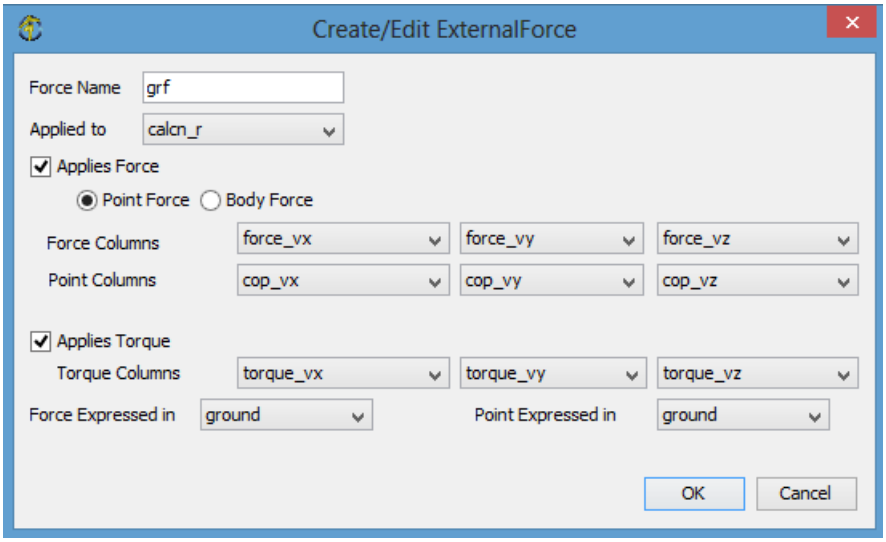

Figure 10.6: Specification of the external loads used in the Inverse Dynamics analysis.

10.5 Static Optimization parameters

The main settings used to run the Static Optimization can be seen in Figure 10.7. In particular as input we used the results of the Inverse Kinematics analysis with a cutting-off frequency of 15 Hz. In the "Objective Function" section we set the coefficient "p" equal to 2 and we unselected the "Use muscle force-length-velocity relation".

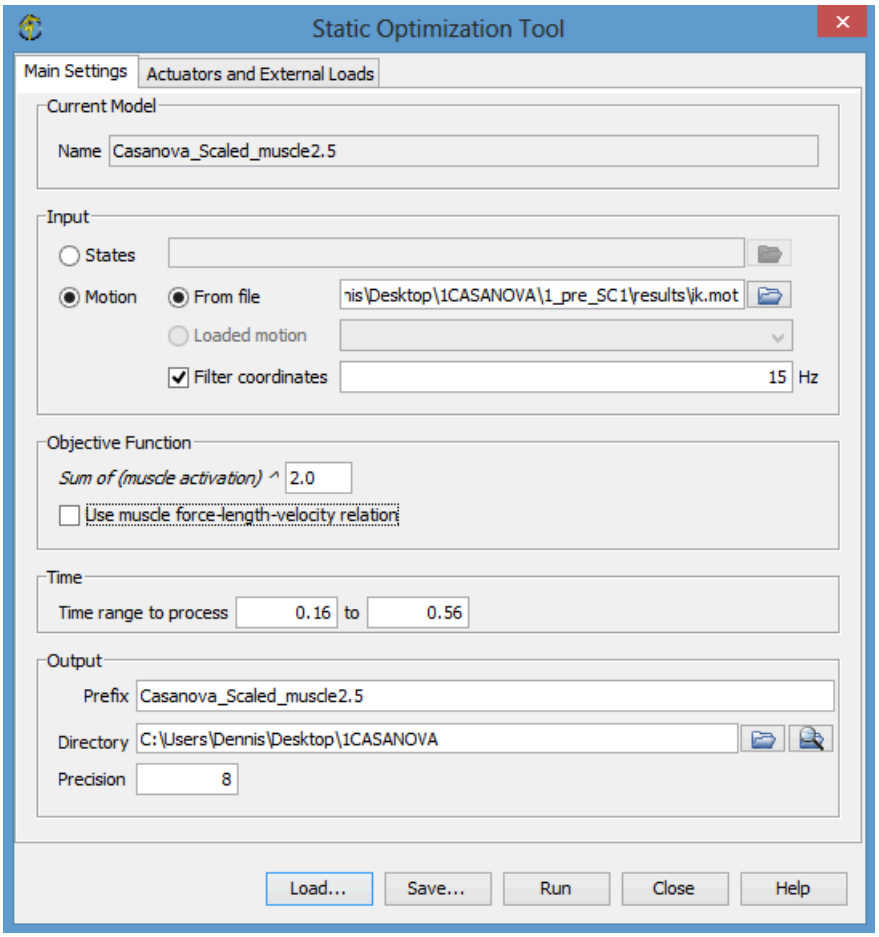

Figure 10.7: Main settings of the Static Optimization.

In the section "Actuators and External Loads" that we can see in Figure 10.8, we set the speification of the external loads as we did for the Inverse Dynamics and we selected a file containing a set of Residual Actuators useful to solve the inconsistency due to the missing parts of the body.

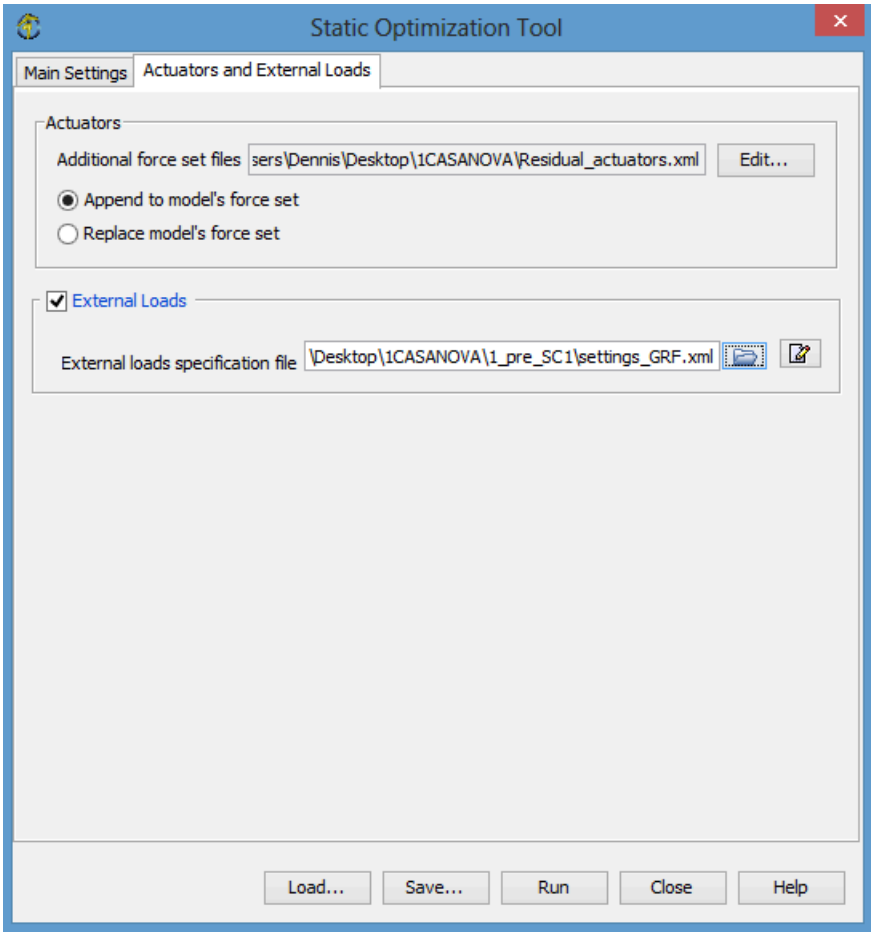

Figure 10.8: Settings of the Actuators and External Loads of the Static Optimization.

The Residual Actuators file contains the definition of 3 forces actuators (x, y and z direction) and 3 torques actuators (x, y and z direction) and these are applied to the pelvis body.

Bibliography

[1] BODYSMART. Anatomi og fysiologi - et overblik. `http://bodysmart.dk/hoften-pelvis`. [Online; accessed 26-January-2014].

[2] WIKIPEDIA COMMONS. Anterior cruciate ligament. `http://en.wikipedia.org/wiki/Anterior_cruciate_ligament`. [Online; accessed 26-January-2014].

[3] WIKIPEDIA COMMONS. Pennation angle of fibers in pennate muscle. `http://commons.wikimedia.org/wiki/File:Pennation_angle_of_fibers_in_pennate_muscle.png`. [Online; accessed 26-January-2014].

[4] KRISTIANSLUND E. and KROSSHAUG T. Comparison of drop jumps and sport-specific sidestep cutting: Implications for anterior cruciate ligament injury risk screening. *41(3):684-8. Am J Sports Med.*, 2013.

[5] DE MORAT G., WEINHOLD P., BLACKBURN T., CHUDIK S., and GARRETT W. Aggressive quadriceps loading can induce noncontact anterior cruciate ligament injury. *32(2):477-83. Am J Sports Med*, 2004.

[6] KAMEN G., ROBERTSON D.G.E., and HAMILL J. *Electromyographic Kinesiology.* 2004.

[7] MYER G.D., FORD K.R., and HEWETT T.E. New method to identify athletes at high risk of acl injury using clinic-based measurements and freeware computer analysis. *45(4):238-44. Brit J Sport Med.*, 2010.

[8] LOEB G.E. and GHEZ C. The motor unit and muscle action. `http://www.ib.cnea.gov.ar`. [Online; accessed 26-January-2014].

[9] KOGA H., NAKAMAE A., and SHIMA Y. Mechanisms of noncontact anterior cruciate ligament injuries. *43(4): 396408. Am. J Sports Med.*, 2010.

[10] MATSUMOTO H. Mechanism of the pivot shift. *72(5):816-21. J Bone Joint Surg Br*, 1990.

[11] WANG H. and ZHENG N. Knee rotation and loading during spin and step turn. *31(10):742-6. Int J Sports Med.*, 2010.

[12] HICKS J. Getting started with rra. `http://simtk-confluence.stanford.edu:8080/pages/viewpage.action?pageId=3376194`. [Online; accessed 27-January-2014].

[13] SPEER K., SPRITZER C.E., BASSETT F.H., FEAGIN J.A., and GARRETT W.E. Osseous injury associated with acute tears of the anterior cruciate ligament. *20(4):382-9. Am J Sports Med.*, 1992.

[14] CARDINALE M. and LIM J. The acute effects of two different whole body vibration frequencies on vertical jump performance. *Med. Sport*, 2003.

[15] HOUSTON METHODIST ORTHOPEDICS & SPORTS MEDECINE. A patient's guide to meniscal surgery. `http://www.methodistorthopedics.com/bodyortho.cfm?id=41856`. [Online; accessed 26-January-2014].

[16] TOOLOOP HUMAN ANATOMY PICTURE. Back to post: Patella sesamoid bone. `http://www.tooloop.com/patella-sesamoid-bone/patella-sesamoid-bone`. [Online; accessed 26-January-2014].

[17] FAIRFAX COUNTRY PUBLIC SCHOOLS. Contraction of motor units. `http://staff.fcps.net/cverdecc/adv%20a&p/notes/muscle%20unit/contration%20of%20motor/contraction_of_motor_units.htm`. [Online; accessed 26-January-2014].

[18] SENIAM. Sensor placements. `http://www.seniam.org/`. [Online; accessed 26-January-2014].

[19] MCLEAN S.G., HUANG X., SU A., and VAN DEN BOGERT A.J. Sagittal plane biomechanics cannot injure the acl during sidestep cutting. *19(8):828-38. Clin Biomech*, 2004.

[20] SIMBIOS. Simtk. `https://simtk.org/xml/index.xml`. [Online; accessed 26-January-2014].

[21] DELP S.L., ANDERSON F.C., ARNOLD A.S., LOAN P., HABIB A., JOHN C.T., GUENDELMAN E., and THELEN D.G. Opensim: Open-source software to create and analyze dynamic simulations of movement. *54(11):1940-50. IEE Trans Biomed Eng.*, 2007.

[22] HEWETT T.E., MYER G.D., and FORD K.R. Biomechanical measures of neuromuscular control and valgus loading of the knee predict anterior cruciate ligament injury risk in female athletes: a prospective study. *33(4):492-501. Am J Sports Med.*, 2005.

Chapter 11

Ringraziamenti

Questo lavoro di tesi è dedicato a voi Mamma e Papà, che mi avete sempre sostenuto durante tutti questi anni, che mi avete dato l' opportunità di studiare e di poter crescere professionalmente nonchè come persona, pur sapendo che molto probabilmente ciò mi avrebbe portato lontano da casa. Lontano da casa è dove ho trascorso gli ultimi 6 mesi della mia vita, tra un sacco di cose nuove e stimolanti, ma anche senza la sicurezza di avere accanto qualcuno su cui poter contare veramente, qualsiasi cosa potesse accadere. Vi ringrazio per avermi dato l' opportunità di vivere questa esperienza, pur sapendo quanto amara possa esser stata per voi; ne sono ritornato con un importante bagaglio di vita vissuta e di esperienze che mai avrei potuto acquisire senza partire. Finalmente siamo giunti insieme a questo importante traguardo della Laurea Magistrale e l' unica cosa che posso dirvi è GRAZIE.

Vi voglio bene.

Dennis.